NASA-CR-168100
19830013119

NASA CR-168100
PWA-5843-13

# NASA

DEVELOPMENT OF A SIMPLIFIED ANALYTICAL METHOD FOR REPRESENTING
MATERIAL CYCLIC RESPONSE

By:
Vito Moreno

UNITED TECHNOLOGIES CORPORATION
POWER SECTOR
PRATT & WHITNEY AIRCRAFT GROUP
COMMERCIAL ENGINEERING

Prepared for:
NATIONAL AERONAUTICS AND SPACE ADMINISTRATION

NASA Lewis Research Center
Contract NAS 3-22821

| 1. Report No.<br>NASA CR-168100 | 2. Government Accession No. | 3. Recipient's Catalog No. |
|---|---|---|
| 4. Title and Subtitle<br>DEVELOPMENT OF A SIMPLIFIED ANALYTICAL METHOD FOR REPRESENTING MATERIAL CYCLIC RESPONSE | | 5. Report Date<br>**January 1983** |
| | | 6. Performing Organization Code |
| 7. Author(s)<br>Vito Moreno | | 8. Performing Organization Report No.<br>**PWA-5843-13** |
| | | 10. Work Unit No. |
| 9. Performing Organization Name and Address<br>United Technologies Corporation<br>Pratt & Whitney Aircraft Group<br>Commercial Engineering - East Hartford, CT 06108 | | |
| | | 11. Contract or Grant No.<br>NAS 3-22821 |
| 12. Sponsoring Agency Name and Address<br>National Aeronautics and Space Administration<br>Washington, D. C. 20546 | | 13. Type of Report and Period Covered<br>**Contractor Report** |
| | | 14. Sponsoring Agency Code |

16. Abstract

Development of a simplified method for estimating structural inelastic stress and strain response to cyclic thermal loading is presented. The method assumes that high temperature structural response is the sum of time independent plastic and time dependent elastic/creep components. The local structural stress and strain response predicted by linear elastic analysis is modified by the simplified method to predict the inelastic response. Simulations of both isothermal and variable temperature (thermomechanical) Hastelloy X uniaxial specimen tests were conducted to assess the capability of the method to predict relevant response characteristics. Comparison of these results with simulations made with a nonlinear finite element analysis, using time independent plasticity and unified time dependent material models, show comparable accuracy of the simplified material with the more rigorous analyses. The cyclic Hastelloy X specimen response data base used in this work is also presented.

| 17. Key Words (Suggested by Author(s))<br>Time Independent Plasticity and Creep<br>Unified Time Dependent<br>Simplified Response Prediction<br>Hastelloy X Cyclic Response Data Base | 18. Distribution Statement | | |
|---|---|---|---|
| 19. Security Classif. (of this report)<br>Unclassified | 20. Security Classif. (of this page)<br>Unclassified | 21. No. of Pages | 22. Price* |

* For sale by the National Technical Information Service, Springfield, Virginia 22151

N83-21390#

This Page Intentionally Left Blank

TABLE OF CONTENTS

iii

# LIST OF ILLUSTRATIONS

LIST OF ILLUSTRATIONS (Continued)

## LIST OF ILLUSTRATIONS (Continued)

# 1.0 SUMMARY

In this program, a simplified method of estimating structural inelastic stress and strain response, produced as a result of cyclic thermal loading, was developed.

The procedure was evaluated using a data base developed from uniaxial, strain controlled Hastelloy X specimen tests. The data base included isothermal and thermomechanical cycles. Hastelloy X was selected because of prior structural analysis and material model development with this material conducted under two previous contracts.

Isothermal cyclic response data were included to document fundamental material response characteristics (strain rate dependent yield stress, effect of cyclic hold times, etc.) over the range of temperatures experienced during a typical thermal loading cycle. The isothermal data were considered to be "fundamental building block" information necessary in the development of a response model. The thermomechanical cyclic response data consisted of a series of increasingly complex cycles ultimately leading to the response for a gas turbine combustor liner defined from previous structural analysis. Accurate prediction of the thermomechanical cycles is considered as verification of the cyclic response model.

For comparison, simulations of Hastelloy X specimen tests were made with two existing Hastelloy X material behavior models: 1) a classical time independent plasticity and creep model, and 2) a unified time dependent plasticity model. The classical plasticity and creep model assumes decomposition of the response into uncoupled plasticity and creep components. This is considered the current state of the art in material models available in most general purpose nonlinear finite element codes. Simulation of the thermomechanical cycles with this model generally produced stress-strain response predictions that were more elastic than the experimental data.

The unified time dependent model considers inelastic response as a continuous function of stress and several state variables which recognize prior history loading. Predicted response with this model for the thermomechanical cycles were in good agreement with the experimental results. The major area of discrepancy was in the lower temperature region where the material displays a smaller degree of rate sensitivity.

The simplified procedure was developed recognizing characteristics of both material models. The time independent yield surface concept was used to define discrete yield points, while a unified equation predicts integrated elastic and creep response. This method assumes that, for a structure in which the inelastic regions are constrained by the surrounding elastic material, the local mechanical strain and temperature history can be defined by linear elastic analysis. The actual stress response is then determined by considering the nonlinearity produced by time independent plasticity and time dependent creep. Comparisons of the predicted results for the thermomechanical cycles show the simplified procedure to be of comparable accuracy with the two other models. Yet, implementation of the model requires material properties available either from design handbooks or simple monotonic specimen testing and a definition of the local strain-temperature history.

## 2.0 INTRODUCTION

Requirements for increased durability of gas turbine hot section structural components have placed greater importance on accurate structural analysis and life prediction. The high temperatures experienced by these components (combustor liner, turbine blades and vanes, support structures) often result in significant amounts of cyclic time-dependent plasticity which makes the basic development and calibration of structural analysis and life prediction tools a challenging job. Therefore, improvements in hot section structural durability will rely heavily on the ability to accurately define local response for life prediction through computer-based analytical methods.

Details of the high temperature structural analysis problem are best defined by considering a component on which extensive analysis has been performed such as a combustor liner.

Most combustor liners are constructed of sheet metal louvers which rely on convective film cooling. Details of a louver geometry are shown in Figure 2-1 where the individual formed pieces are seam welded together to make the louver liner. Each individual louver is cooled by compressor discharge air introduced into the chamber created by the louver lip and knuckle region to generate an insulating film of cooling air on the downstream panel. Degradation of the cooling film as it moves along the panel results in increased metal temperature in the seam weld and louver lip regions. The thermal gradient between these regions and the knuckle of the next louver is a function of the engine operating condition. Figure 2-2 indicates the typical knuckle location, (B), which is generally cooler than the typical lip location, (A). The temperature difference between these two locations creates thermal stresses in the combustor liner. At the maximum power point, the thermally induced stress and strain state has significant amounts of plasticity which, when repeated over subsequent engine flight cycles, results in creep/fatigue failure of the liner. In large diameter annular combustion liners, fatigue cracks initiate in the louver lip region and grow axially toward the seam weld.

While the specific geometry and heat transfer mechanisms may vary, the combustor liner is a representative high temperature thermomechanical analysis problem requiring accurate structural analysis and life prediction.

In recent years, the finite element analysis procedure has been used with increasing frequency in the analysis of gas turbine structural components. In general, durability considerations limit design stress levels below the material yield strength and, as such, linear elastic finite element analysis is sufficient for the analysis of most components. These solutions can be generally obtained quickly and economically for a series of loading conditions throughout a flight cycle using specifically developed or commercially available codes. For structures operating at moderate to high temperatures, the local stresses can exceed the material yield strength and/or time dependent deformation (creep) can occur. In this case, a non-linear analysis is considered necessary for an accurate prediction of the local stress and

strain response. This is illustrated by considering the combustor liner analysis performed in Reference 1. The three-dimensional finite element model of a segment of the combustor liner is shown in Figure 2-3. Predicted stress and strain results at the fatigue critical location (end of the louver lip) using both a linear elastic analysis and a non-linear analysis are shown in Figure 2-4. The linear elastic, thermoelastic, analysis was conducted at a number of specific points throughout the thermal loading cycle. The results show a large negative stress and a closed loop response. The incremental non-linear analysis predicts a more realistic stress and strain response which contains initial yielding and cyclic plasticity at the expense of considerably more set-up and computer run time than the thermoelastic analyses. From these results the need and objective of the current program become clear; the development of a simplified procedure for the prediction of local cyclic structural response to thermomechanical loading using the result of thermoelastic analysis and readily available material property data. As a measure of success, the procedure or model would have to predict results of comparable accuracy to those obtained with the more rigorous non-linear analysis.

In this program, a simplified method for predicting material cyclic response was developed and compared to two existing material behavior models for a series of isothermal and thermomechanical Hastelloy-X loading cycles. To meet the objectives of the program, three technical tasks were established.

Task I    SPECIMEN FABRICATION AND TESTING - Uniaxial, strain controlled specimens fabricated from fine grain Hastelloy-X material were tested to provide cyclic constitutive response data for the loading cycles defined in Task II.

TASK II   CYCLIC RESPONSE DATA BASE DEFINITION - A Hastelloy-X data base, consisting of uniaxial cyclic response for six types of loading cycles, was established for evaluation of three cyclic response methods defined in Task III.

TASK III  METHODS EVALUATION, DEVELOPMENT AND RANKING - Three cyclic response methods were evaluated and compared as to their suitability for the prediction of the relevant cyclic response characteristics. The three analysis methods included a state of the art time independent plasticity and creep representation, a time dependent unified representation, and the simplified procedure.

Section 3.0 of this report describes the Hastelloy-X specimens and the six categories of response data used in the establishment of the data base. Section 4.0 describes the cyclic response prediction methods and explains how each was evaluated for the isothermal loading cycles. The comparison of the three methods in predicting thermomechanical loading cycles is described in Section 5.0, Results. Section 6.0 presents the Conclusions and a Summary of the Results.
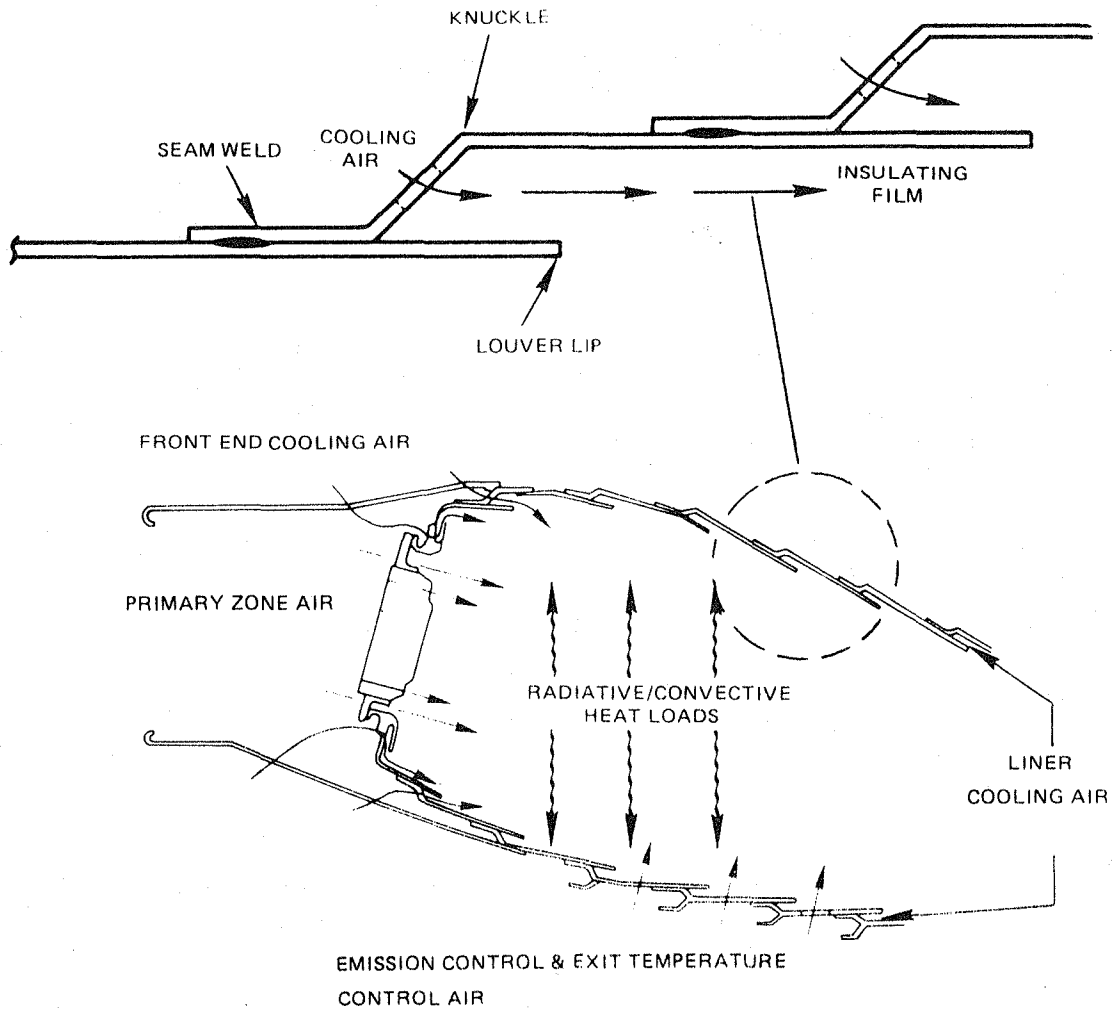
Figure 2-1    Typical Louver Liner Construction and Airflow Distribution
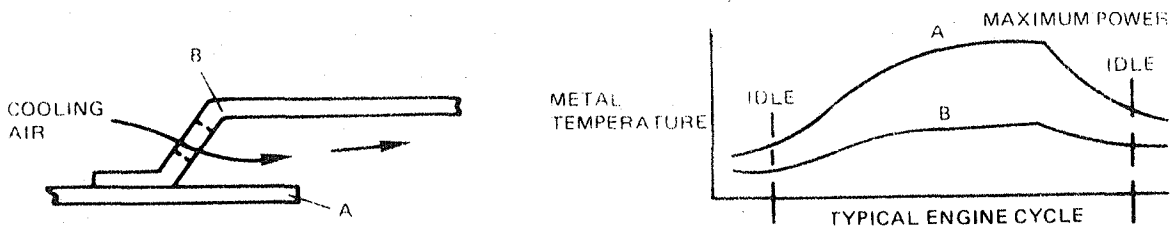


Figure 2-2    Representative Thermal Gradient in Louver Cooling Scheme
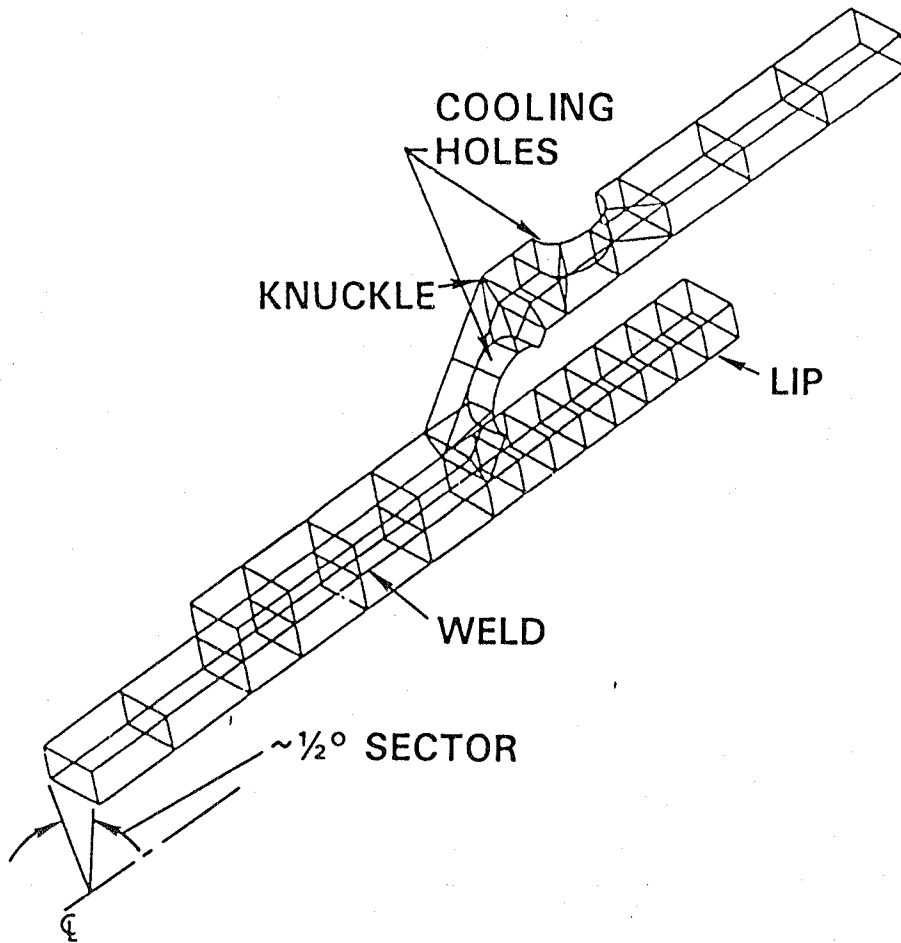
Figure 2-3    Combustor Liner Finite Element Model
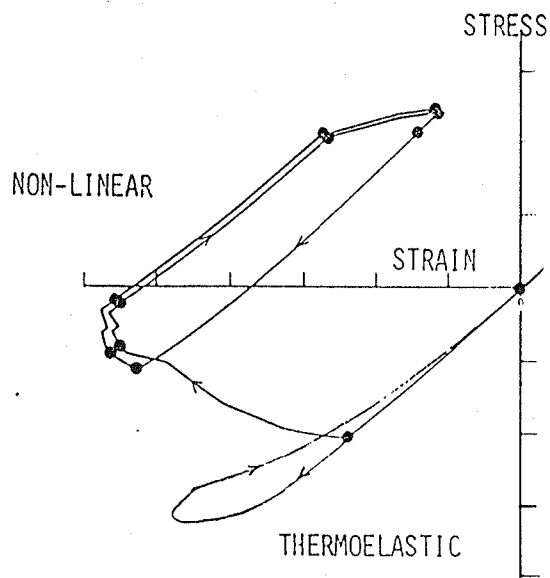


Figure 2-4    Comparison of Linear and Non-linear Analysis

## 3.0  SPECIMEN DESCRIPTION AND HASTELLOY-X RESPONSE DATA BASE

Previous analysis of the combustor liner discussed in Section 2.0 indicated that the area of maximum inelastic stress and strain was concentrated at the end of the louver lip in (Figure 2-3). The strain controlled nature of the response, together with the essentially one-dimensional stress field (circumferential hoop stress), suggested that a uniaxial test specimen could be used to investigate the local stress-strain response to a given loading history. The intent of the data base was to study the component thermomechanical response through a series of simpler response cycles. This would identify fundamental characteristics which a successful analytical model should predict. The data base consisted of uniaxial stress versus strain data generated in two earlier contracts (References 1 and 2), and additional testing conducted in Task I of the current program. Specimen geometry, test procedures, and the specific test conditions that comprised the data base are discussed below.

### 3.1  SPECIMEN DESCRIPTION

### 3.1.1  Material

Specimens in this program were fabricated from 2.54 cm (1 inch) diameter Hastelloy X base stock taken from the same heat of material used in references 1 and 2. This bar material had been specifically processed to have a grain size (ASTM 8 or finer) consistent with the rolled sheet metal used in the construction of many combustor liners. Previous testing had shown similar tensile, creep, and fatigue properties between the bar and sheet materials.

### 3.1.2 ` Internal Ridge Specimens

Two tubular, internal ridge geometry specimens were fabricated for thermomechanical testing. A representative specimen is pictured in Figure 3.1-1. The hollow geometry, together with low frequency induction heating and cooling air, permitted testing with the mechanical strain and temperature histories included in the data base. An axial extensometer was attached to the internal ridges for strain control.
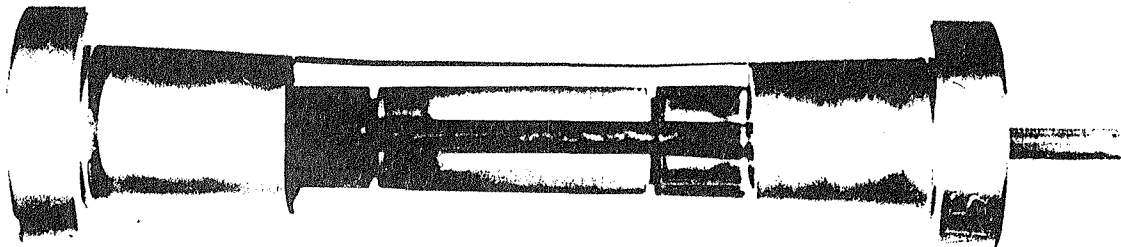
Figure 3.1-1  Strain  Control  Fatigue  Specimen  With  Internal  Ridges
(78-441-8492)

6

### 3.1.3 External Ridge Specimens

Three solid, external ridge geometry specimens were fabricated for isothermal cyclic testing. A representative specimen is pictured in Figure 3.1-2. Tests were conducted in a clamshell resistance heated oven. The integral ridges were used for attachment of an axial extensometer for strain control.
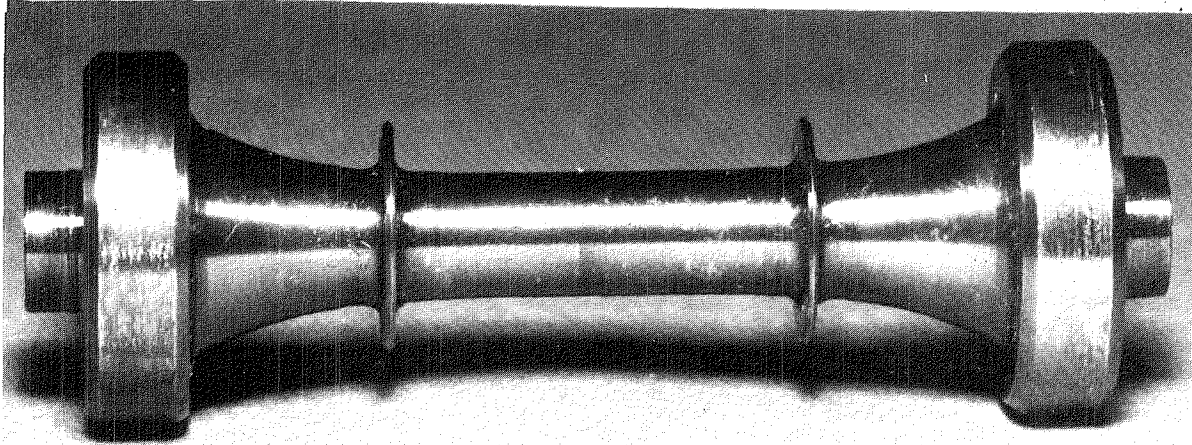


Figure 3.1-2  External Ridge Solid Strain Controlled Specimen

## 3.2  CYCLIC RESPONSE DATA BASE

The data base consisted of the uniaxial cyclic response for six types of loading cycles, shown schematically in Figure 3.2-1. Isothermal and thermomechanical loading histories were selected that addressed the important response characteristics associated with high temperature structural cyclic loading. The six loading cycles used to define the data base were:

  a.) Isothermal, fully reversed, strain controlled cycling at 538, 649, 760, 871, and 982°C (1000, 1200, 1400, 1600, and 1800°F) to define strain rate dependence. Figure 3.2-1a

  b.) Isothermal, fully reversed with stress relaxation at maximum compressive strain at 760, 871, and 982°C (1400, 1600, and 1800°F) to define the effect of the relaxation on subsequent inelastic response. Figure 3.2-1b

  c.) Isothermal, strain controlled with creep hold at maximum compressive strain at 760, 871, and 982°C (1400, 1600, and 1800°F) to define the effect of creep on subsequent inelastic response. Figure 3.2-1c

  d.) Thermomechanical cycling with step temperature changes to investigate the temperature rate effect on subsequent response. Figure 3.2-1d

  e.) Thermomechanical, strain controlled with linear strain-temperature histories from 427 to 982°C (800 to 1800°F), 649 to 982°C (1200 to 1800°F), and 760 to 982°C (1400 to 1800°F) for evaluation of the analytical models on "simple" thermomechanical cycles. Figure 3.2-1e

f.) Thermomechanical, strain controlled with faithful cycle strain-temperature from a combustor liner nonlinear analysis (Reference 1). This represents a more representative component loading and was considered a "final" verification of the simplified procedure. Figure 3.2-1f

The isothermal cycles (a-c) were used primarily in the development and calibration of the three response prediction models, described in Section 4.0, while the thermomechanical cycles (d-f) were used in a comparison of prediction accuracy.

The step temperature tests (condition d) represent the simplest thermomechanical cycle considered. Here, the specimen is cycled at a isothermal condition under sinusoidal strain control. The temperature is then instantaneously (less than 3 seconds) raised at the point of minimum strain and the subsequent isothermal response at the new temperature is observed. These tests were intended to determine if a temperature rate effect could be observed in Hastelloy X.

The linear strain-temperature cycles (condition e) were included to provide an intermediate step for model evaluation from an isothermal to a faithful cycle. The 760 to 982°C (1400 to 1800°F) cycle represents a nearly isothermal cycle while the 427 to 982°C (800 to 1800°F) cycle extends beyond the temperature range experienced in the faithful cycle. All three cycles were run with sinusoidal strain and temperature variation with a 1 minute period.

Condition f in the data base contains the stress-strain response of a uniaxial specimen when subjected to the strain temperature history in Figure 3.2-2. This history was determined from the analysis of a representative combustor louver liner, described in Reference 1, using nonlinear finite element analysis with classical time independent plasticity and creep theory. The results shown in the figure represent the predicted response at the end of the louver lip.

The experimental data assembled in this task is presented in Appendix A, Figures A-1 through A-17.

8

ISOTHERMAL CONDITIONS

a. FULLY REVERSED

$\epsilon$
(IN/IN)

TIME

b. FULLY REVERSED
WITH RELAXATION

$\epsilon$
(IN/IN)

TIME

HOLD TIME

c. FULLY REVERSED
WITH CREEP

$\epsilon$
(IN/IN)

TIME

CREEP
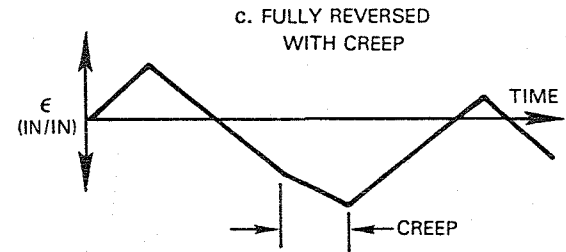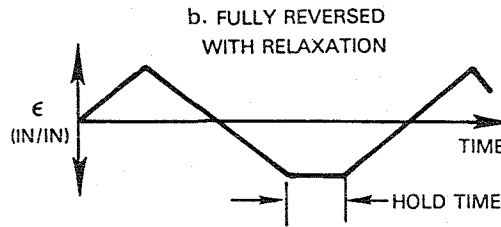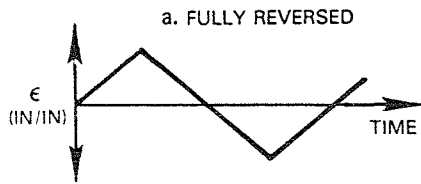
THERMOMECHANICAL CONDITIONS

d. TEMPERATURE
STEP CHANGE

$\epsilon$
(IN/IN)

TIME

TEMPERATURE

TIME

e. LINEAR STRAIN — TEMPERATURE HISTORY

$\epsilon_A$

$\epsilon$
(IN/IN)

$T_B$

$T_A$

TEMPERATURE

$\epsilon_B$

f. FAITHFUL CYCLE HISTORY*

$\epsilon$
(IN/IN)
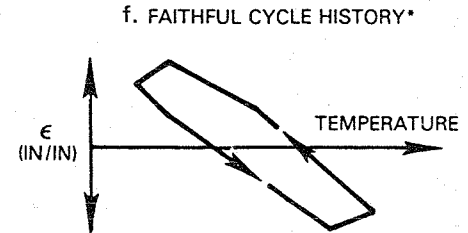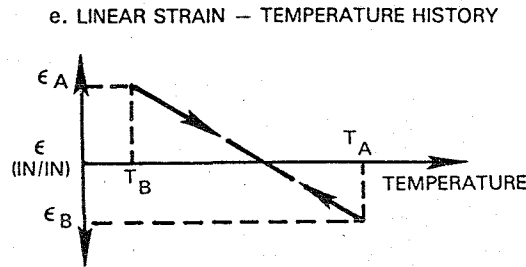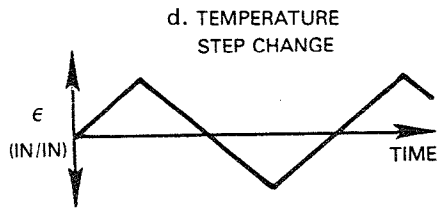
TEMPERATURE

*CYCLE DEFINED IN REFERENCE 1 (SECTION 3.0)

6
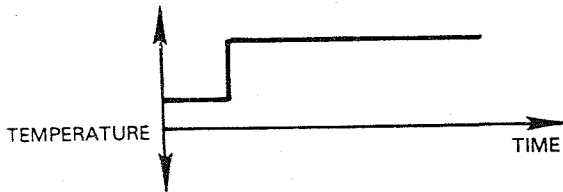
Figure 3.2-1  Loading Cycles Used to Define Cyclic Resppnse Bata Base
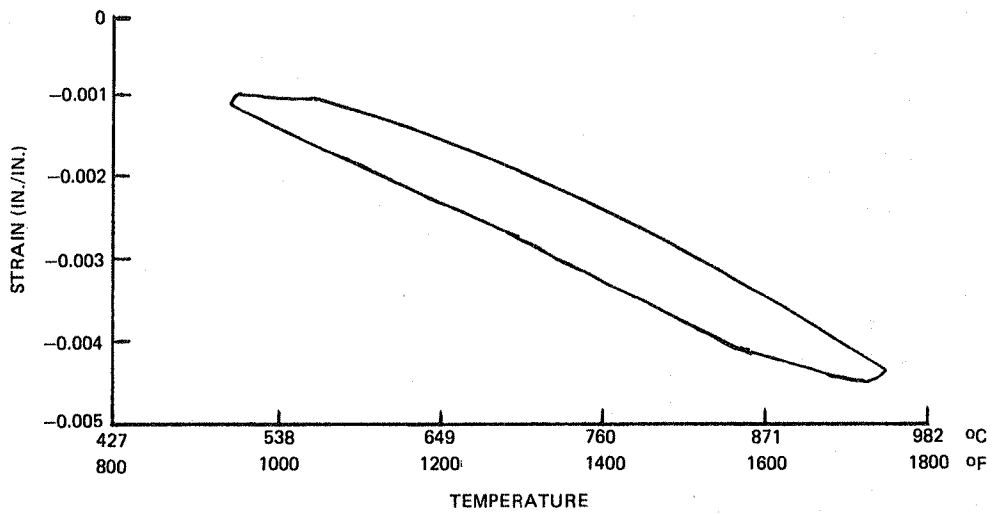
Figure 3.2-2  Sixth Cycle Mechanical Strain-Temperature History

## 4.0  EVALUATION AND DEVELOPMENT OF MATERIAL MODELS

Within the gas turbine engine, certain hot section components experience a degree of inelastic (non-linear) stress and strain response. These components (combustor liners, turbine vanes, cases and other support structures) are subjected to thermomechanical loading, that is, the predominate stress is produced by temperature differentials within the structure. In general, the resulting inelastic response is localized to the area of maximum temperature gradient while the remainder of the structure remains elastic. The stiffer elastic material acts as a constraining body and controls the cyclic strain range experienced by the inelastic area. A comparison of predicted results from non-linear and linear elastic finite element analyses, conducted in reference 1 and 2, have shown that the cyclic strain range and history at the location of maximum inelastic response can be accurately estimated from the linear elastic (thermoelastic) analyses. Thus, it is assumed for the simplified procedure, that the local mechanical strain and temperature history at a location in a structure is known from previous linear analysis. The procedure also assumes that the predominate stress field at a actual location in the structure is one-dimensional. As an example, the major stress component at the fatigue critical location in the louver of Reference 1 (Figure 2-3) is the circumferential (hoop) stress. In developing the simplified procedure, two existing material behavior models used in non-linear finite element analysis were examined. The models are a "state-of-the-art" classical time independent plasticity and creep model and a viscoplastic or time dependent plasticity model. Aspects of each model, discussed below, were selected for the simplified procedure. The overall evaluation process consisted of comparison of the predicted response for the various loading cycles included in the data base (Section 3.2) by the two models and the simplified procedure.

The models were evaluated for each loading cycle by performing nonlinear finite element analysis on a single element representation of the gage section of the specimens described in Section 3.1. This representation, shown in Figure 4-1, is a single MARC (Reference 3) element, number 28 (8 node axisymmetric - 9 integration points). The appropriate boundary conditions are also shown in the figure.



MARC ELEMENT TYPE NO. 28
8 NODE AXISYMMETRIC
9 INTEGRATED POINTS

0.22 IN.

0.050 IN.

DISPLACEMENT
APPLIED ALONG
THIS FACE

0.050 IN.
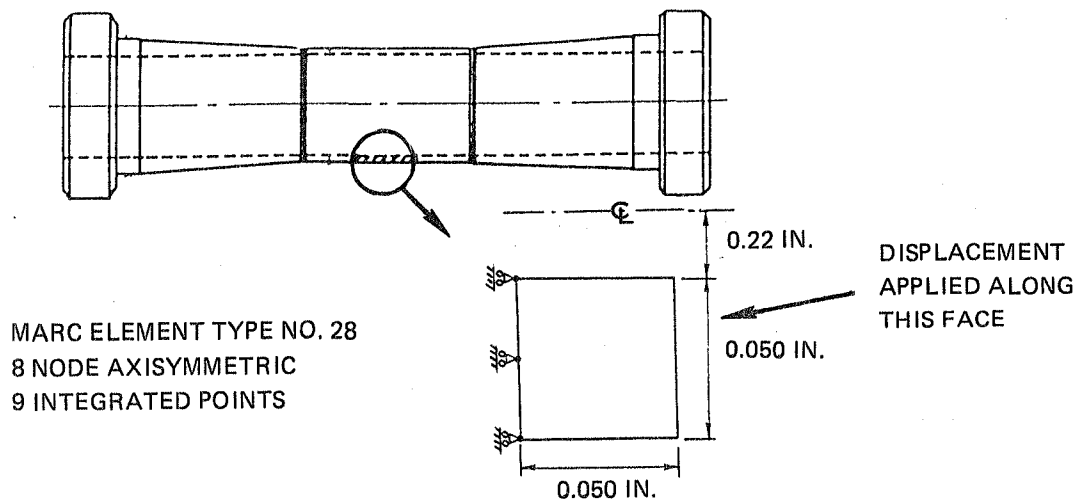
Figure 4-1    Single Element Model of Test Specimen Gage Section

The simplified procedure was evaluated using the known mechanical strain and temperature histories (where appropriate) for each of the loading cycles together with the procedure defined in Section 4.3.

A brief discussion of the existing models and the particular characteristics of each, incorporated into the simplified procedure, is presented below.

## 4.1 TIME INDEPENDENT PLASTICITY AND CREEP MODEL

Development of this model and application in the three-dimensional nonlinear finite element analysis of a Hastelloy X gas turbine combustor liner is fully documented in Reference 1. The general material model available in the MARC code (and most other nonlinear codes) is based on the assumption that the total mechanical strain can be decomposed into elastic, time independent plastic, and time dependent creep components. This may be written as:

$$\varepsilon = \varepsilon_{elastic} + \varepsilon_{plastic} + \varepsilon_{creep} \tag{1}$$

Development of the Hastelloy X cyclic plasticity model was based on the VonMises yield criterion, a tri-linear representation of the monotonic tensile curves, and the combined hardening (isotropic-kinematic) rule. In constructing the model for each temperature within the analysis, the elastic modulus, work hardening slope, and stress level (at large strains) were chosen based on previous testing conducted at a strain rate of $0.008$ min$^{-1}$. The yield point was determined using the tangency point of the actual stress-strain curve and by equating the areas under the experimental and analytical curves. Figure 4.1-1 shows a representative construction. Using this approach, the monotonic stress-strain curves for temperatures between 427°C (800°F) and 982°C (1800°F) were constructed and incorporated into the MARC WKSLP user subroutine. Simulation of the 760°C (1400°F) and 815°C (1500°F) monotonic stress-strain response is shown in Figures 4.1-2.

A series of isothermal, uniaxial simulations were run to verify the accuracy of the representation under cyclic loading. Figures 4.1-3 through 4.1-5 show the predicted results at 760°C (1400°F), 871°C (1600°F), and 982°C (1800°F) for cyclic strain controlled loading between +0.6 percent strain. Shown are the stable 5th cycle MARC results versus available cyclic test data for two representative strain rates ($\dot{\varepsilon} = 2.4 \times 10^{-2}$ min$^{-1}$ and $\dot{\varepsilon} = 2.4 \times 10^{-3}$ min$^{-1}$). Note that while the predicted stress amplitude falls between the data, the model is not capable of predicting the strain rate dependence.

A creep solution was included in an attempt to model time dependent material response. This was accomplished using the MARC subroutine CRPLAW and required that the incremental plasticity solution be periodically stopped and "creep allowed to occur".

12
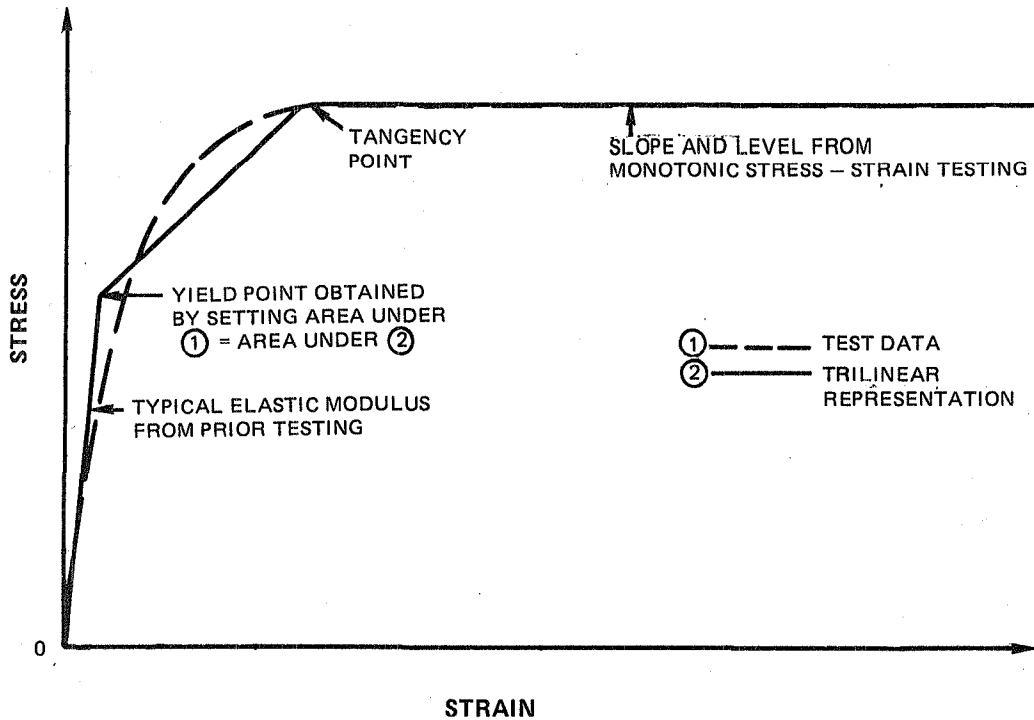
Figure 4.1-1  Construction of Stress-Strain Input for Analyses

The form of the creep equation used to model the Hastelloy X time dependent response is:

$$\epsilon_{CR} = A\sigma^n t \tag{2}$$

where:

$\epsilon_{CR}$ = creep strain
$\sigma$ = stress (ksi)
$t$ = time (hours)
$A, n$ = temperature dependent constants.

Simulation of the instantaneous time dependent nature of the high temperature material response required that the constants be determined from short time (less than 1 minute), high stress level ($\sigma_{applied} \geq 0.5\ \sigma_{yield}$) Hastelloy X creep data.

The accuracy of this constant rate model was demonstrated by simulation of monotonic stress relaxation tests. Stress relaxation, not creep, is appropriate in judging the model since, with thermal loading, time dependent structural response is predominantly stress relaxation. Comparison of these results are shown in Figure 4.1-5. Good agreement is obtained with the model, particularly for the higher temperatures (871°C or higher (1600°F)).

13
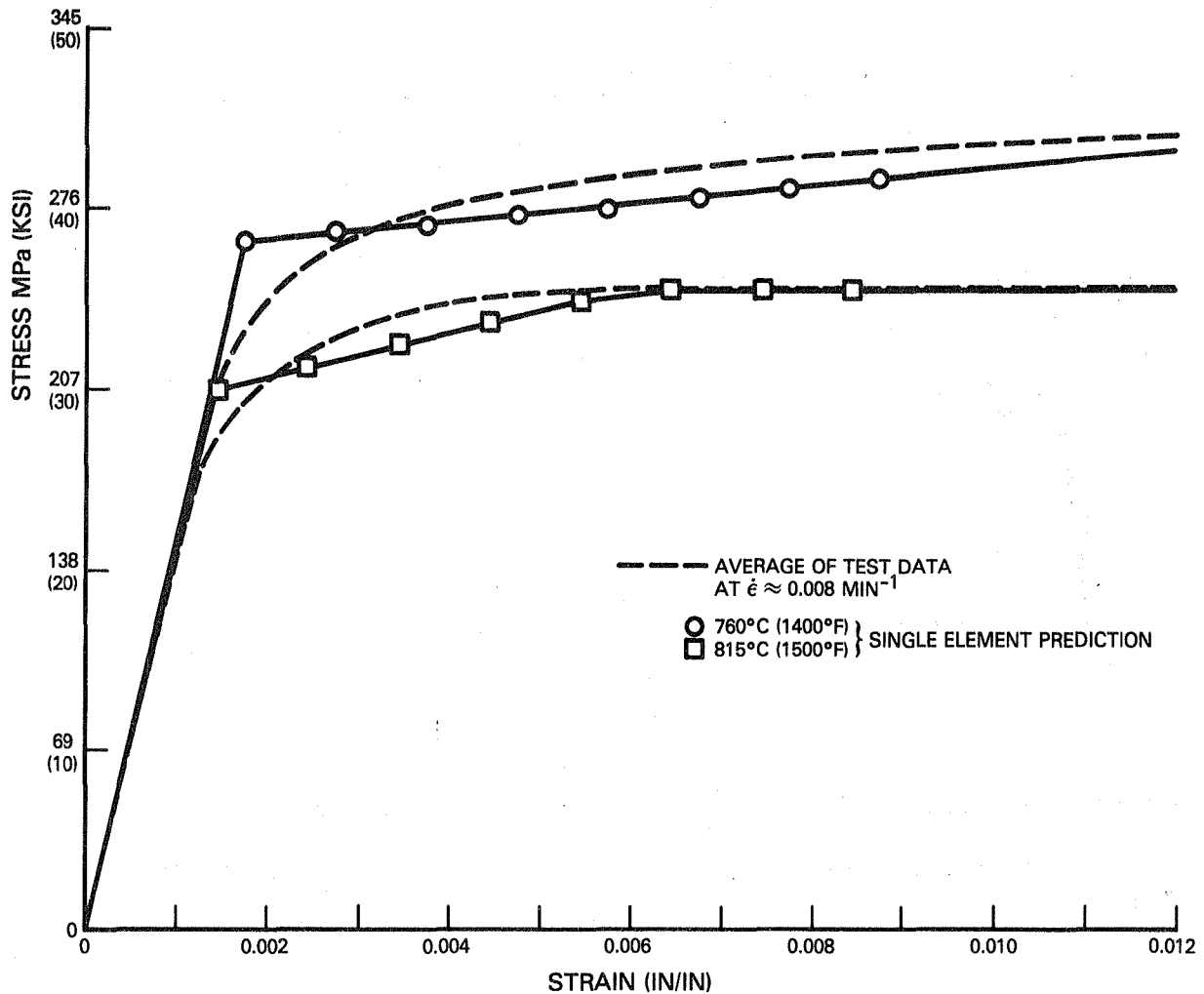
Figure 4.1-2   Prediction of Hastelloy X Monotonic Stress-Strain Response at 538 and 649°C (1000 and 1200°F) Using Classical Time Independent Plasticity and Creep Model

A piecewise interpolation scheme was developed for the temperature dependence of the constants A and n. The values of the constants were determined by:

704°C-871°C (1300°F-1600°F)
$$A = 3.05 \times 10^{-12} \left(\frac{T}{1000}\right)^{17.87} \qquad n = 3.39 \times 10^{-3} (T) \tag{3}$$

871°C-927°C (1600°F-1700°F)
$$A = 9.48 \times 10^{-30} \left(\frac{T}{1000}\right)^{103.64} \qquad n = -1.63 \times 10^{-2} (T) + 31.49 \tag{4}$$

927°C-982°C (1700°F-1800°F)
$$A = 2.49 \times 10^{-23} \left(\frac{T}{1000}\right)^{75.78} \qquad n = -1.27 \times 10^{-2} (T) + 25.39 \tag{5}$$

where T = metal temperature, °C (°F).

14

MPA
(KSI)

276
(40)

138
(20)

STRESS

-0.8   -0.6   -0.4   -0.2   0   0.2   0.4   0.6   0.8

STRAIN (%)

(-20)
-138

(-40)
-276

(-60)
-414

— — —  $\dot{\epsilon}$ = 0.0024 MIN$^{-1}$ }  TEST
- - - - -  $\dot{\epsilon}$ = 0.024 MIN$^{-1}$ }  DATA
———  $\dot{\epsilon}$ = 0.008 MIN$^{-1}$  MARC ANALYSIS
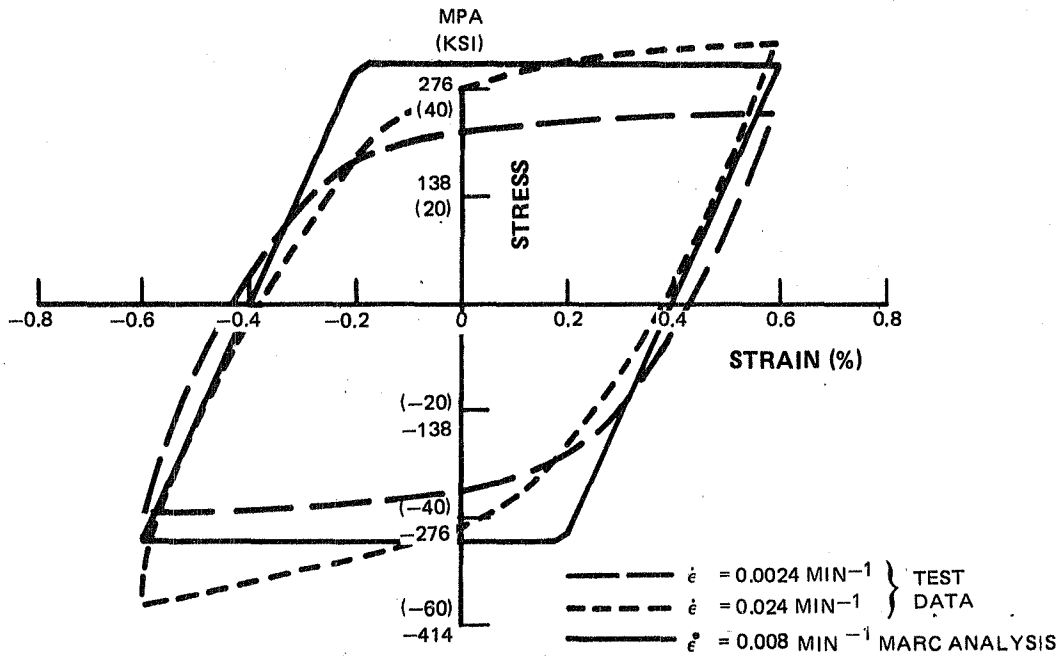
Figure 4.1-3   Prediction of Cyclic Response at 760°C (1400°F) Using Classical Time Independent Plasticity and Creep Model



MPA
(KSI)

138
(20)

69
(10)

STRESS

-0.8   -0.6   -0.4   -0.2   0   0.2   0.4   0.6   0.8

STRAIN (%)

-69
(-10)

(-30)
-207

— — —  $\dot{\epsilon}$ = 0.0024 MIN$^{-1}$ }  TEST
- - - - -  $\dot{\epsilon}$ = 0.024 MIN$^{-1}$ }  DATA
———  $\dot{\epsilon}$ = 0.008 MIN.$^{-1}$  MARC ANALYSIS
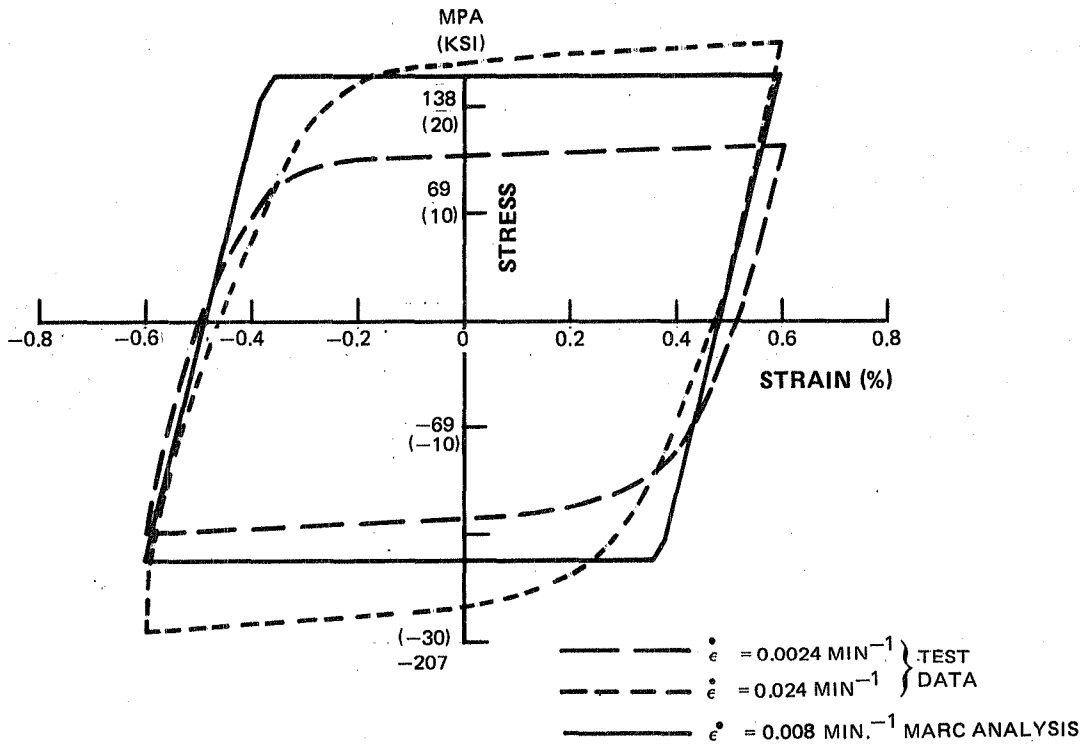
Figure 4.1-4   Prediction of Cyclic Response at 871°C (1600°F) Using Classical Time Independent Plasticity and Creep Model
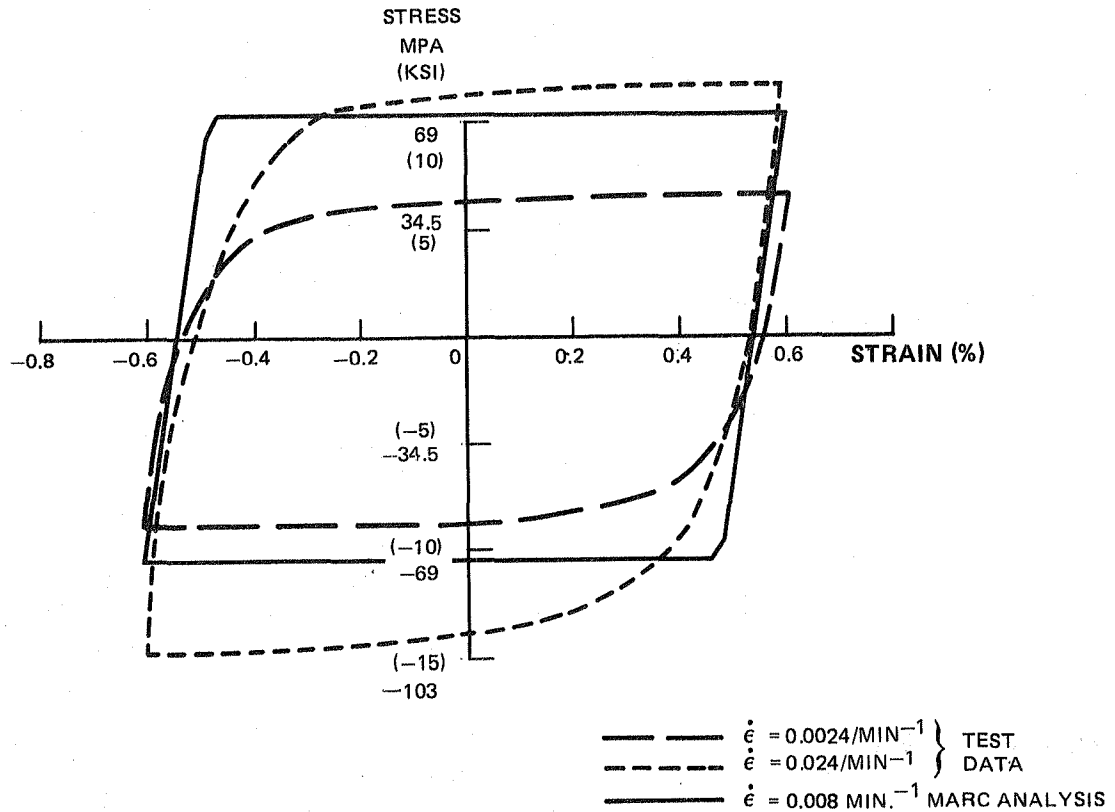
Figure 4.1-5 Prediction of Cyclic Response at 982°C (1800°F) Using Classical Time Independent Plasticity and Creep Model

Within this formulation, the plasticity and creep are independent of each other, creep does not influence subsequent plasticity nor does prior plasticity influence the predicted creep response. This is demonstrated in Figure 4.1-7 where the reverse yield point is unaffected by the previous 1 minute stress relaxation. Under continuous cycling isothermal conditions, the amount of cyclic hardening is determined only by the equivalent plastic strain, not the combined plastic and creep strains. A representative prediction is presented in Figure 4.1-8 for a 871°C (1600°F) cycle with a 1 minute compressive strain hold. Similar results are obtained at the other temperatures considered in the data base.

16
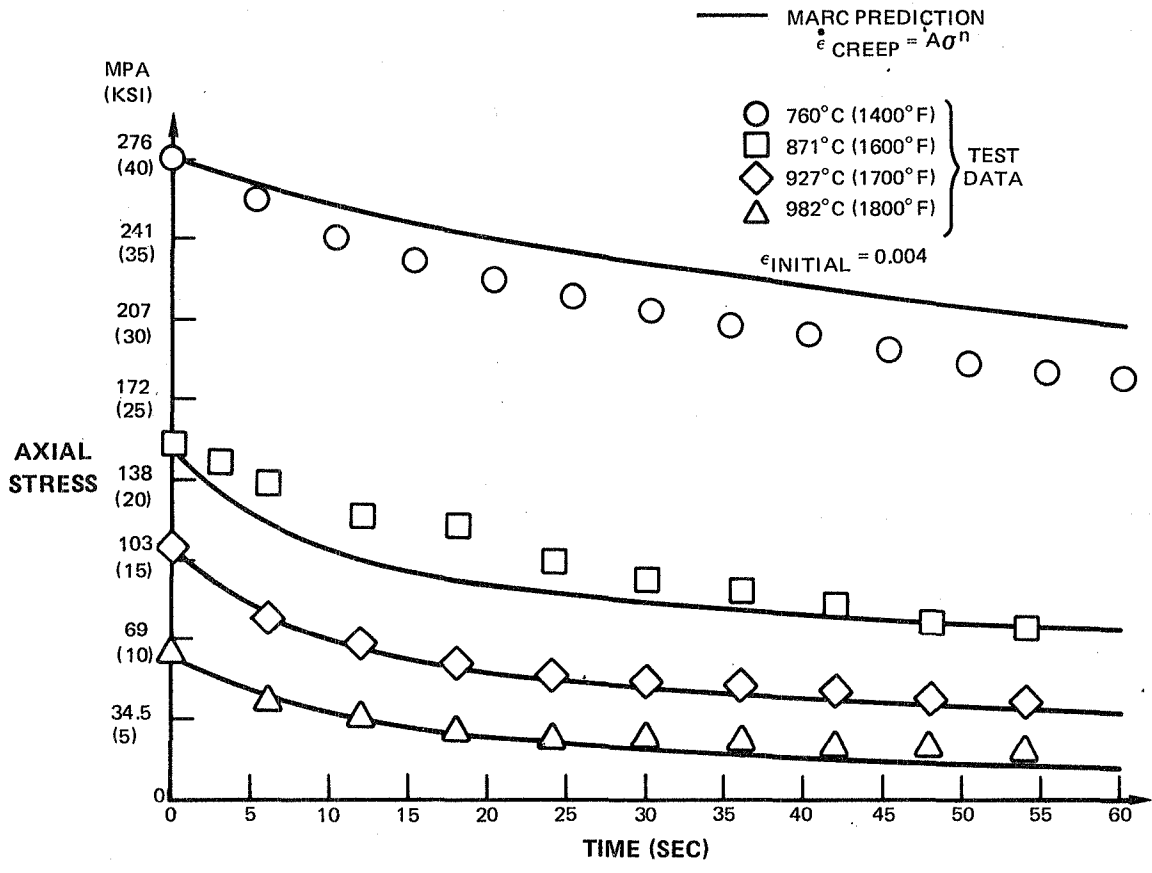
Figure 4.1-6 Comparison of Short-term Uniaxial Stress Relaxation Data with Prediction of Classical Time Independent Plasticity and Creep Model
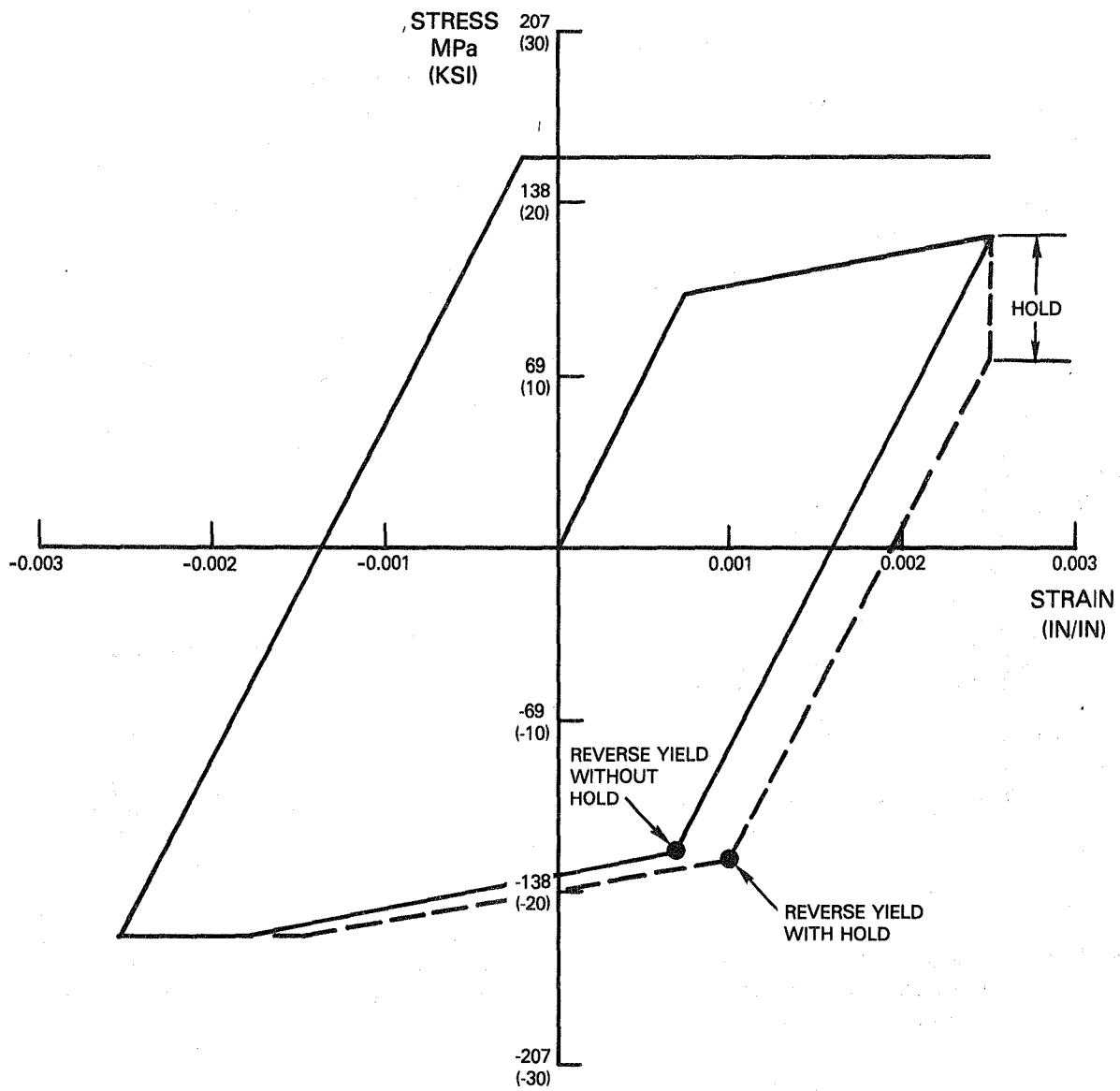
Figure 4.1-7  Influence of Creep on Yield Points for Hastelloy X at 871°C
              (1600°F)

18
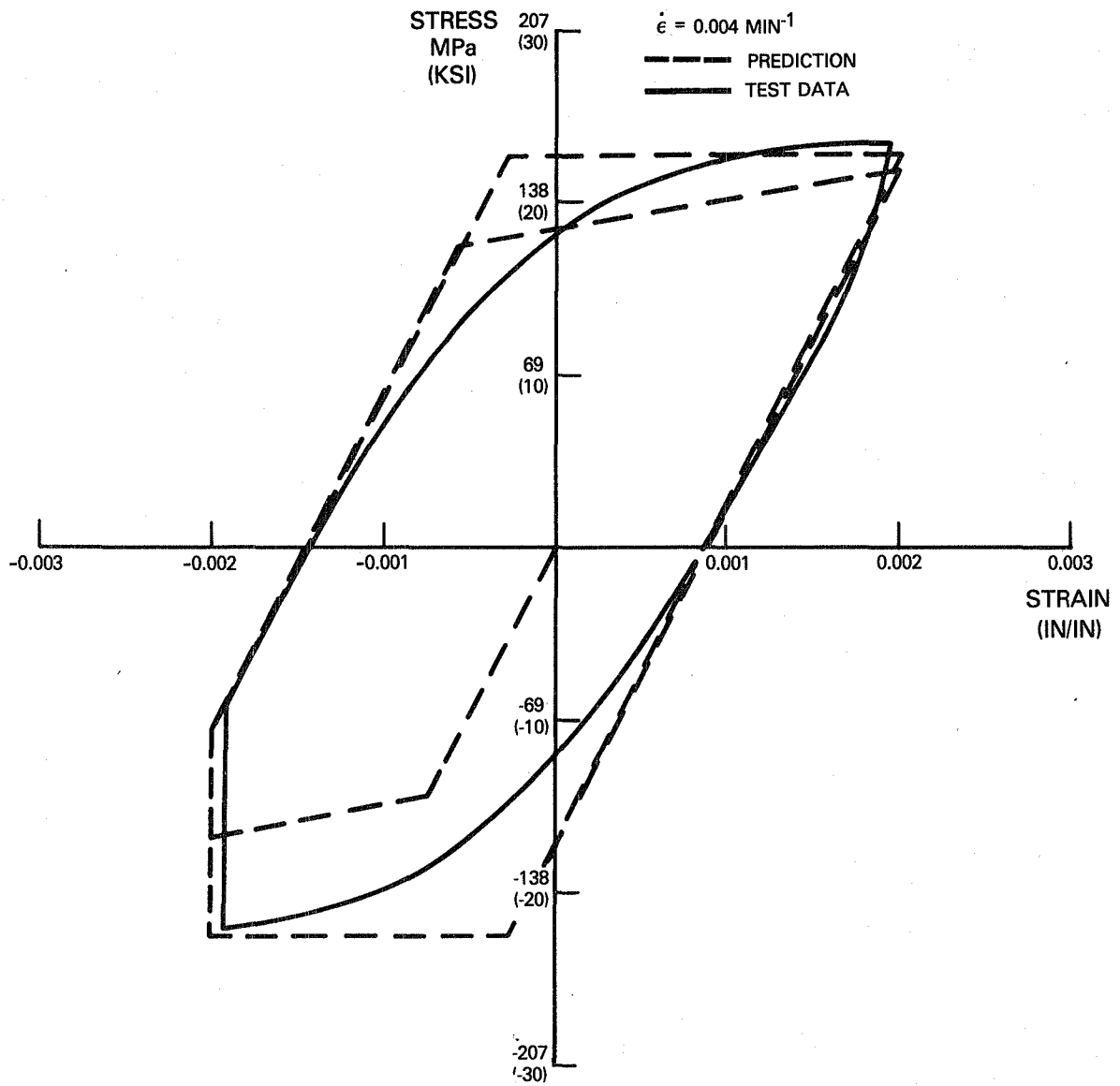
Figure 4.1-8  Rate Independent Plasticity and Creep Model Predicted Response
with Strain Hold for Hastelloy X at 871°C (1600°F)

## 4.2 UNIFIED TIME DEPENDENT MODEL

Development of the viscoplastic model, implementation into the MARC code, and application to the combustor liner thermomechanical analysis is fully documented in Reference 2.

The model also assumes decomposition of the mechanical strain response, however, all of the inelastic strain is contained in a single parameter which recognizes interaction and load history effects.

$$\varepsilon = \varepsilon_{elastic} + \varepsilon_{inelastic} \tag{6}$$

This time dependent theory was developed by modifying the constitutive relation for a three parameter viscoelastic solid and is presented in equations 7-13 below. The differential form of the theory is written as:

$$\dot{c}_{ij} = \left( \frac{\sqrt{\frac{2}{3}\left(\frac{3}{2}s_{ij} - \Omega_{ij}\right)\left(\frac{3}{2}s_{ij} - \Omega_{ij}\right)}}{K} \right)^n \frac{\left(\frac{3}{2}s_{ij} - \Omega_{ij}\right)}{\sqrt{\frac{2}{3}\left(\frac{3}{2}s_{ij} - \Omega_{ij}\right)\left(\frac{3}{2}s_{ij} - \Omega_{ij}\right)}} \tag{7}$$

$$\dot{\Omega}_{ij} = (n_1 + n_2)\dot{c}_{ij} + \dot{c}_{ij}\frac{\partial n_1}{\partial \Theta}\dot{\Theta} - \left(\Omega_{ij} - \overset{0}{\Omega}_{ij} - n_1 c_{ij}\right)\left(\dot{G} - \frac{1}{n_2}\frac{\partial n_2}{\partial \Theta}\dot{\Theta}\right) \tag{8}$$

$$K = K_1 - K_2 e^{-n_7 R}, \tag{9}$$

$$\dot{c}_{ij} = (\delta_{ij}\lambda\dot{\varepsilon}_{kk} + 2\mu\dot{\varepsilon}_{ij} - \dot{\sigma}_{ij} - \delta_{ij}(3\lambda + 2\mu)\alpha\dot{\Theta})/2\mu, \tag{10}$$

$$\dot{G} = (n_3 + n_4 e^{-n_5 R})\dot{R} + n_6\left(\frac{2}{3}\Omega_{ij}\Omega_{ij}\right)^{\frac{m-1}{2}} \tag{11}$$

$$\dot{R} = \sqrt{\frac{2}{3}\dot{c}_{ij}\dot{c}_{ij}}, \tag{12}$$

$$s_{ij} = \sigma_{ij} - \frac{1}{3}\delta_{ij}\sigma_{kk} \tag{13}$$

where:  $c_{ij} \equiv$ inelastic strain rate
  $\Omega_{ij} \equiv$ equilibrium stress
  $K \equiv$ drag stress
  $\Theta \equiv$ temperature

Material constants: $\lambda, \mu, \overset{0}{\Omega}, n, m, n_1, n_2, n_3, n_4, n_5, n_6, n_7, K_1, K_2$ depend on temperature

20

Creep, relaxation and strain rate effects are modelled by a power law for the inelastic strain rate. Two state variables, $\Omega_{ij}$ and K, are introduced into the viscoelastic theory to account for the effects of viscoplasticity. The equilibrium (rest or back) stress, $\Omega_{ij}$, introduces nonlinear kinematic hardening into the model to account for the Bauschinger effect, while the drag stress, K, introduces isotropic hardening into the model to account for cyclic hardening or softening of the material.

The growth law for the equilibrium stress contains both dynamic recovery and static thermal recovery terms. At high strain rates, the thermal recovery term becomes insignificant in comparison with the dynamic recovery term and the equilibrium stress becomes independent of strain rate. In the growth law for drag stress, static thermal recovery terms have been omitted. This form has been found adequate in the modelling of Hastelloy X behavior, but future applications may require the inclusion of static thermal recovery in the drag stress evolution law.

The theory is capable of modelling the cyclic hardening and softening of hysteresis loops without the use of a yield surface. Material constants required to model cyclic hardening/softening are obtained from cyclic hysteresis tests so that cyclic hardening and softening can be modeled. Both the equilibrium stress, $\Omega$, and the drag stress, K, contribute to the cyclic hardening in the theoretical formulation.

Application of the viscoplastic model to the prediction of 760°C (1400°F) and 815°C (1500°F) monotonic stress-strain response is shown in Figure 4.2-1. As shown, the model is in good agreement with both the experimental data and the predictions from model 1.

The prediction of isothermal cyclic material response is demonstrated in Figure 4.2-2. In this figure, the Hastelloy X experimental data at 1600°F for two different strain rates ($\dot{\varepsilon}$ = 0.024 min$^{-1}$ and $\dot{\varepsilon}$ = 0.0324 min$^{-1}$) is presented. As shown, the viscoplastic model accurately predicts the saturated stress amplitudes associated with the two strain rates and the transition from elastic to fully plastic loading. The predictions of the cyclic response at 760°C (1400°F) and 649°C (1200°F) are shown in Figure 4.2-3 and 4.2-4. The viscoplastic model again accurately predicts the stress amplitude and the shape of the stress strain curves. At temperatures greater than 649°C (1200°F), Hastelloy X displays little cyclic strain hardening thus the increase in stress between the monotonic and cyclic response is small. At temperatures below 649°C (1200°F) significant cyclic strain hardening is observed. In the prediction shown in Figure 4.2-4, the model was developed from the cyclically stable stress-strain response. This results in a predicted response for the first loading cycle which is significantly different than the initial experimental data but closely agrees with the cyclically stable results as shown.
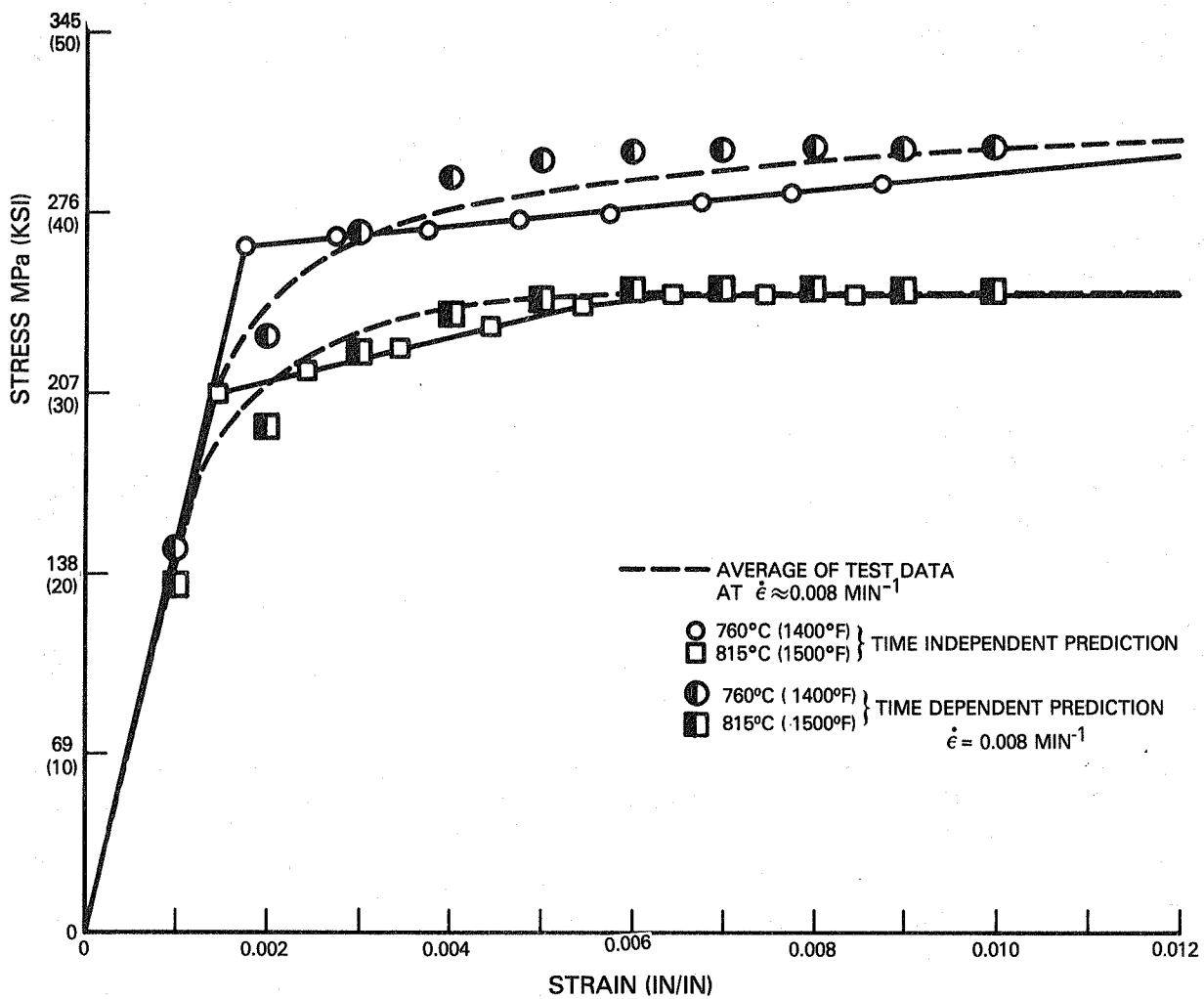
Figure 4.2-1 Prediction of Hastelloy X Monotonic Stress-Strain Response at 760 and 815°C (1400 and 1500°F) Using Unified Time Dependent Model

22
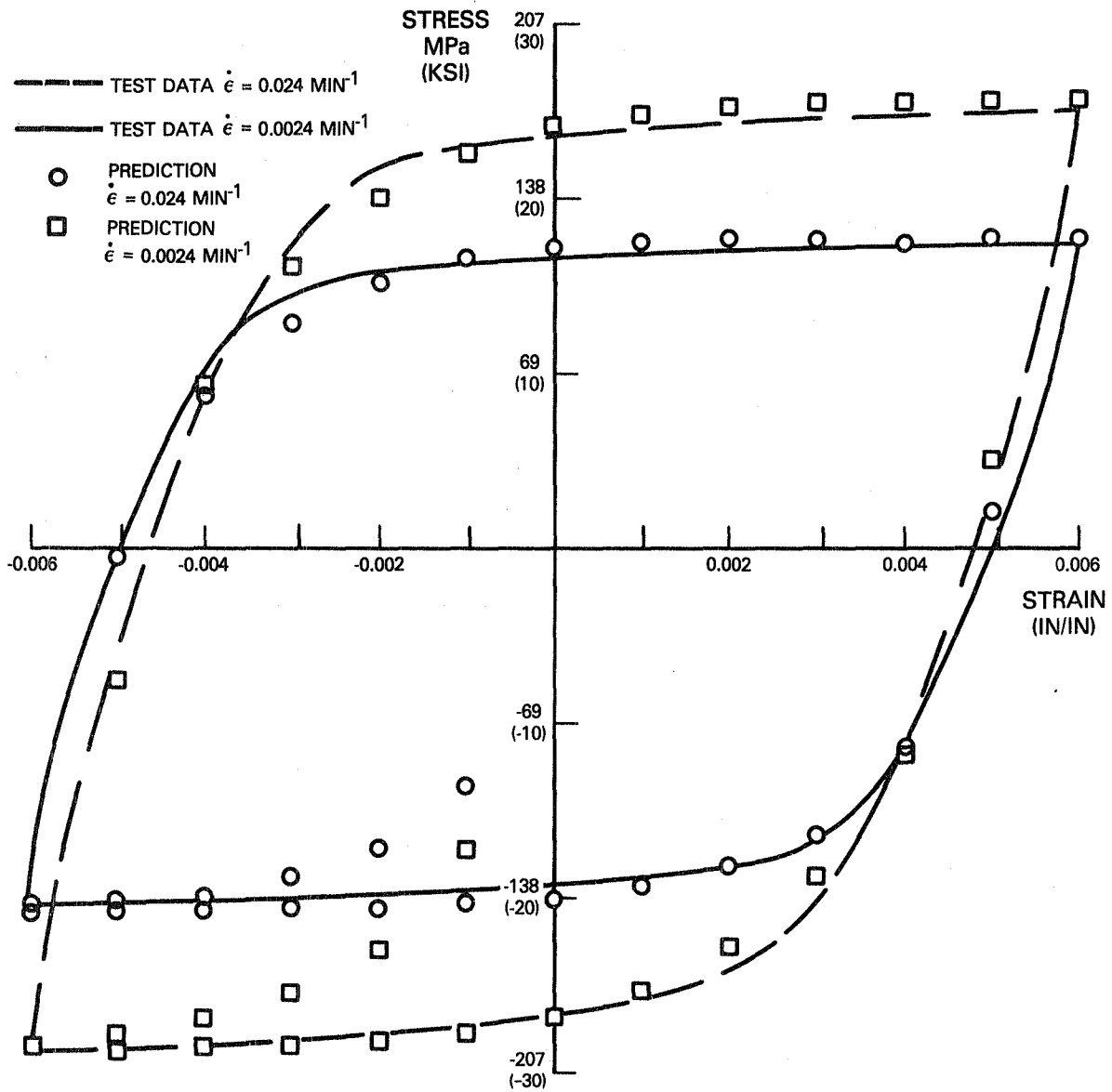
Figure 4.2-2 Prediction of Hastelloy X Isothermal Response at 871°C (1600°F) Using Unified Time Dependent Model
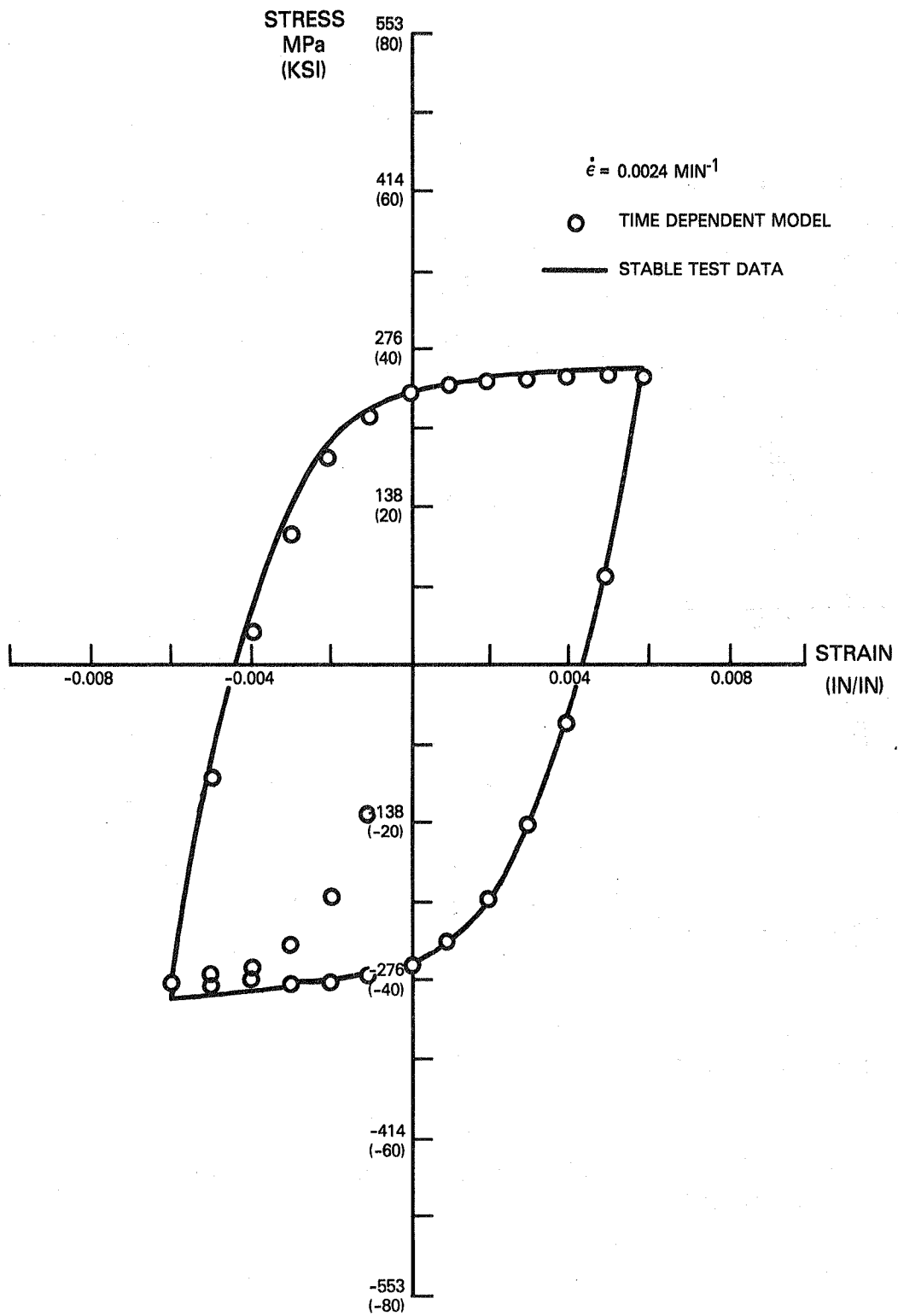
Figure 4.2-3  Prediction of Hastelloy X Isothermal Cyclic Response at 760°C (1400°F) Using Unified Time Dependent Model
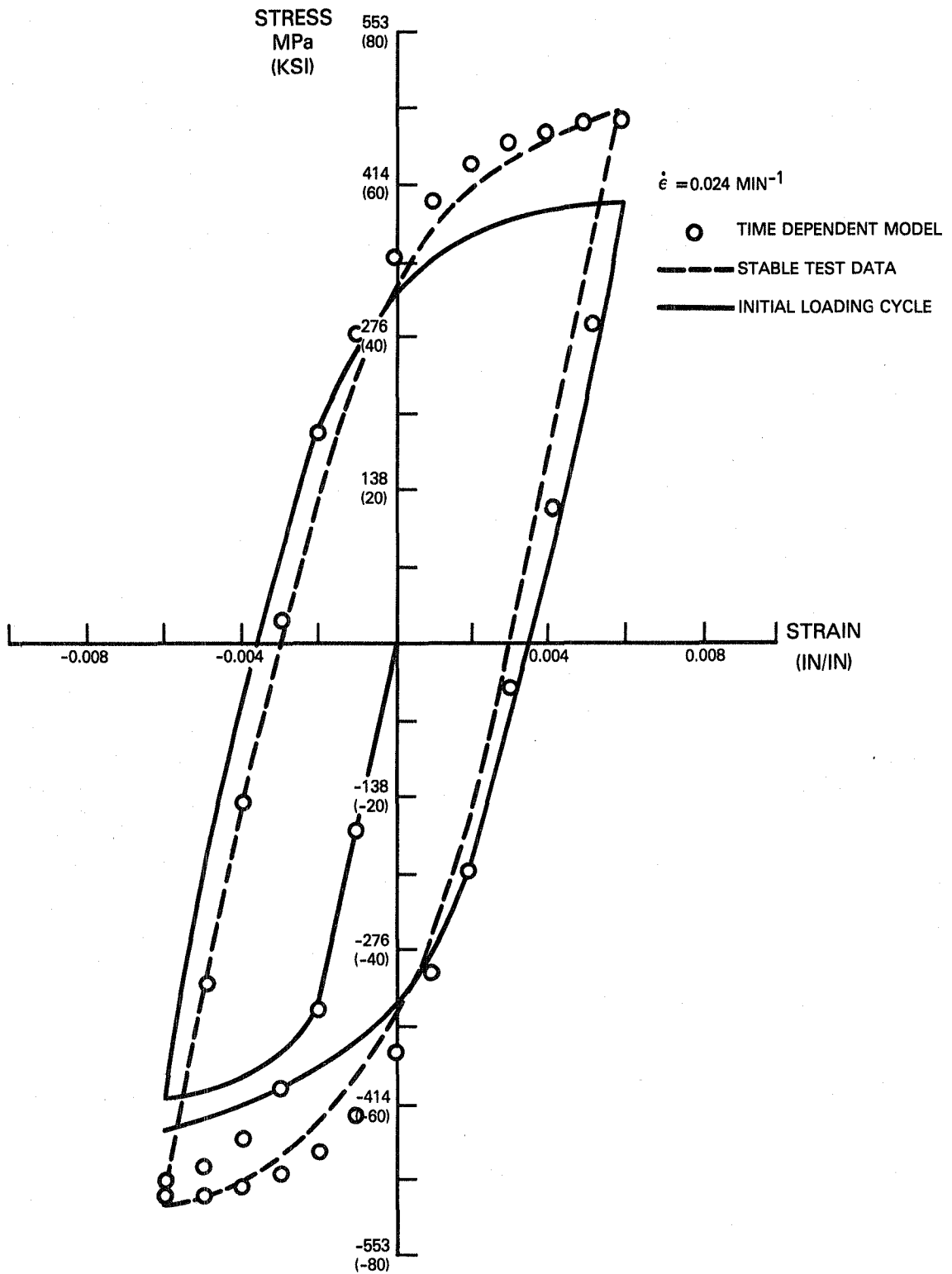
Figure 4.2-4  Prediction of Hastelloy X Isothermal Cyclic Response at 649°C (1200°F) Using Unified Time Dependent Model

## 4.3 APPROXIMATE, SIMPLIFIED PROCEDURE

Development of the simplified procedure for predicting local stress and strain response assumes that the strain and temperature histories produced by a loading cycle is known from previous analysis. An incremental description of the histories (strain - $\Delta\varepsilon$, temperature - $\Delta T$, and time - $\Delta t$) together with the procedure described below, is used to predict the resulting stress history. Each increment in strain is assumed to be composed of either, time independent plastic or time dependent elastic and creep response:

$$\Delta\varepsilon = \Delta\varepsilon \text{ plastic} \tag{14a}$$

$$\text{or} \quad \Delta\varepsilon = \Delta\varepsilon \text{ elastic} + \Delta\varepsilon \text{ creep} \tag{14b}$$

Since the solution strategy is based on the prediction of stress increments, equations (14) are rewritten:

$$\Delta\sigma = \Delta\sigma \text{ plastic} \tag{15a}$$

$$\Delta\sigma = \Delta\sigma \text{ elastic} + \text{creep} \tag{15b}$$

During a loading cycle, the onset of plastic action is determined by the conventional yield surface concept taken from the classical time independent plasticity model. The yield surface is assumed to be temperature dependent and isotropic, with zero strain hardening (fixed size and equal in tension and compression). Using the definition of yield stress shown in Figure 4.1-1, the Hastelloy X yield surface developed for this analysis procedure is shown in Figure 4.3-1. Justification for this definition of the yield surface is based on two observations from the data base: 1) at higher temperatures, Hastelloy X displays little cyclic hardening and 2) the variable temperature experienced in a thermomechanical cycle (the primary application of the simplified procedure) reduces the amount of cyclic hardening developed at the lower temperatures.

The stress increment associated with time independent plastic action is then calculated as:

$$\sigma_{i+1} - \sigma_i = \Delta\sigma \text{ plastic} = \sigma_{yi+1} - \sigma_{yi} \qquad \begin{array}{l} \text{for } \sigma_i = \sigma_{yi} \\ T_{i+1} \geq T_i \end{array} \tag{16}$$

or

$$\Delta\sigma_{i+1} - \sigma_i = \Delta\sigma_{plastic} = \frac{E_{pi+1} + E_{pi}}{2} \Delta\varepsilon \qquad \begin{array}{l} \text{for } \sigma_i = \sigma_{yi} \\ T_{i+1} < T_i \end{array} \tag{17}$$

where:
| | | |
|---|---|---|
| $\Delta\sigma_{plastic}$ | = | total stress increment |
| $\sigma_y$ | = | yield stress |
| $T$ | = | temperature |
| $E_p$ | = | strain hardening slope of monotonic stress-strain curve |
| $\Delta\varepsilon$ | = | total strain increment |
| $i$ | = | beginning of increment |
| $i+1$ | = | end of increment |

26
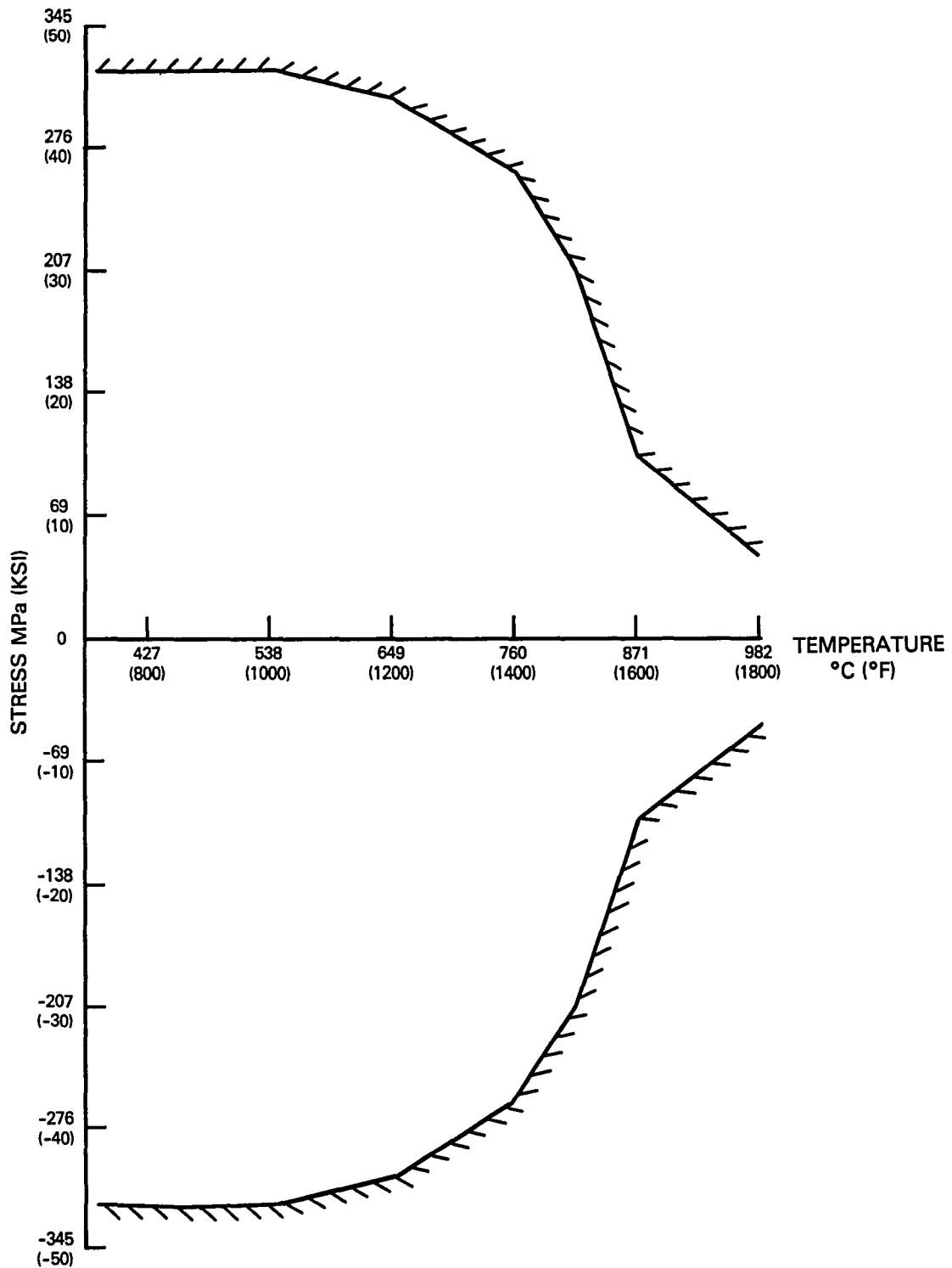
Figure 4.3-1 Temperature Dependent Hastelloy X Yield Surface for Simplified Procedure

As an example, point A in Figure 4.3-2 represents a stress state on the yield surface at time i. Applying a total increment of strain $\Delta\epsilon$ will result in the stress at time i+1 at point B, if the temperature is increasing during the increment (decreasing size of the yield surface), or at point C if the temperature is decreasing during the increment (increasing size of the yield surface).
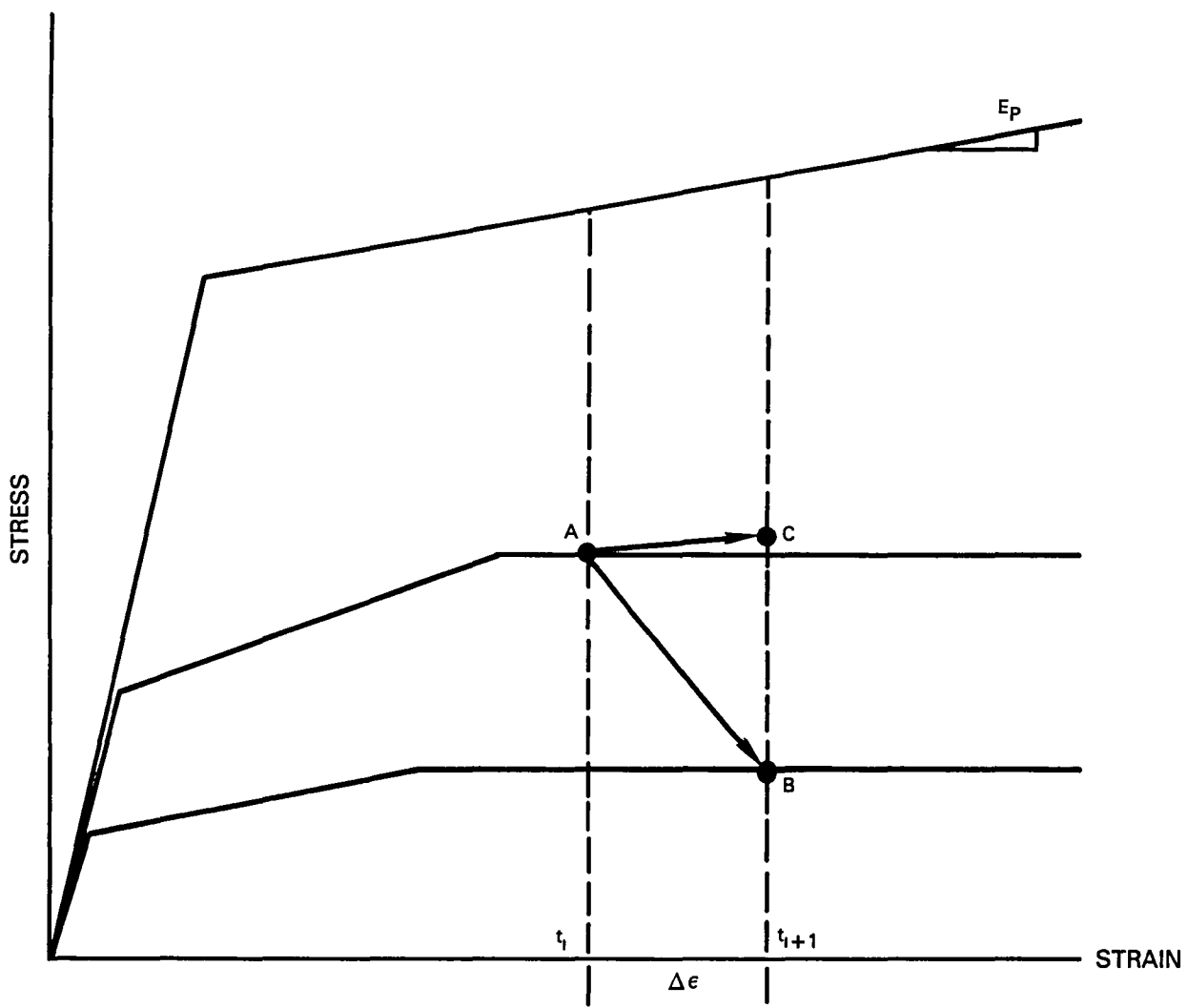


Figure 4.3-2  Prediction of Time Independent Plastic Stress Increment

28

For all other loading conditions the strain (stress) is assumed to be time dependent elastic and creep response.

$$\Delta\varepsilon_{total} = \Delta\varepsilon_{elastic} + \Delta\varepsilon_{creep} \qquad (18)$$

However, rather than consider a separate, uncoupled creep model as used in the time independent model, an integrated or viscoplastic approach is used. This approach was pursued based on observations from the data base that the cyclic material response is not purely elastic in either the loading or unloading portions of the response curves. Instead, the response represents a simultaneous elastic and creep action. Development of the model is as follows:

$$\dot{\varepsilon}_{total} = \dot{\varepsilon}_{elastic} + \dot{\varepsilon}_{creep} \qquad (19)$$

where:   $\dot{\varepsilon}_{total}$ = total strain rate

$\dot{\varepsilon}_{elastic}$ =   $1/E\ \dot{\sigma}$ (Young's modulus "E" assumed to be   (20)
temperature dependent but constant over
and increment of loading

For the creep rate term, use is made of the short time monotonic creep model developed in Reference 1. The expression used in the simplified procedure is:

$$\dot{\varepsilon}_{creep} = A\sigma^n \qquad (21)$$

where:   A, n are temperature dependent constants.

$$\dot{\varepsilon}_{total} = \frac{1}{E}\dot{\sigma} + A\sigma^n \qquad (22)$$

or

$$\dot{\sigma} = E\ \dot{\varepsilon}_{total} - EA\sigma^n \qquad (23)$$

An incremental solution of this nonlinear equation was developed using a Taylor series expansion. Equation 23 is then written:

$$\sigma_{i+1} = \sigma_i + \dot{\sigma}_i\ \Delta t + \frac{\ddot{\sigma}_i\Delta t^2}{2!} + \frac{\dddot{\sigma}_i\Delta t^3}{3!} + \ldots \qquad (24)$$

where;

$\sigma_i$ = stress at beginning of increment,

$\sigma_{i+1}$ = stress at end of increment,

$\Delta t$ = time increment,

$\dot{\sigma}$ = $E\dot{\varepsilon}_T - EA|\sigma|^{n-1}\sigma$,

$\ddot{\sigma}$ = $-n\ EA|\sigma|^{n-2}\sigma\dot{\sigma}$

$\dddot{\sigma}$ = $-n(n-1)EA|\sigma|^{n-3}\sigma\dot{\sigma}^2 - n\ EA\ \sigma^{n-2}\sigma\ddot{\sigma}$.

Solution of this equation results in a total stress increment which is either greater than or less than the stress increment that would be produced by purely elastic loading. This is demonstrated at various points in a response cycle in Figure 4.3-3. At location A, the total strain increment and the initial stress are negative, the actual stress response is less than (relaxed) an elastic increment. The same condition holds at point B, where all incremental values are positive. Relaxation of the response produces a smaller stress amplitude than the elastic response. At locations C and D, the strain increment and the initial stress are of opposite signs. The resulting creep strain increment (due to relaxation) produces a stress increment that is larger than the elastic increment. This steeper slope immediately after strain reversal is characteristic of a time dependent cyclic response.

In the viscoplastic model discussed in Section 4.2, the backstress, ij, is included in the power law expression for plastic strain rate (equation 7). In a physical sense, the backstress is an internal stress generated by plastic deformation which changes the reference point for the measurement of global stress. The same concept of backstress was applied in the development of the elastic and creep equation. The importance of this is demonstrated in Figure 4.3-4 for the prediction of 871°C (1600°F) Hastelloy X fully reversed ($\Delta\epsilon$ = 1.2 percent, $\dot{\epsilon}$ = 0.024 $min^{-1}$) stress-strain response. Initially, the incremental equation 24 is applied in loading from points A to B. This represents monotonic loading and the stress is "measured" from the coordinate axes shown. For this calculation, the backstress is assumed to be zero and the maximum stress is -207 MPa (-30 ksi). When the direction of straining is reversed (points B to D), and the backstress is again assumed to be zero, equation 24 predicts a rapid stress relaxation to approximately zero stress (point C) followed by a response which is essentially identical to the predicted initial response (A-B). Examination of the figure shows that this prediction does not agree with the experimental data. Instead, if we assume that, upon reversal of the direction of straining, the prior deformation (A-B) produced a backstress of -10 Ksi, the predicted results from points B to E agree closely with the experimental response. This shifting of the reference for the stress measurement produced an initial relaxation response and a reverse yield response more consistent with the data. Equation 23 can now be written as:

$$\dot{\sigma}^* = E\dot{\epsilon}_{total} - EA\sigma^{*n} \qquad (25)$$

where: $\qquad \sigma^* = \sigma - \Omega \qquad\qquad\qquad (26)$

For the isothermal cycle, a constant value of $\Omega$ was used in the example above. During a thermomechanical cycle, the temperature changes throughout the cycle will result in a different value of $\Omega$ for each loading increment.

A summary of all Hastelloy X constants developed for the simplified procedure is presented in Table 4.3-I.

30

STRESS

$\Delta\varepsilon_T$ (+)

$\sigma$ (+)

B

$\Delta\sigma$   $\Delta\sigma_e$

$\Delta\varepsilon_T$ (-)

$\sigma$ (+)

D

È

STRAIN

$\Delta\varepsilon_T$ (+)

$\sigma$ (-)

C

$\Delta\varepsilon_T$

A

$\Delta\sigma_e$   $\Delta\sigma$

E

$\Delta\varepsilon_T$ (-)

$\sigma$ (-)

$\Delta\sigma_e$   ≡   ELASTIC STRESS INCREMENT
$\Delta\sigma$   ≡   ACTUAL STRESS INCREMENT
$\Delta\varepsilon_T$   ≡   TOTAL STRAIN INCREMENT
E   ≡   YOUNG'S MODULUS
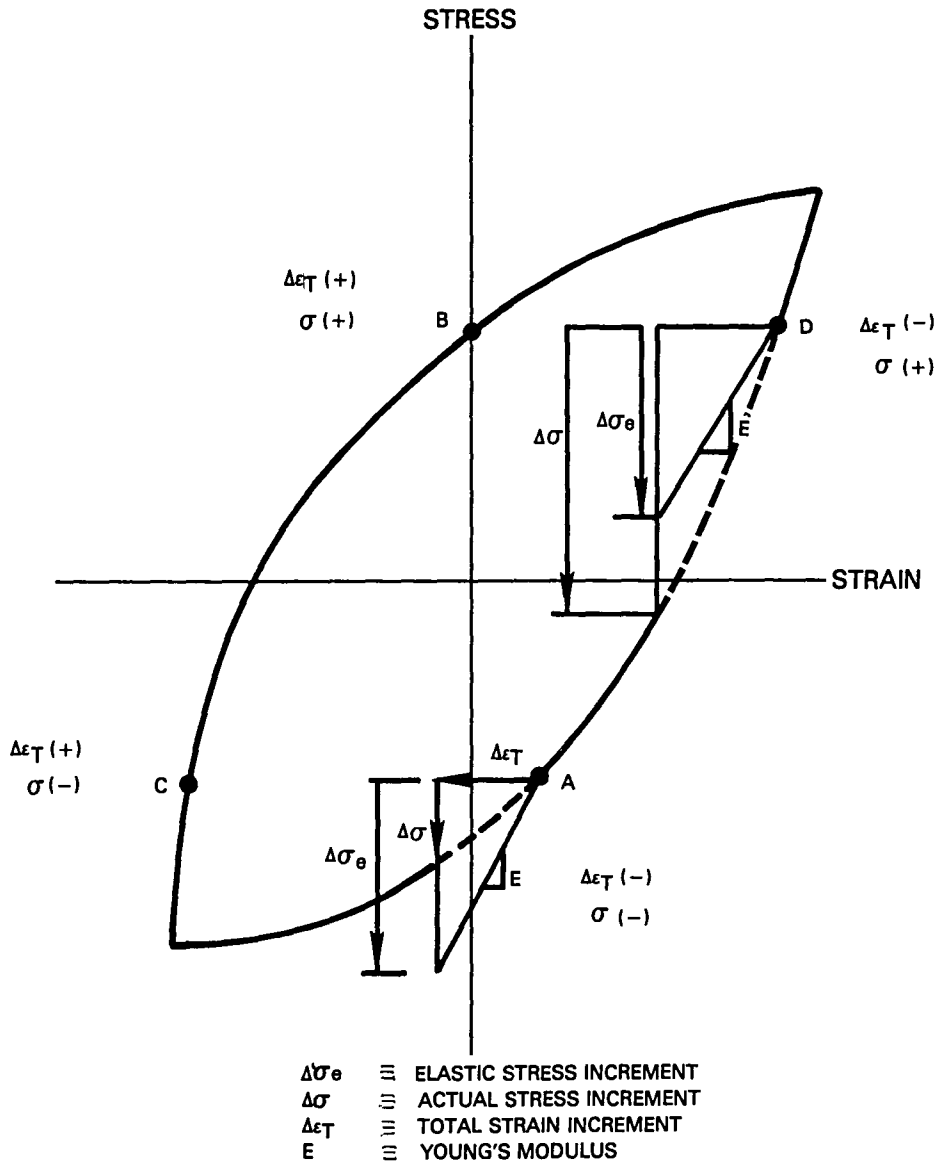
Figure 4.3.3  Typical Time Dependent Cyclic Response
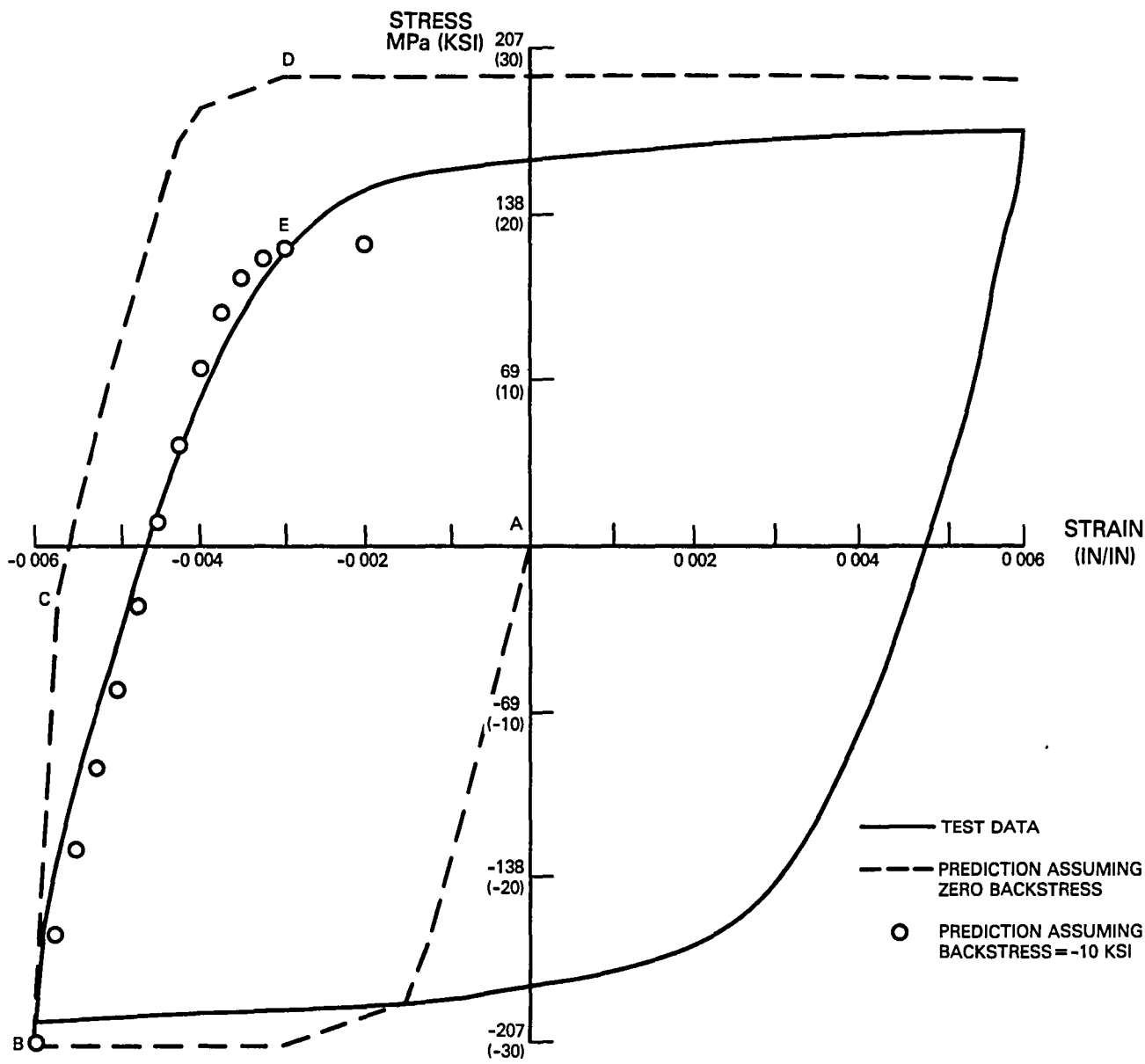
Figure 4.3-4 Effect of Assumed Backstress on Unloading Response of Hastelloy X at 871°C (1600°F)

## TABLE 4.3-I

## TEMPERATURE DEPENDENT PARAMETERS FOR APPROXIMATE RESPONSE PROCEDURE

| Temperature °C, (°F) | Young's Modulus, MPa (ksi) | | Yield Stress, MPa (ksi) | A | | n MPa (ksi) |
|---|---|---|---|---|---|---|
| 427 (800) | 170 (24.6 | 03 03) | 314 (45.6) | - | | - |
| 538 (1000) | 170 (24.6 | 03 03) | 314 (45.6) | - | | - |
| 649 (1200) | 161 (23.3 | 03 03) | 303 (44.0) | - | | - |
| 760 (1400) | 152 (22.05 | 03 03) | 262 (38.0) | 9.4 | -09 | 28.6 (4.15) |
| 815 (1500) | 146 (21.15 | 03 03) | 207 (30.0) | 1.65 | -08 | 32 7 (4.75) |
| 871 (1600) | 137 (19.8 | 03 03) | 103 (15.0) | 2.9 | -08 | 36.2 (5.25) |
| 927 (1700) | 130 (18.85 | 03 03) | 76 (11.0) | 1.9 | -05 | 23.1 (3.35) |
| 982 (1800) | 123 (17.9 | 03 03) | 48 (7.0) | 2.9 | -04 | 21.7 (3.15) |

## 5.0 RESULTS OF CYCLIC THERMOMECHANICAL RESPONSE PREDICTIONS

The three types of thermomechanical cycles considered in the comparison of the models: a pseudo thermomechanical cycle in which the temperature was rapidly changed from one isothermal condition to another (condition d); a simple continuous thermomechanical cycle having the mechanical strain and temperature in phase (sinusoidal strain and temperature variation) resulting in a linear strain-temperature history (condition e); and "the faithful cycle" which was representative of actual structural component response to thermal loading (condition f). Details of the faithful cycle were described in Reference 1 for the analysis of a gas turbine engine combustor liner.

### 5.1 PREDICTION OF TEMPERATURE STEP CHANGE CYCLE

This cycle was selected to determine if a temperature rate effect in the material could be observed. This would be important in the prediction of thermomechanical response with a model developed from a series of isothermal conditions. Tests were run at cyclic rates of 2 cpm and 4 cpm with no appreciable difference observed in the response immediately after the temperature change or the subsequent steady-state response. Simulation of one of the tests using the time independent plasticity model is shown in Figure 5.1-1. Since the test results did not appear to have a significant temperature rate effect, no additional work with this data was conducted. The assumption of an instantaneous change in material properties with temperature was assumed valid for the remaining simulations.

### 5.2 PREDICTION OF LINEAR STRAIN TEMPERATURE CYCLES

Three temperature histories were selected for the evaluation, 760°C to 982°C (1400°F to 1800°F), 649°C to 982°C (1200°F to 1800°F) and 427°C to 982°C (800°F to 1800°F). Each temperature cycle and a single mechanical strain cycle (-0.001 to -0.0045) were imposed on a tubular test specimen shown in Figure 3.1-1 and the resulting stress and strain response from start up through stabilization recorded. A description of the cycle parameters and loading sequence for the three cycles is presented in Figure 5.2-1, each test started at a constant 982°C (1800°F) - point A, the specimen was than compressed to a mechanical strain of -0.0045 in/in, desingated point B in the figure. A sinusoidal variation in temperature from 982°C (1800°F) to the minimum value of either 760°C (1400°F), 649°C (1200°F) or 427°C (800°F) was then generated on the specimen together with a simultaneous sinusoidal variation in mechanical strain from -0.0045 in/in to -0.0010 in/in. The period for both the temperature and strain histories was 1 minute. Cross plotting of these quantities results in the linear paths shown, B-C, B-D or B-E.

34
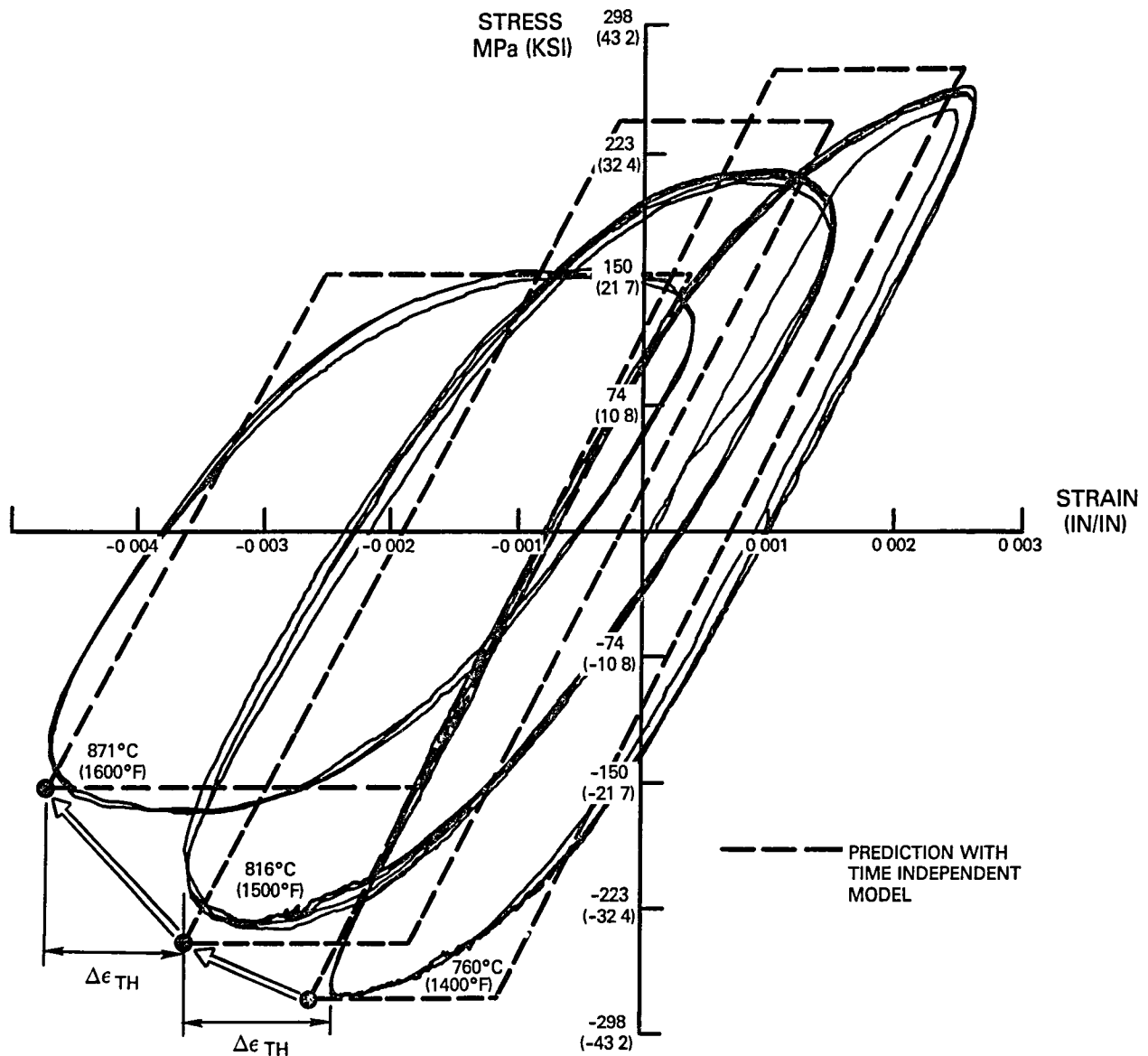
Figure 5.1-1   Simulation of Step Temperature Tests

Simulations of the 760 to 982°C (1400 to 1800°F) test using time independent plasticity and viscoplastic models described in Section 4.0 are shown in Figures 5.2-2 and 5.2-3. Due to the high average temperature, this cycle displays the greatest amount of time dependent inelastic response of the thermomechanical cycles analyzed. The analytical simulations with the two finite element analyses indicate that the rate dependent model more accurately captures the overall response shape. The prediction with the time independent plasticity model predicts a stiffer (more elastic) stress-strain response and a smaller amount of inelastic strain range. A greater amount of inelastic strain could have been predicted by intermittently stopping the loading cycle and including a creep period consistent with the elapsed time in the actual cycle. However, the uncoupled nature of the elastic, plastic and creep

35

components would not have altered the basic shape of the prediction relative to the data. In addition, analyses described in Reference 1 showed that, under continued cycling, the model displays a tendency for elastic shakedown as opposed to the experiment which stabilized after several loading cycles.
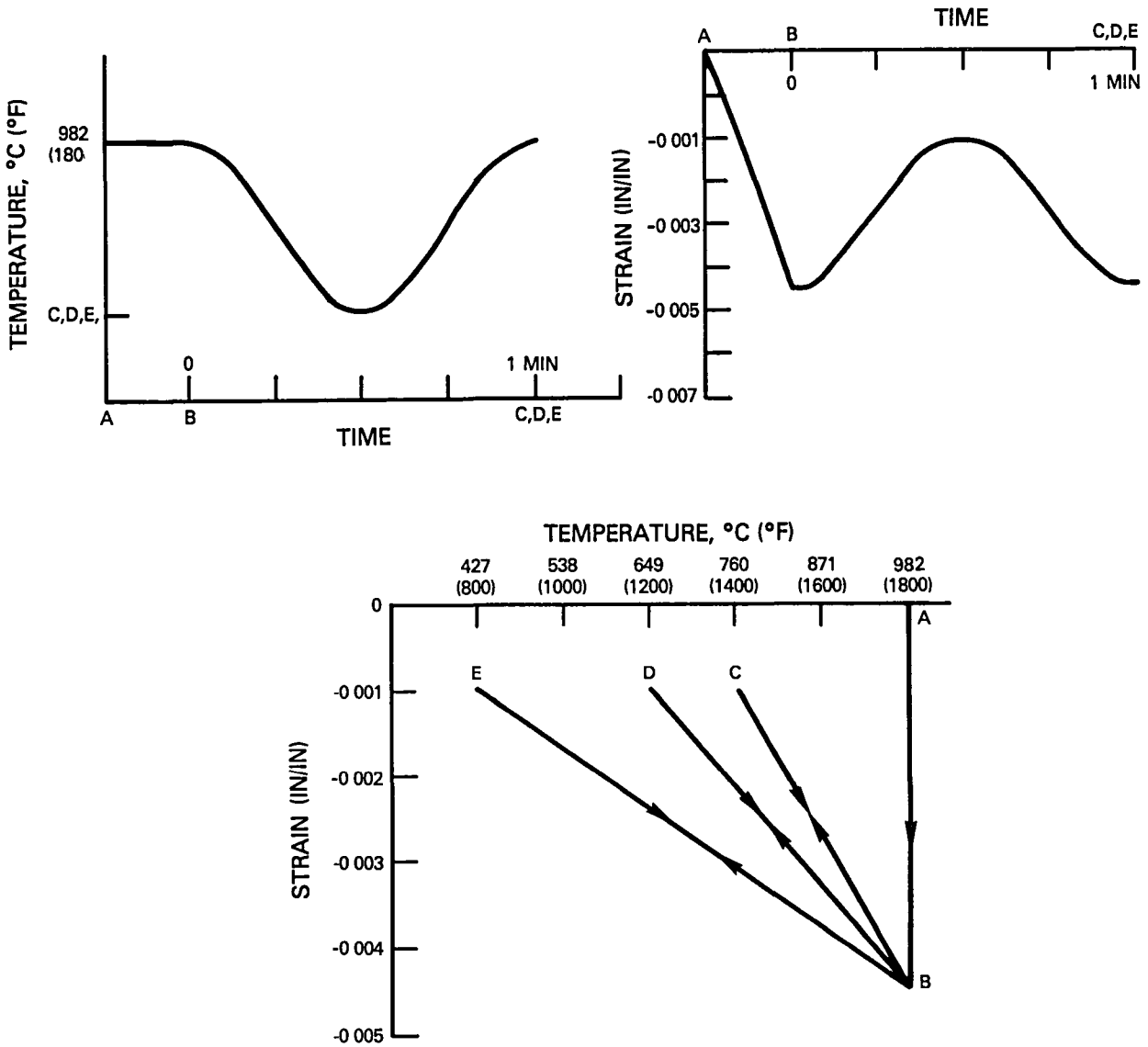


Figure 5.2-1 Temperature and Strain Input Histories for Linear Thermomechanical Cycle
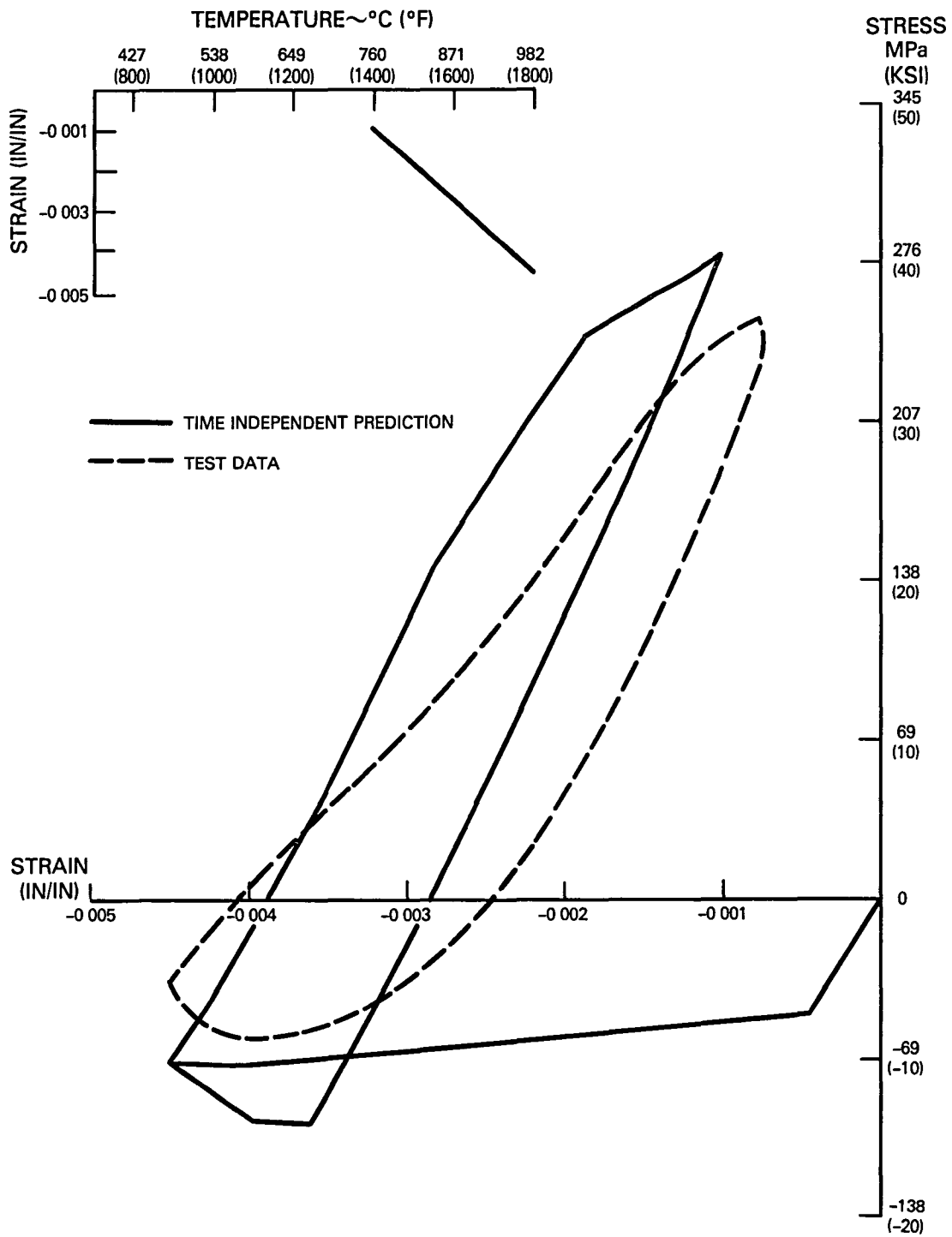
Figure 5.2-2   Simulation of 760 to 982°C (1400 to 1800°F) Test with Time
Independent Model
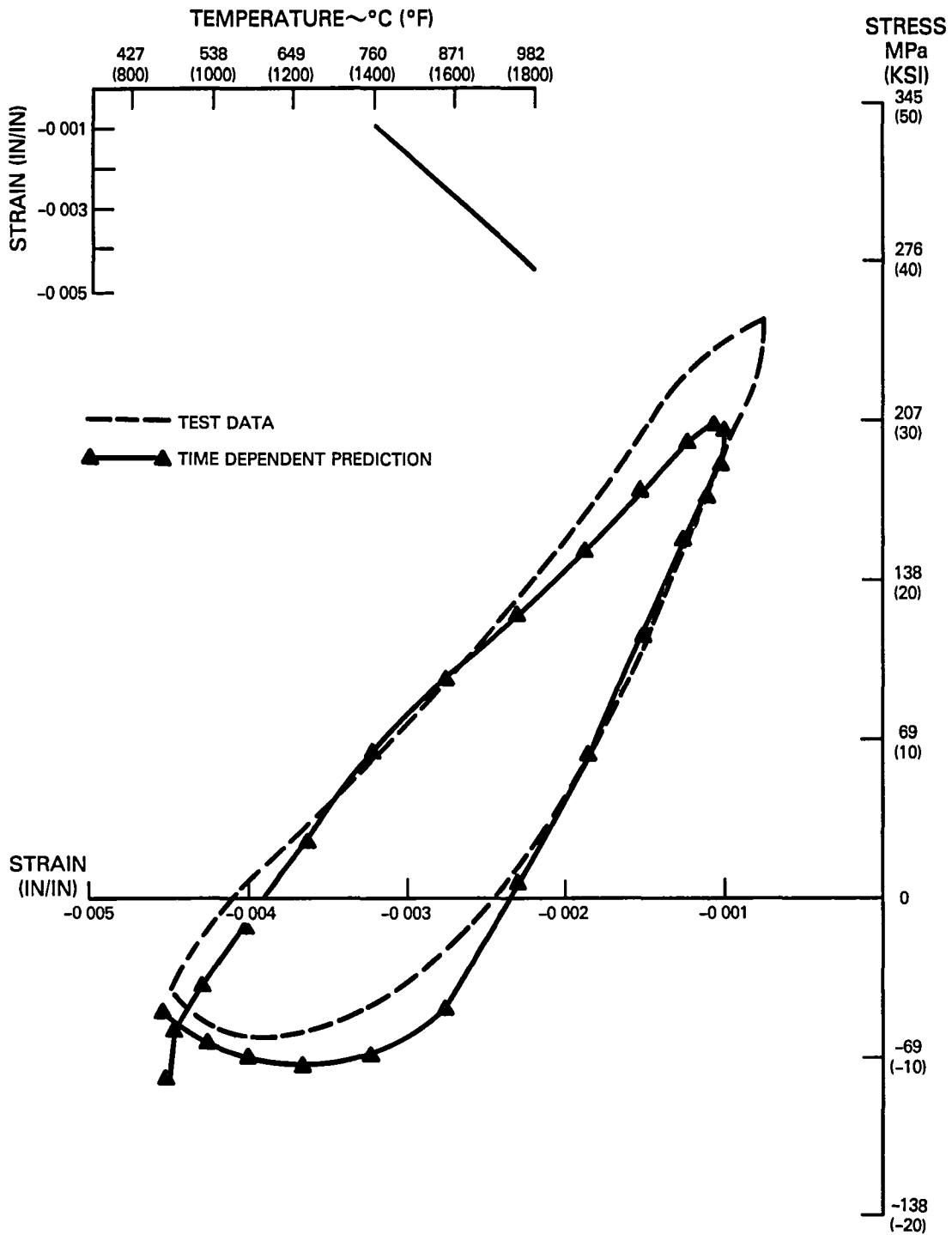
Figure 5.2-3 Simulation of 760 to 982°C (1400 to 1800°F) Test with Time Dependent Model

As shown in Figure 5.2-4, the prediction using the simplified method, also captures the relevant cyclic response characteristics. Implementation of the procedure for this cycle is described below.
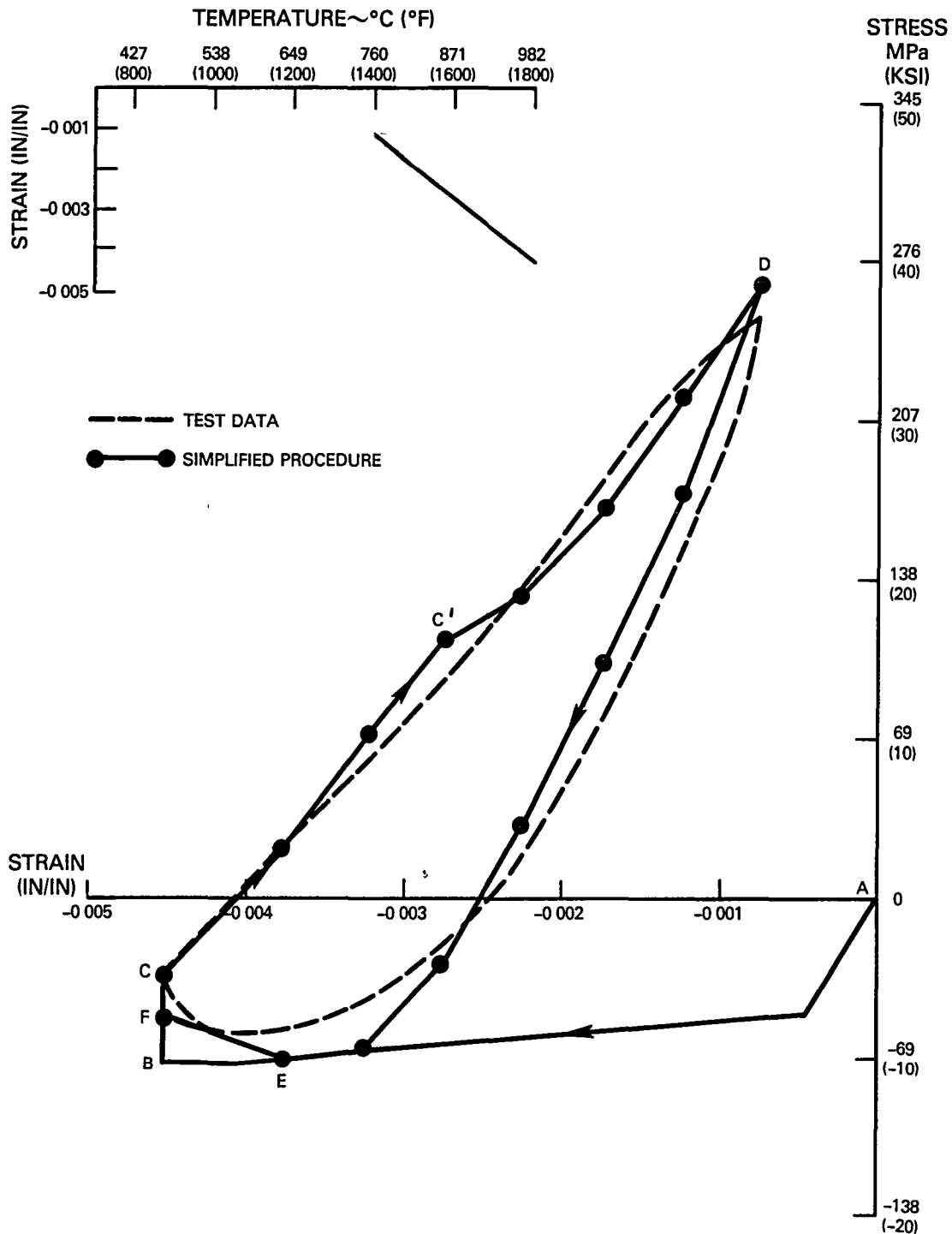


Figure 5.2-4   Simulation of 760 to 982°C (1400 to 1800°F) Test with Simplified Response

1.  Initial Loading A-B. Consistent with the test procedure described above, the analytical simulation from zero strain to the minimum strain point (-0.0045 in/in) follows the 982°C (1800°F) isothermal stress-strain relationship.

2.  Stress Relaxation B-C. This response is produced by a short (< 5 seconds) hold time in which the strain is held constant (at -0.0045 in/in) prior to the initiation of strain and temperature cycling. Equation 24 was used to predict this response by assuming an initial stress of -69 MPa (-10 Ksi) and a zero strain rate ($\dot{\varepsilon}$ = 0).

3.  Unloading C-D. From point C, the strain and temperature are simultaneously changing. This represents movement "away" from a yield surface due to the reversal of the direction of loading and the decreasing temperature (increasing yield surface size). Equation 24 is used to predict the incremental elastic-creep stress history, however, the initial value of stress at point C is assumed to be zero. This shift in the stress origin is equivalent to assuming that the prior deformation at 982°C (1800°F) develops an internal back stress equal to the external stress. Thus by equation 26, the effective stress ($\sigma^*$), at the beginning of the incremental calculation, is zero. The back stress is assumed to remain constant throughout the unloading from points C to D. This is based on the notion that the internal stress generated by the deformation at the hottest temperature in the cycle, 982°C (1800°F), tends to get "locked in" as the temperatures decrease during the unloading.

The predicted response is considered as time dependent elastic-creep response up to the point where the stress intersects the yield stress boundary. Continued loading beyond this point is assumed to produce a time independent plastic response as described in Equation 17.

In Figure 5.2-5, the intial stress at point C in the 982°C (1800°F) to 760°C (1400°F) cycle is -34.5 MPa (-5Ksi). The incremental prediction using the elastic-creep equation results in a final stress at point D of +262 MPa (+38.7Ksi) that lies on the yield stress vs. temperature boundary. Thus, plastic action is not predicted on this leg of the cycle. At the intermediate point C', the stress history does penetrate the yield stress boundary, this is consistent with the area in the stress-strain response (Figure 5.2-4) where the predicted stress is greater than the experimental response. Reduction of the predicted stress in this area, consistent with the yield stress boundary, would improve the correlation. This implies that in a thermomechanical cycle plastic action can occur at an intermediate strain as a function of the rates of strain and temperature change.

A summary of the incremental calculations for the predicted response between parts C and D is presented in Table 5.2-I.

40
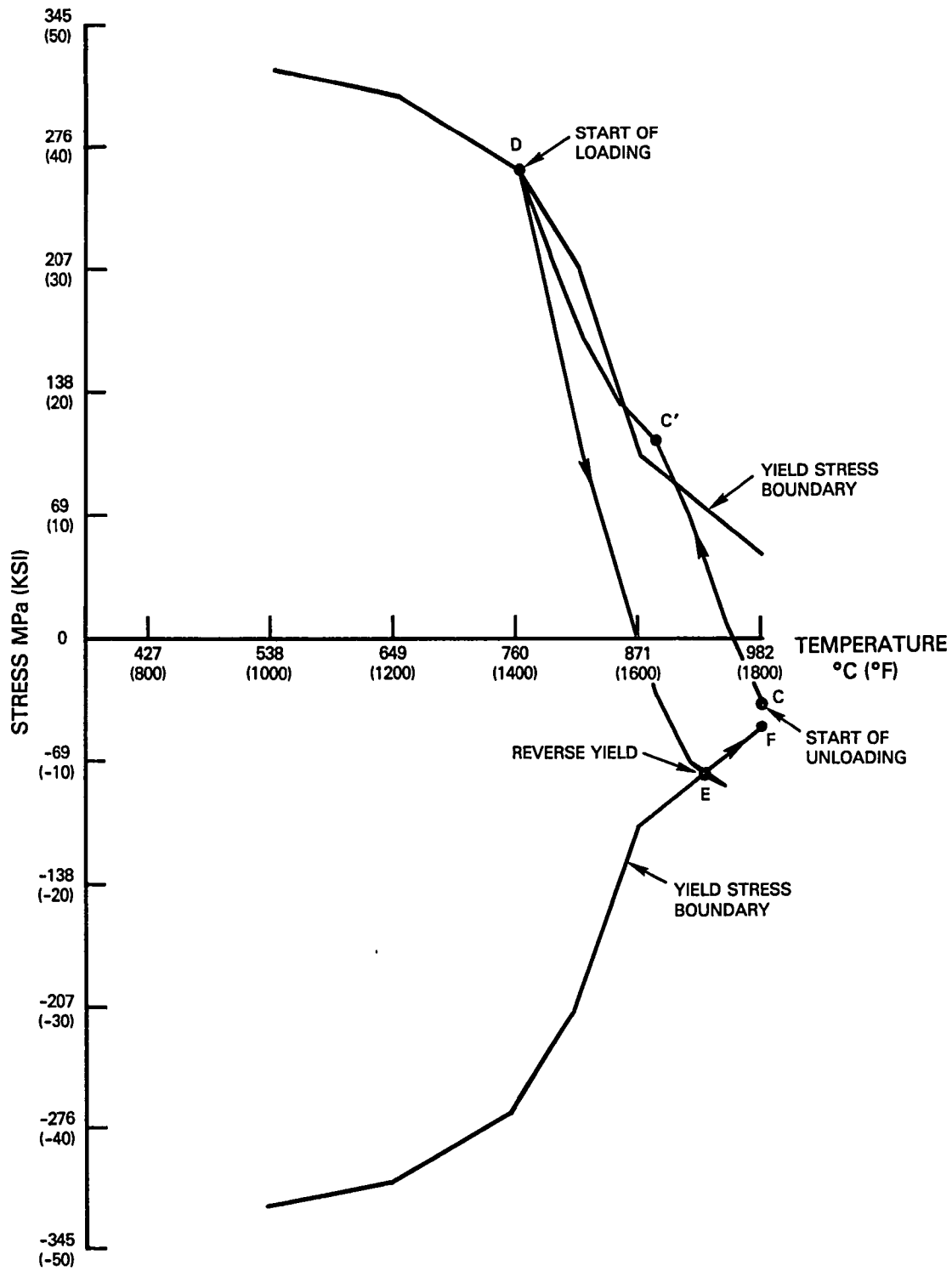
Figure 5.2-5  Prediction of Yield Points for 760 to 982°C (1400 to 1800°F) Test

TABLE 5.2-I

PREDICTION OF STRESS FROM C TO D IN FIGUR .2-4

| Strain ε | Temp. (°F) | Ave. Temp. (°F) | Time Increment (hr) | Strain Rate in/in/hr | E (ksi) | A | n (ksi) | $\sigma_{yield}$ (ksi) | (1) (ksi) | $\sigma^*$(2) (ksi) | $\Delta\sigma^*$(3) (ksi) | $\sigma$ (ksi) |
|---|---|---|---|---|---|---|---|---|---|---|---|---|
| -0.0045 | 1800 | | | | | | | 7.5 | -5.0 | - 0.0 | | - 5.0 (C) |
| | | 1770 | 2.08-03 | +0.243 | 18.2+03 | 1.25-04 | 3.2 | | | | +8.1 | |
| -0.0040 | 1740 | | | | | | | 9.5 | -5.0 | + 8.1 | | + 3.1 |
| | | 1710 | 9.36-04 | +0.534 | 18.75+03 | 25-04 | 3.32 | | | | +7.4 | |
| -0.0035 | 1680 | | | | | | | 11.5 | -5.0 | +15.5 | | +10.5 |
| | | 1653 | 7.94-04 | +0.630 | 19.3+03 | 1.02-06 | 4.15 | | | | +6.3 | |
| -0.0030 | 1625 | | | | | | | 14.0 | -5.0 | +21.8 | | +16.8 |
| | | 1598 | 7.61-04 | +0.657 | 19.8+03 | 2.8-08 | 5.3 | | | | +2.4 | |
| -0.0025 | 1570 | | | | | | | 20.5 | -5.0 | +24.2 | | +19.2 |
| | | 1540 | 7.95-04 | +0.630 | 20.6+03 | 2.05-08 | 5.0 | | | | +5.2 | |
| -0.0020 | 1510 | | | | | | | 33.5 | -5.0 | +29.4 | | +24.4 |
| | | 1483 | 9.36-04 | +0.534 | 21.3+03 | 1.5-08 | 4.65 | | | | +6.8 | |
| -0.0015 | 1455 | | | | | | | 36.5 | -5.0 | +36.2 | | +31.2 |
| | | 1428 | 2.08-03 | +0.243 | 21.75+03 | 1.1-08 | 4.3 | | | | +7.0 | |
| -0.0010 | 1400 | | | | | | | 38.0 | -5.0 | +43.2 | | +38.2 (D) |

(1) Backstress assumed constant -34.5 MPa (-5 ksi)

(2) $\sigma^* = \sigma - \Omega$

(3) Four subincrements used for each increment shown

TABLE 5.2-I (SI Units)

PREDICTION OF STRESS FROM C TO D IN FIGURE 5.2-4

| Strain ε | Temp. (°C) | Ave. Temp. (°C) | Time Increment (hr) | Strain Rate in/in/hr | E (MPa) | A | n (MPa) | $\sigma_{yield}$ (MPa) | (1) (MPa) | $\sigma^*$ (2) (MPa) | $\Delta\sigma^*$ (3) (MPa) | σ (MPa) |
|---|---|---|---|---|---|---|---|---|---|---|---|---|
| -0.0045 | 932 | | | | | | | 58 | -34 | - 0.0 | | - 34 (C) |
| | | 965 | 2.08-03 | +0.243 | 125+03 | 1.25-04 | 22 | | | | +56 | |
| -0.0040 | 948 | | | | | | | 66 | -34 | +56 | | + 21 |
| | | 932 | 9.36-04 | +0.534 | 129+03 | 25-04 | 23 | | | | +51 | |
| -0.0035 | 915 | | | | | | | 79 | -34 | +107 | | + 72 |
| | | 900 | 7.94-04 | +0.630 | 133+03 | 1.02-06 | 29 | | | | +43 | |
| -0.0030 | 885 | | | | | | | 97 | -34 | +150 | | +116 |
| | | 870 | 7.61-04 | +0.657 | 136+03 | 2.8-08 | 37 | | | | +17 | |
| -0.0025 | 854 | | | | | | | 141 | -34 | +167 | | +132 |
| | | 837 | 7.95-04 | +0.630 | 142+03 | 2.05-08 | 34 | | | | +36 | |
| -0.0020 | 821 | | | | | | | 231 | -34 | +208 | | +168 |
| | | 806 | 9.36-04 | +0.534 | 147+03 | 1.5-08 | 32 | | | | +47 | |
| -0.0015 | 790 | | | | | | | 252 | -34 | +250 | | +215 |
| | | 775 | 2.08-03 | +0.243 | 150+03 | 1.1-08 | 30 | | | | +48 | |
| -0.0010 | 760 | | | | | | | 262 | -34 | +298 | | 263 (D) |

(1) Backstress assumed constant -34 MPa

(2) $\sigma^* = \sigma - \Omega$

(3) Four subincrements used for each increment shown

4. Reloading D-F. From point D, the direction of straining is reversed and the temperature is increasing from 760°C (1400°F) to 982°C (1800°F). This represents movement toward a yield surface with the increase in strain and the decreasing size of the temperature dependent yield surface. Prediction of the elastic-creep response again uses equation 24 and is tabulated in Table 5.2-II. Here, the internal stress (backstress) varies to reduce the effective stress at the cooler temperatures (early in the unloading) and increase the effective stress at the hotter temperatures to produce a more nonlinear response. The function used to estimate the value of the backstress in these calculations is:

$$\Omega = \sigma_{max} - \sigma_{yield} \text{ for } \sigma_{max} \leq 2x\sigma_{yield} \tag{27}$$

$$\Omega = \sigma_{yield} \text{ for } \sigma_{max} > 2x\sigma_{yield} \tag{28}$$

where: $\sigma_{max}$ = maximum stress at start of unloading

This is equivalent to considering a series of temperature dependent circular yield surfaces "pinned" at the maximum tensile stress in the cycle and the backstress as the centers of the yield circles. The limiting condition occurs when the diameter of the yield circle equals the maximum stress, then a smaller (hotter) yield circle would predict reverse plasticity at the same sign of stress as the maximum stress (in this case positive). This is generally considered not possible, so the backstress is limited to the value of the yield stress for these temperatures. Prediction of the stress-temperature history is shown in Figure 5.2-4. At point E, the stress lies on the yield boundary, continued loading from point E to F with the corresponding increase in temperature from 932°C (1710°F) to 982°C (1800°F) follows the yield boundary as described in section 4.3. Using this approach, the predicted stress-strain response shown in Figure 5.2-4 is in good agreement with the stabilized experimental data.

A summary of the key equations of the simplified procedure is included in Appendix B.

A program written for the incremental solution of equation 24 using a Hewlett Packard HP67 programmable calculator is presented in Appendix C.

Simulations of the 649 to 982°C (1200 to 1800°F) test by the three models are shown in Figures 5.2-6 and 5.2-7. The time independent model again predicts a stiffer response with less inelastic strain range than the experimental data. The simulation with the simplified procedure shows good correlation with the data. For this cycle, reverse yielding is predicted during the unloading portion of the cycle at a stress of 276 MPa (40 ksi) at 721°C (1330°F), Figure 5.2-8. Prediction with the time dependent model (Figure 5.2-7) shows good agreement with the experimental data, especially at the high temperature end of the cycle. At the lower temperature end, the prediction is more elastic and does not display the distinct reverse yield point. Further development of this model is in progress and should improve future predictions.

TABLE 5.2-II

PREDICTION OF STRESS FROM D TO E IN FIGURE 5.2-4

| Strain $\varepsilon$ | Temp. (°F) | Ave. Temp. (°F) | Time Increment (hr) | Strain Rate in/in/hr | E (ksi) | A | n (ksi) | $\sigma_{yield}$ (ksi) | (1) $\Omega$ (ksi) | Effective Stress $\sigma^*$(2) (ksi) | $\Delta\sigma^*$(3) (ksi) | External Stress $\sigma$ (ksi) |
|---|---|---|---|---|---|---|---|---|---|---|---|---|
| -0.0010 | 1400 | | | | | | | +38.0 | + 0.2 | +38.0 | | +38.2 (D) |
| | | 1428 | 2.08-03 | -0.243 | 21.75+03 | 1.1-08 | 4.3 | | | | -12.4 | |
| -0.0015 | 1455 | | | | | | | +36.5 | + 1.7 | +24.10 | | +25.8 |
| | | 1483 | 9.36-04 | -0.534 | 21.3+03 | 1.5-08 | 4.65 | | | | -10.9 | |
| -0.0020 | 1510 | | | | | | | 33.5 | + 4.7 | +10.2 | | +14.9 |
| | | 1540 | 7.95-04 | -0.630 | 20.61+03 | 2.05-08 | 5.0 | | | | -10.3 | |
| -0.0025 | 1570 | | | | | | | 20.5 | +17.7 | -13.1 | | + 4.6 |
| | | 1598 | 7.61-04 | -0.657 | 19.8+03 | 2.8-08 | 5.3 | | | | - 8.7 | |
| -0.0030 | 1625 | | | | | | | 14.0 | +14.0 | -18.1 | | - 4.1 |
| | | 1653 | 7.94-04 | -0.630 | 19.3+03 | 1.02-06 | 4.15 | | | | -5.6 | |
| -0.0035 | 1680 | | | | | | | 11.5 | +11.5 | -21.2 | | - 9.7 |
| | | 1710 | 9.36-04 | -0.534 | 18.75+03 | 2.5-04 | 3.32 | | | | -0.9 | |
| -0.0040 | 1740 | | | | | | | 9.5 | + 9.5 | -19.2 | | -10.6[4] |
| | | 1770 | 2.08-03 | -0.243 | 18.2+03 | 1.25-04 | 3.2 | | | | - | |
| -0.0045 | 1800 | | | | | | | 7.5 | + 7.5 | | | (E) |

(1)  $\Omega = \sigma_{max} - \sigma_{yield}$ for $2\sigma_{yield} \geq \sigma_{max}$ ($\sigma_{max} = +38.2$ ksi)

$\Omega = \sigma_{yield}$ for $2\sigma_{yield} < \sigma_{max}$

(2) $\sigma^* = \sigma - \Omega$

(3) Four subincrements used for each increment shown

(4) Time independent plasticity predicted beyond this point

## TABLE 5.2-II (SI Units)

## PREDICTION OF STRESS FROM D TO E IN FIGURE 5.2-4

| Strain ε | Temp. (°C) | Ave. Temp. (°C) | Time Increment hr | Strain Rate in/in/hr | E (MPa) | A | n (MPa) | σyield (MPa) | Ω (1) (MPa) | Effective Stress σ*(2) (MPa) | Δσ*(3) (MPa) | External Stress σ (MPa) |
|---|---|---|---|---|---|---|---|---|---|---|---|---|
| -0.0010 | 760 | | | | | | | +262 | + 1.4 | +262 | | +263 (D) |
| | | 775 | 2.08-03 | -0.243 | 150+03 | 1.1-08 | 30 | | | | -85 | |
| -0.0015 | 790 | | | | | | | +252 | + 12 | +166 | | +178 |
| | | 800 | 9.36-04 | -0.534 | 147+03 | 1.5-08 | 32 | | | | -75 | |
| -0.0020 | 821 | | | | | | | 231 | + 32 | +70 | | +103 |
| | ↑ | 837 | 7.95-04 | -0.630 | 142+03 | 2.05-08 | 34 | | | | -71 | |
| -0.0025 | 854 | | | | | | | 141 | +122 | -90 | | + 32 |
| | | 870 | 7.61-04 | -0.657 | 137+03 | 2.8-08 | 37 | | | | - 60 | |
| -0.0030 | 885 | | | | | | | 97 | +97 | -125 | | - 28 |
| | | 900 | 7.94-04 | -0.630 | 133+03 | 1.02-06 | 29 | | | | -39 | |
| -0.0035 | 915 | | | | | | | 79 | +79 | -146 | | - 67 |
| | | 932 | 9.36-04 | -0.534 | 129+03 | 2.5-04 | 23 | | | | -6 | |
| -0.0040 | 948 | | | | | | | 66 | +65 | -132 | | - 73 (4) |
| | | 965 | 2.08-03 | -0.243 | 126+03 | 1.25-04 | 22 | | | | - | |
| -0.0045 | 962 | | | | | | | 52 | + 52 | | | (E) |

(1) $\Omega = \sigma_{max} - \sigma_{yield}$ for $2\sigma_{yield} \geq \sigma_{max}$ ($\sigma_{max} = +263$ MPa)

   $\Omega = \sigma_{yield}$ for $2\sigma_{yield} < \sigma_{max}$

(2) $\sigma* = \sigma - \Omega$

(3) Four subincrements used for each increment shown

(4) Time independent plasticity predicted beyond this point
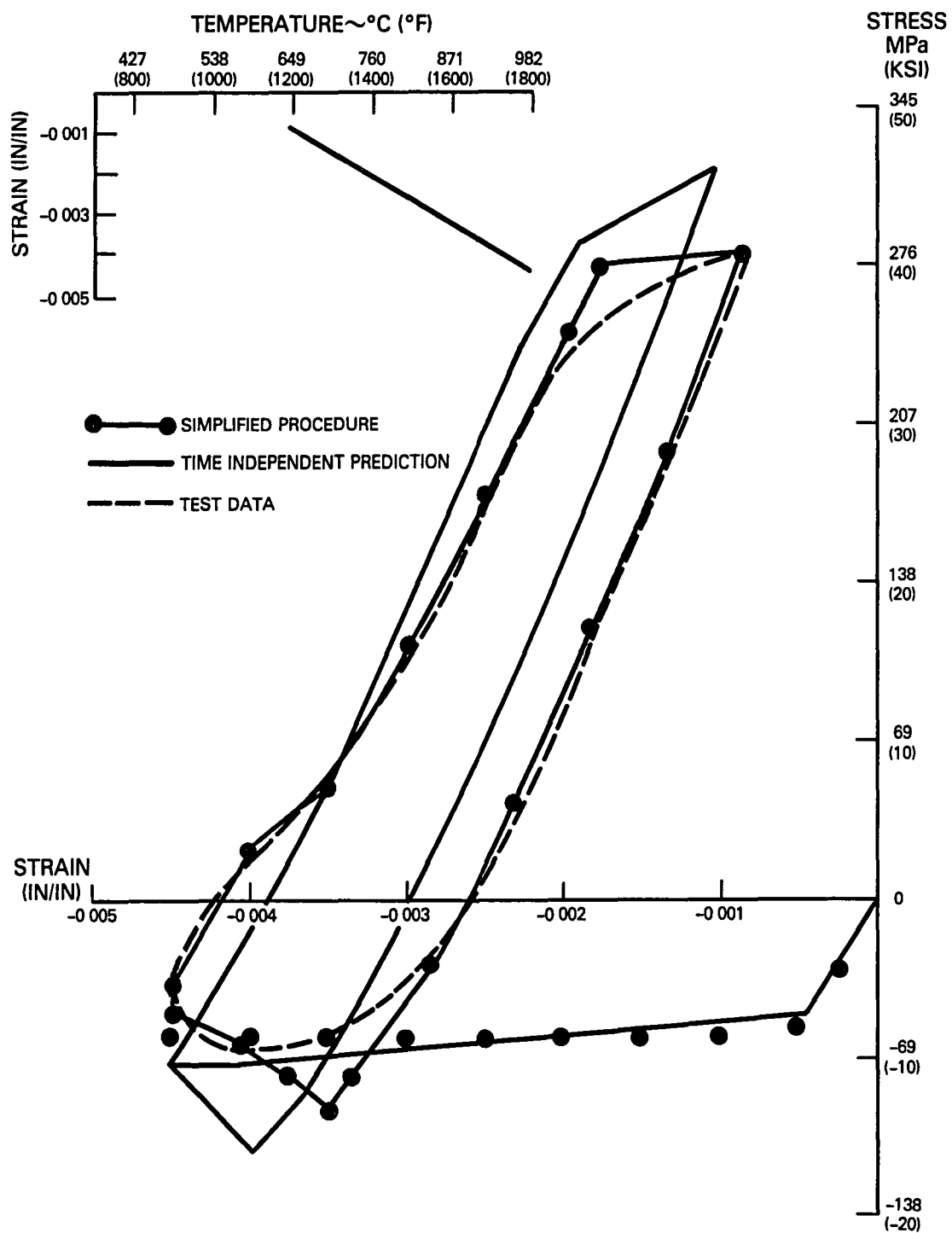
Figure 5.2-6 Prediction of 649 to 982°C (1200 to 1800°F) Response by Time Independent Plasticity and Simplified Models
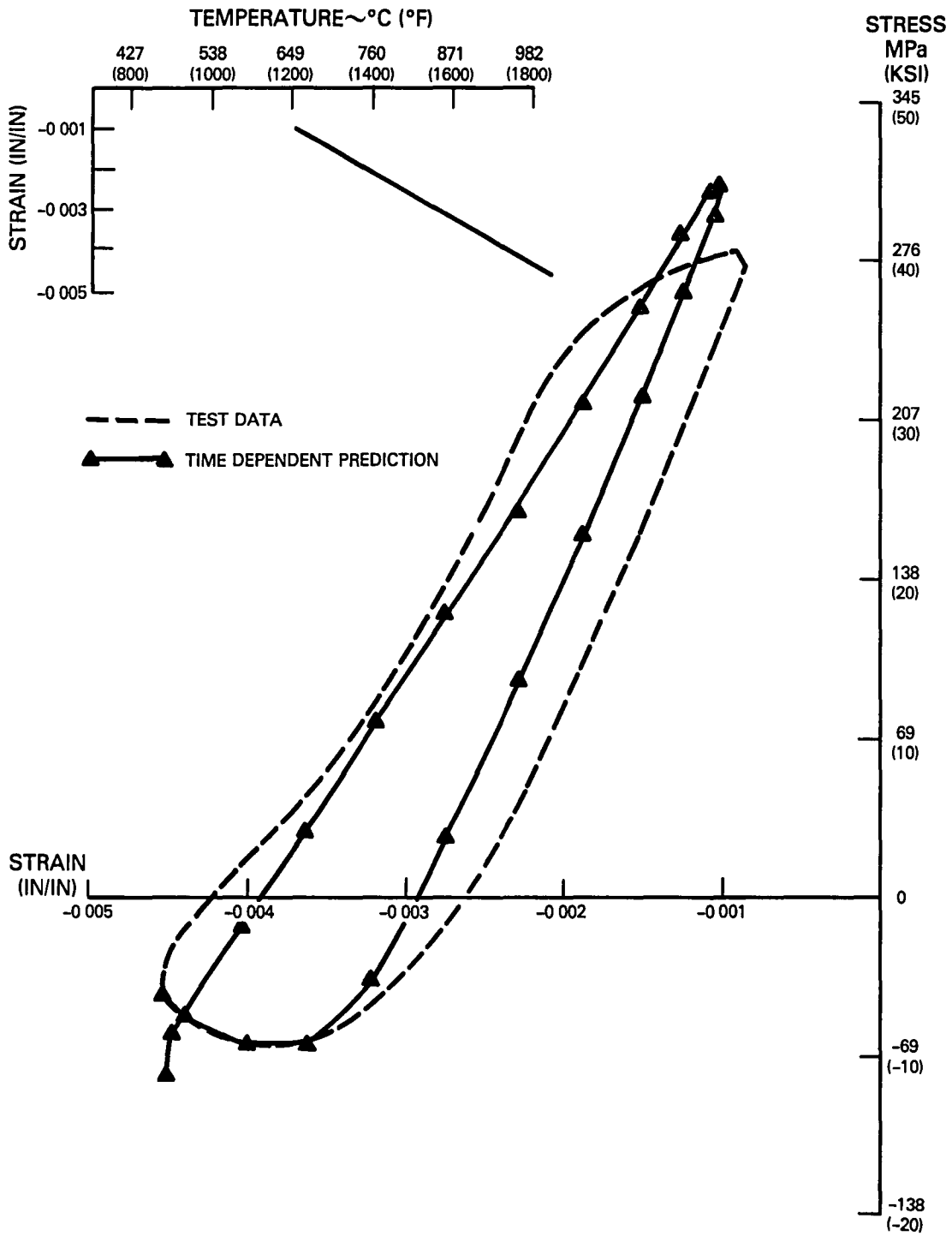
Figure 5.2-7  Prediction of 649 to 982°C (1200 to 1800°F) Response by Time Dependent Model
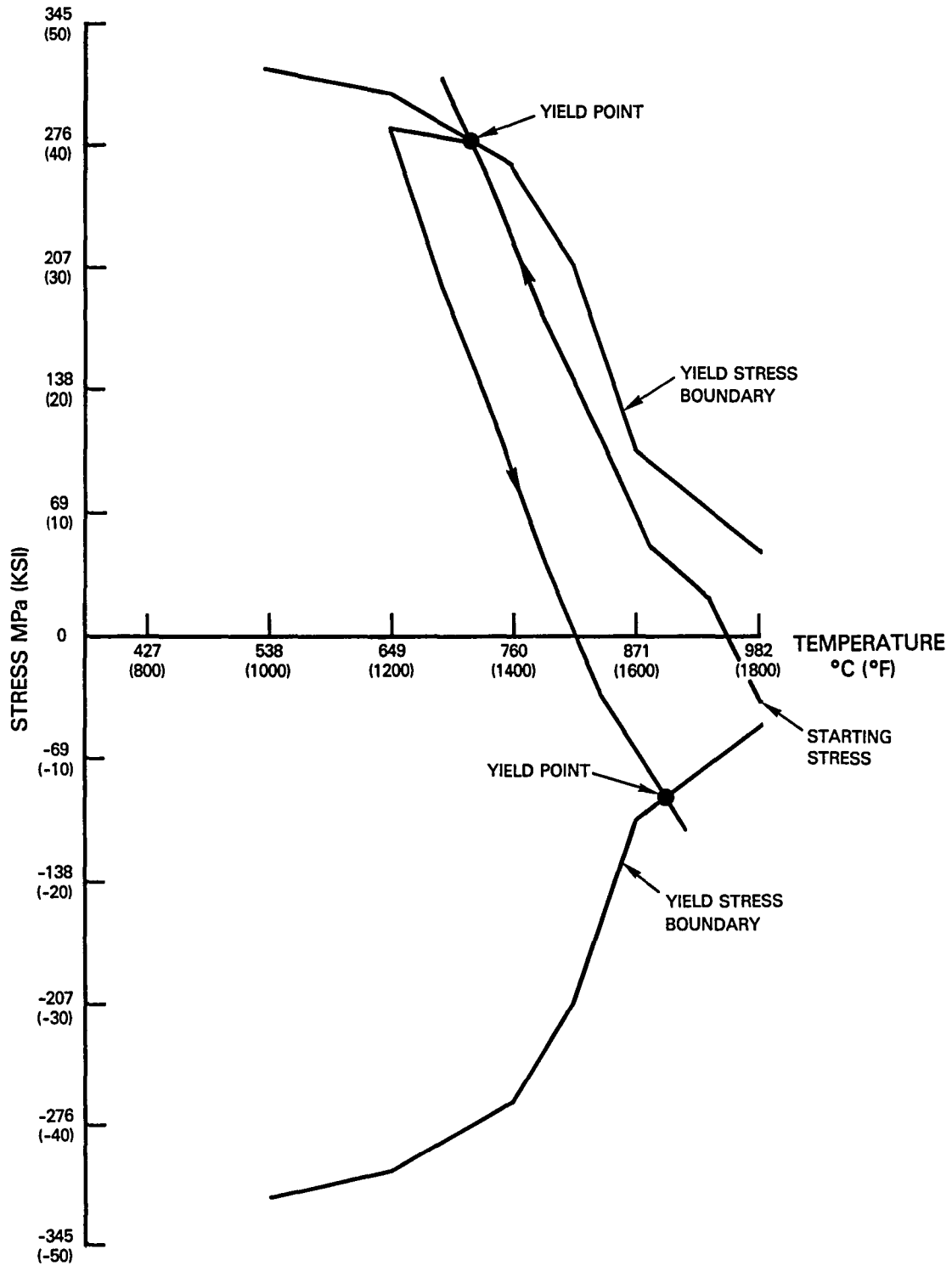
Figure 5.2-8  Prediction of Yield Points for 649 to 982°C (1200 to 1800°F) Simulation

Predicted results for the 427 to 982°C (800 to 1800°F) test are shown in Figures 5.2-9 and 5.2-10. With the overall lower temperatures, the time independent model (Figure 5.2-9) more closely agrees with this cycle than the previous two. Prediction with the simplified procedure closely agrees with the experimental data. Again reverse yielding is predicted on the unloading by the method described above (See Figure 5.2-11). Calculation of the response with the time dependent model (Figure 5.2-10) reproduces the cycle's major characteristics.
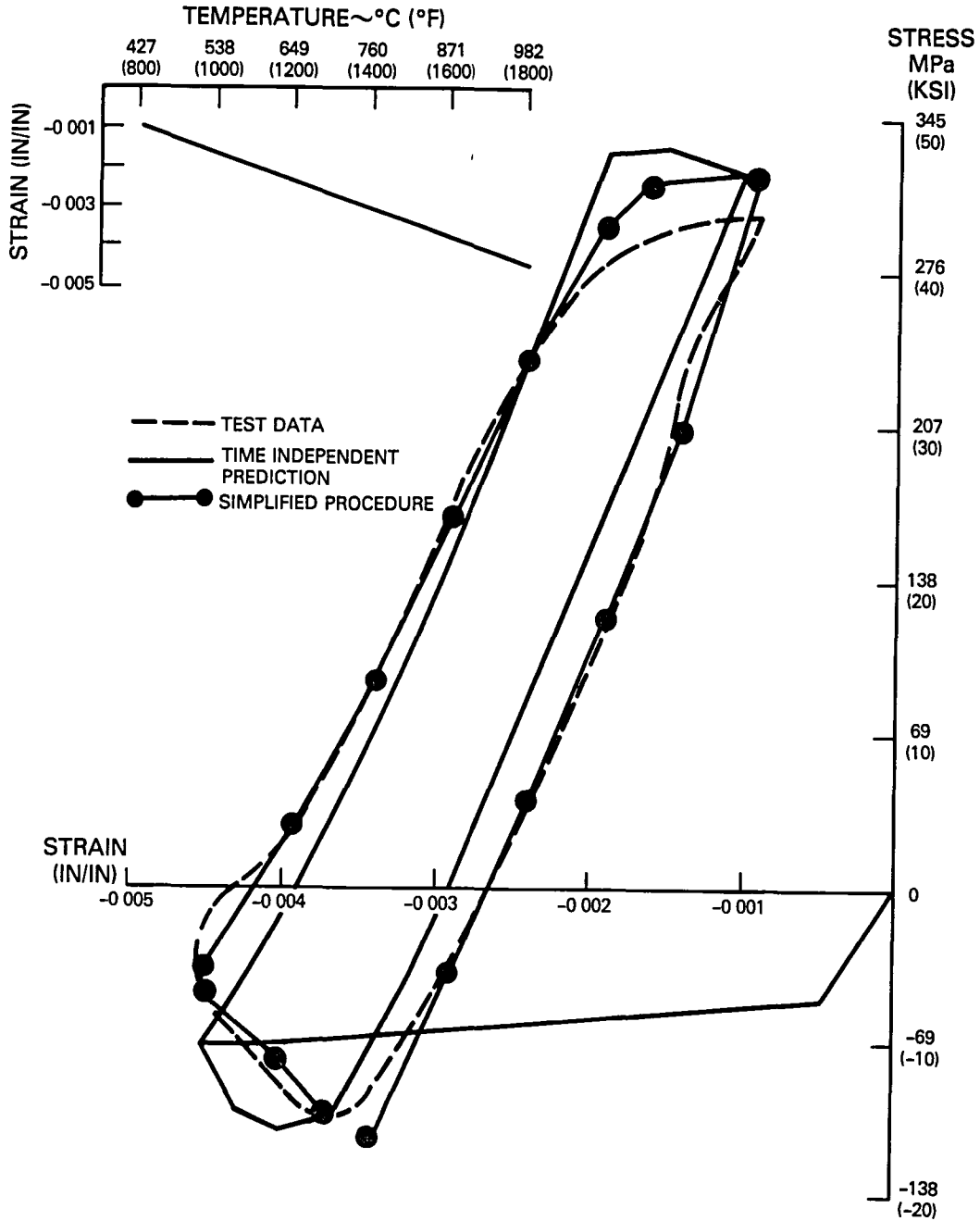


Figure 5.2-9  Simulation of 427 to 982°C (800 to 1800°F) Response with Time Independent and Simplified Models
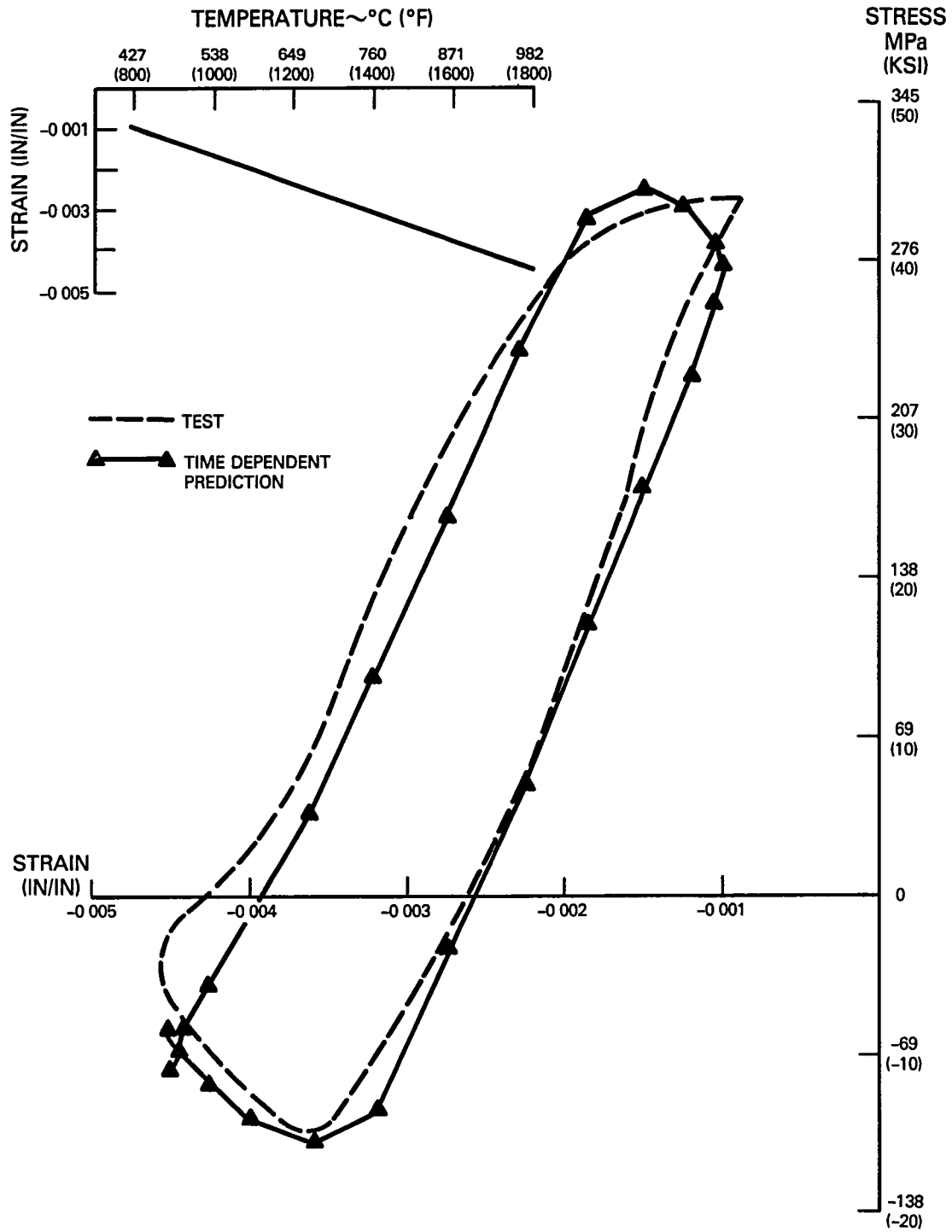
Figure 5.2-10 Prediction of 427 to 982°C (800 to 1800°F) Response by Time Independent Model
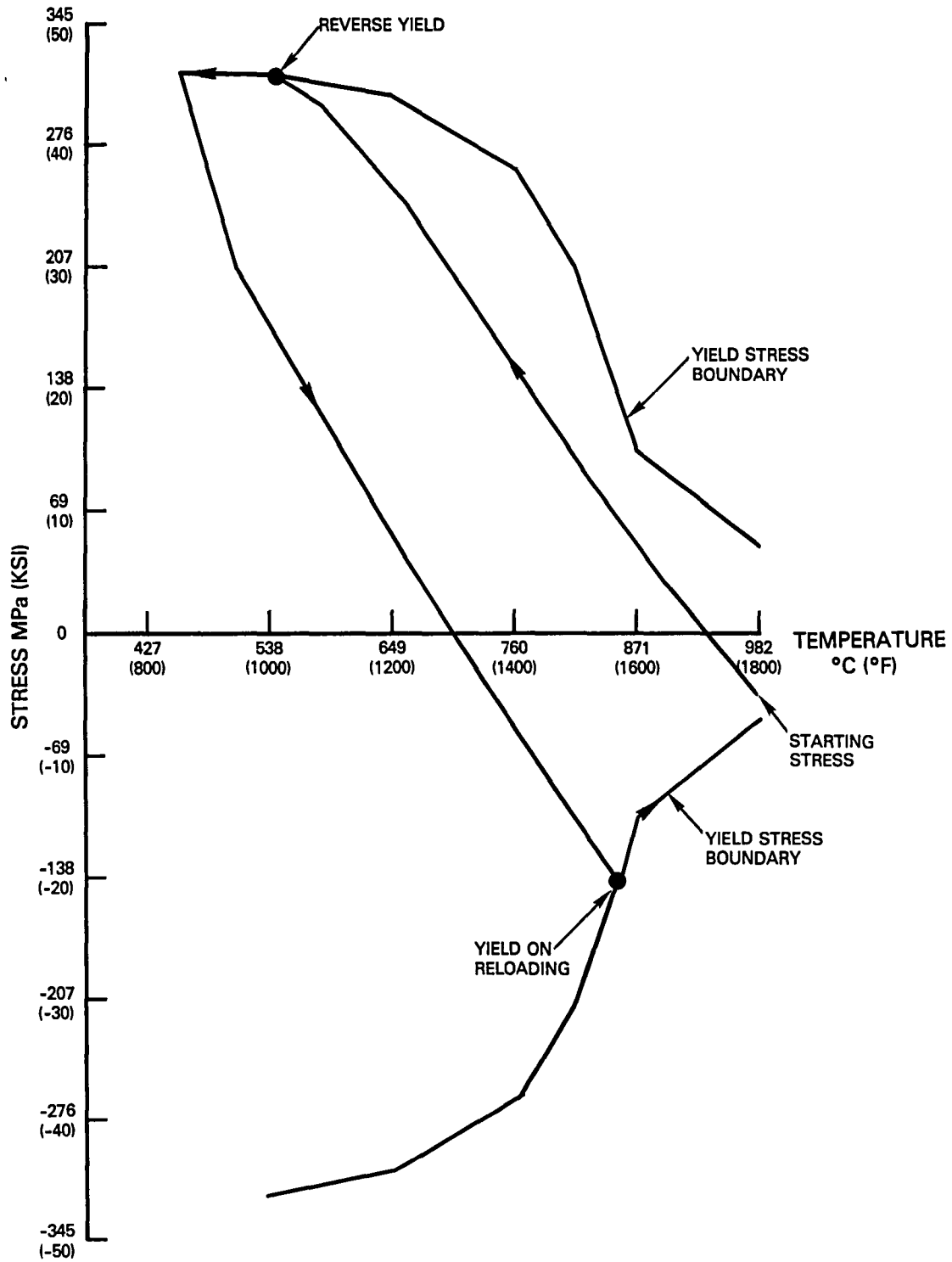
Figure 5.2-11 Prediction of Yield Points for 427 to 982°C (800 to 1800°F)

## 5.3 PREDICTION OF FAITHFUL CYCLE THERMOMECHANICAL RESPONSE

Final evaluation of three models considered the combustor liner faithful cycle defined in Reference 1. The predicted strain-temperature response at the end of the louver lip differs from the previously defined conditions in that the strain and temperature are not continually in phase and the heatup and cool-down portion of the cycle are not identical. The strain-time and temperature-time conditions for this cycle are presented in Figures 5.3-1 and 5.3-2. Application of these loading functions on the thermomechanical specimen shown in Figure 3.1-1 produced a stress-strain response considered to be representative of the local louver lip response. Figure 5.3-3 shows a comparison between input and measured history obtained during the specimen test.
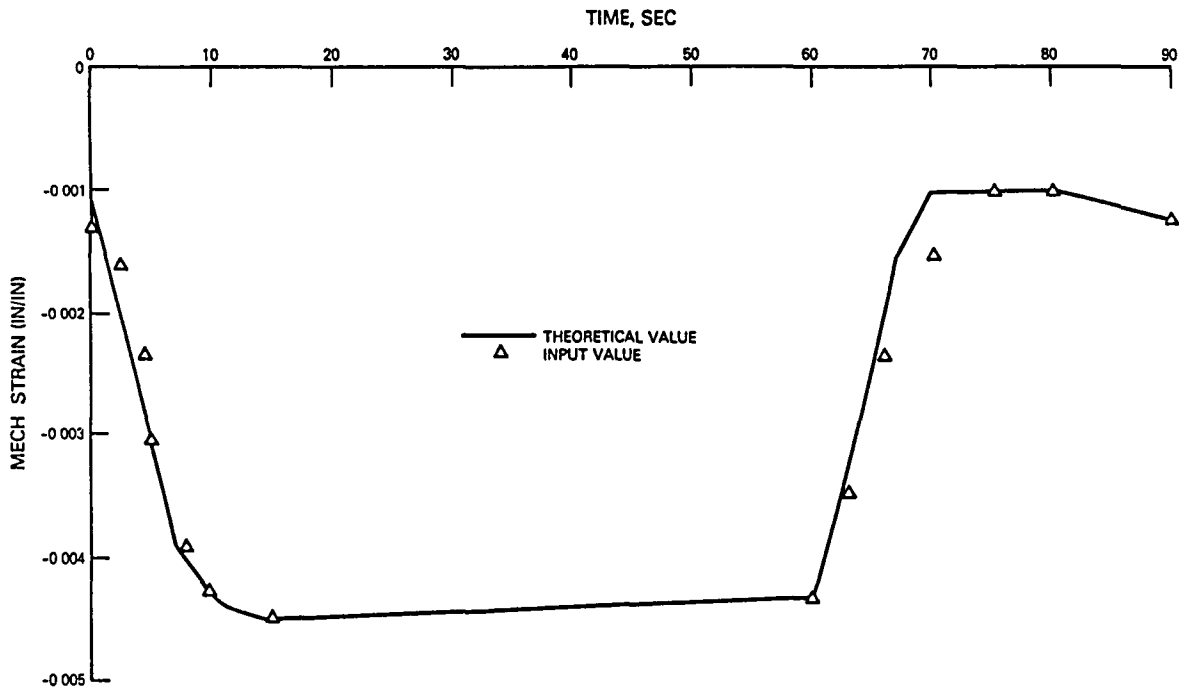


Figure 5.3-1  Strain History for Faithful Cycle Specimen Test
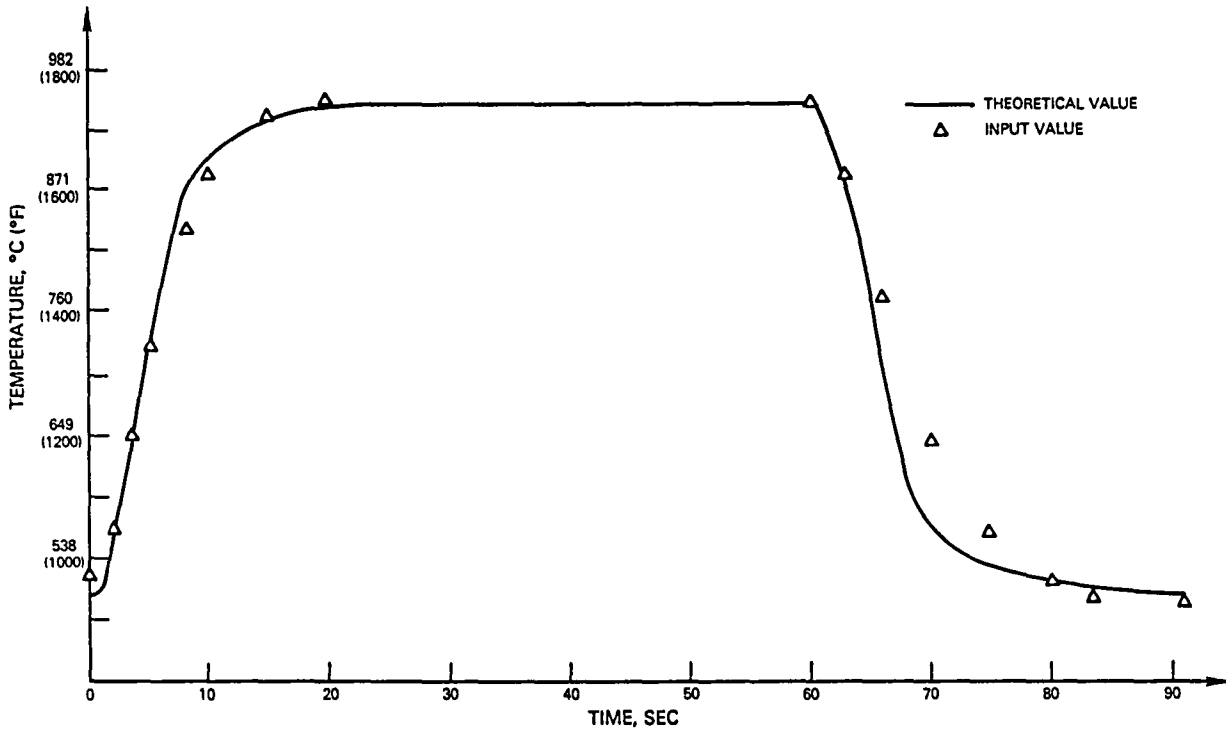
Figure 5.3-2  Temperature History for Faithful Cycle Specimen Test
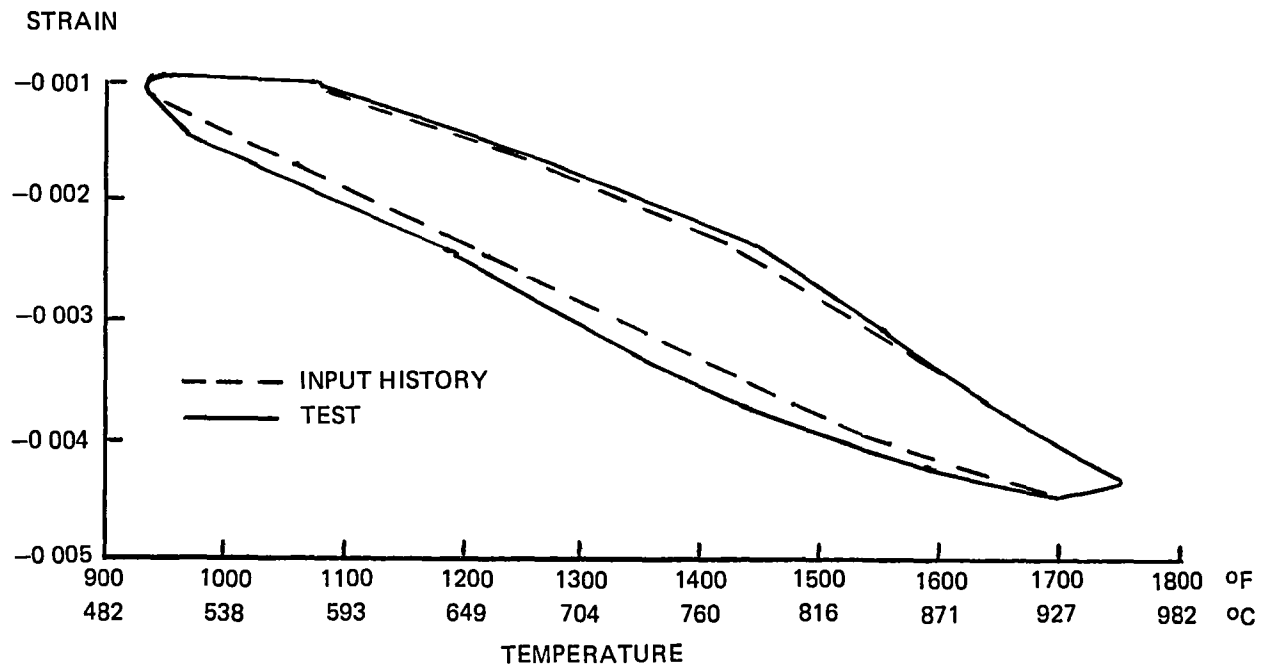


Figure 5.3-3  Strain-temperature History from Thermomechanical Specimen Test

54

Prediction of the faithful cycle with the time independent plasticity and creep model is shown in Figure 5.3-4. To account for the time dependent material response, a creep solution was included. In determining at what point in the loading cycle creep should be included, the variation in strain rate throughout the cycle was considered. Figure 5.3-5 shows the predicted variation in strain rate at the end of the louver lip for the thermal loading cycle. The strain rate was evaluated based on the predicted mechanical strain increments and the time associated with the temperature change for that increment. The results show a rapid (faster than 0.01 $min^{-1}$) initial strain rate, a peak value occurring at 6 seconds and a dramatic drop in strain rate after 10 seconds. Since the predicted response during most of the first 10 seconds of the cycle is elastic and less rate sensitive, only the remaining 50 seconds of the heatup was considered for the creep simulation. The 50 seconds of creep time was arbitrarily divided into three segments and applied as follows:

| | |
|---|---|
| 5 seconds (10 to 15 seconds) | applied at the 12.5 second point |
| 15 seconds (15 to 30 seconds) | applied at the 20 second point |
| 30 seconds (30 to 60 seconds) | applied at the 45 second point |

A creep solution was not included on the unloading portion of the cycle (increasing strain and decreasing temperature). The resulting elastic slope is steeper than the experiment and the stress levels are larger. Prediction of the reverse yield point with the combined hardening model occurs at a stress level of 287 MPa (+41 ksi) versus the experiment at 248 MPa (+36 ksi). On reloading, (decreasing strain and increasing temperature), the prediction is not as steep as the experiment. These differences between the prediction and the experimental results are consistent with the idea of an integrated elastic and creep response included in the development of the simplified procedure. Yielding on reloading (heating) is predicted by the combined hardening model at a stress of -165.5 MPa (-24 ksi) versus -131 MPa (-19 ksi) from the test. While these results for the second analysis cycle agree reasonably well with the experimental data, the prediction after 10 analytical cycles, shown in Figure 5.3-6, is beginning to have significant variation with the data. This is produced by the increase in reverse yield point, from 283 MPa to 317 MPa, (+41 ksi to +46 ksi) predicted by the cyclic hardening model and the lower temperature stress-strain curves. The resulting increase in peak tensile stress and reduction in inelastic strain range is not consistent with the experimental data which stabilized after the first few loading cycles. The uncoupling of the creep and plasticity and the cyclic shakedown at the lower temperature response are considered to be the major deficiencies of this model in predicting thermomechanical stress-strain response.
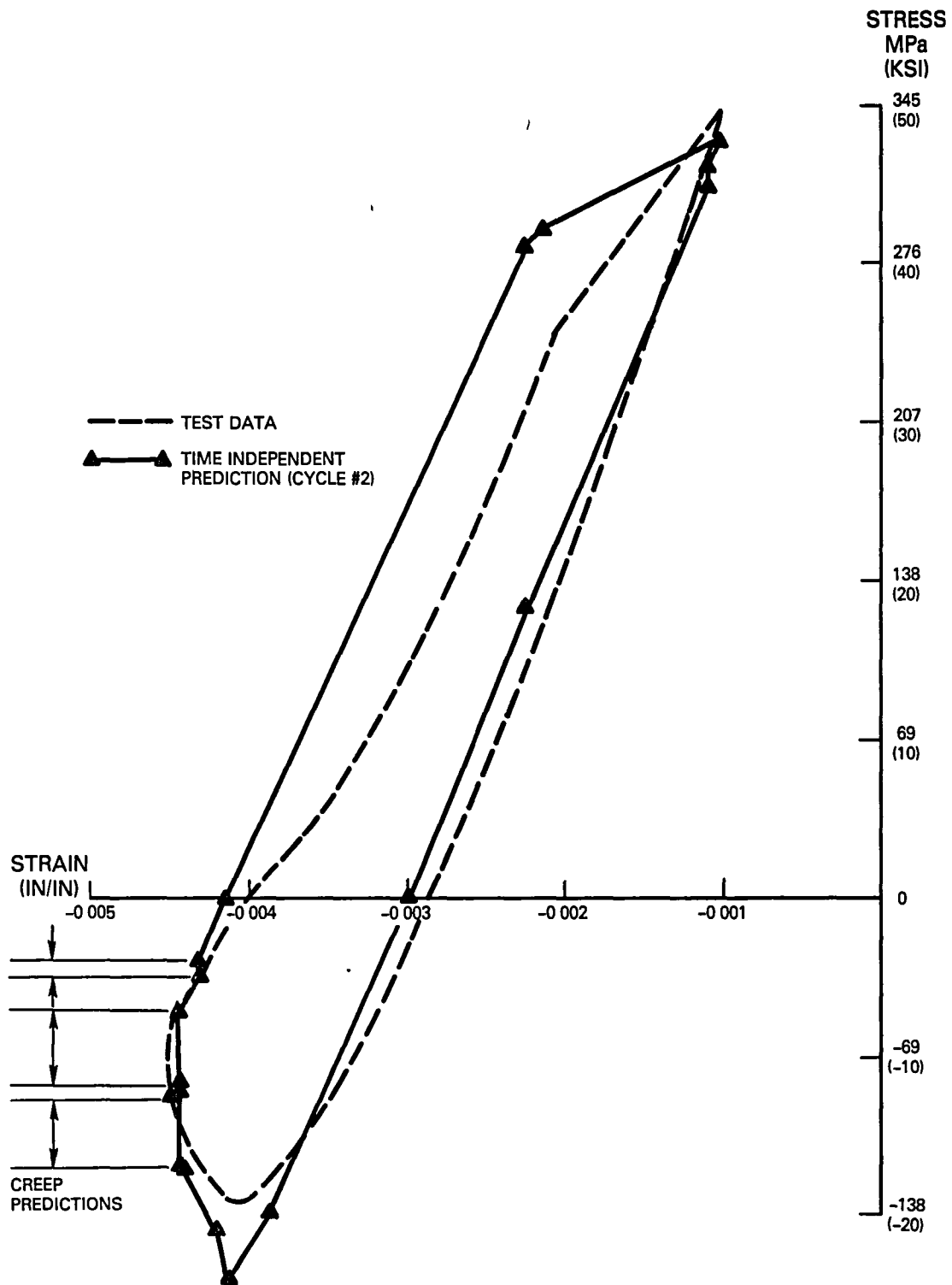
Figure 5.3-4 Prediction of Faithful Cycle Response by Time Independent
Plasticity and Creep Model (2nd Cycle)
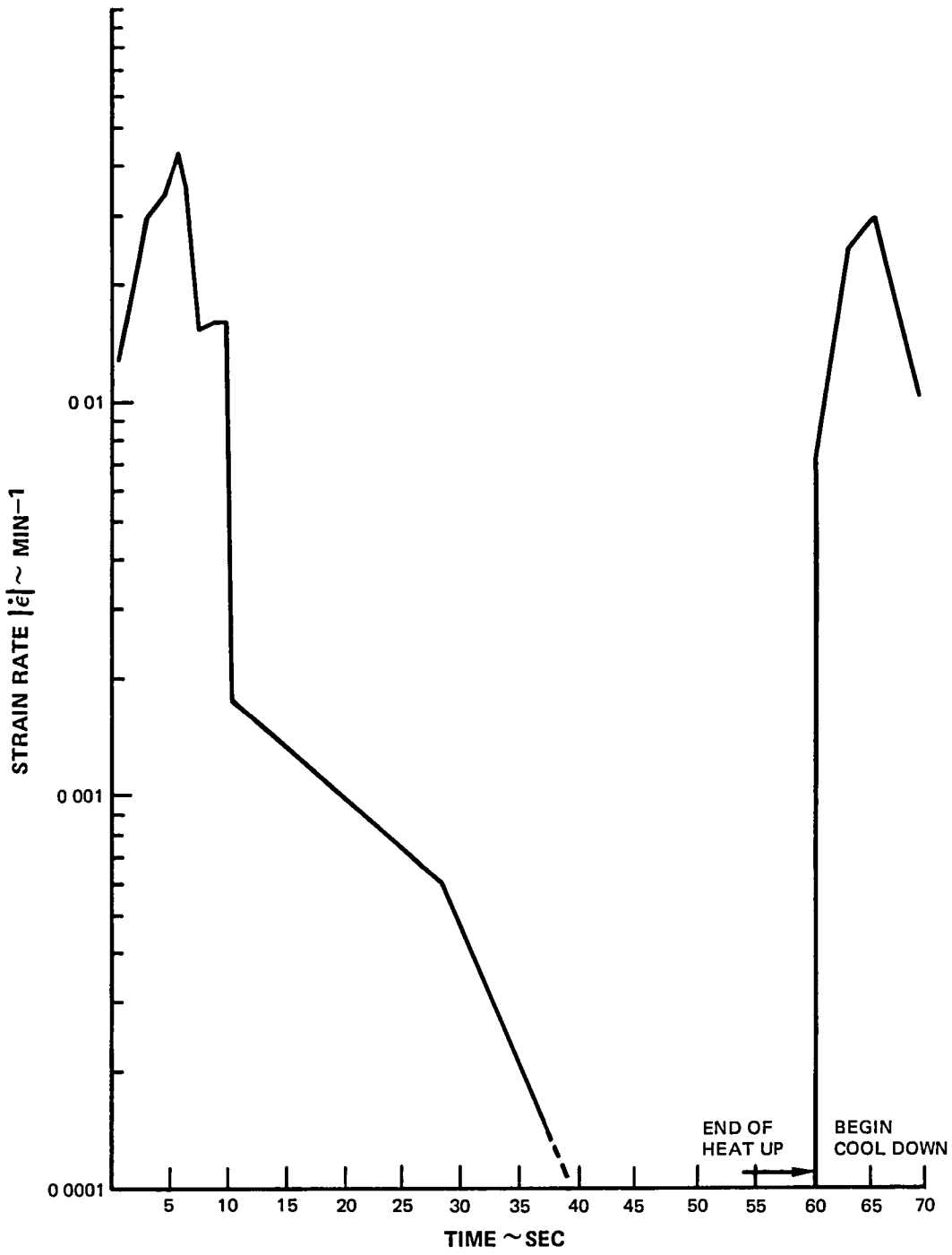
Figure 5.3-5   Strain Rate Variation at End of Louver Lip
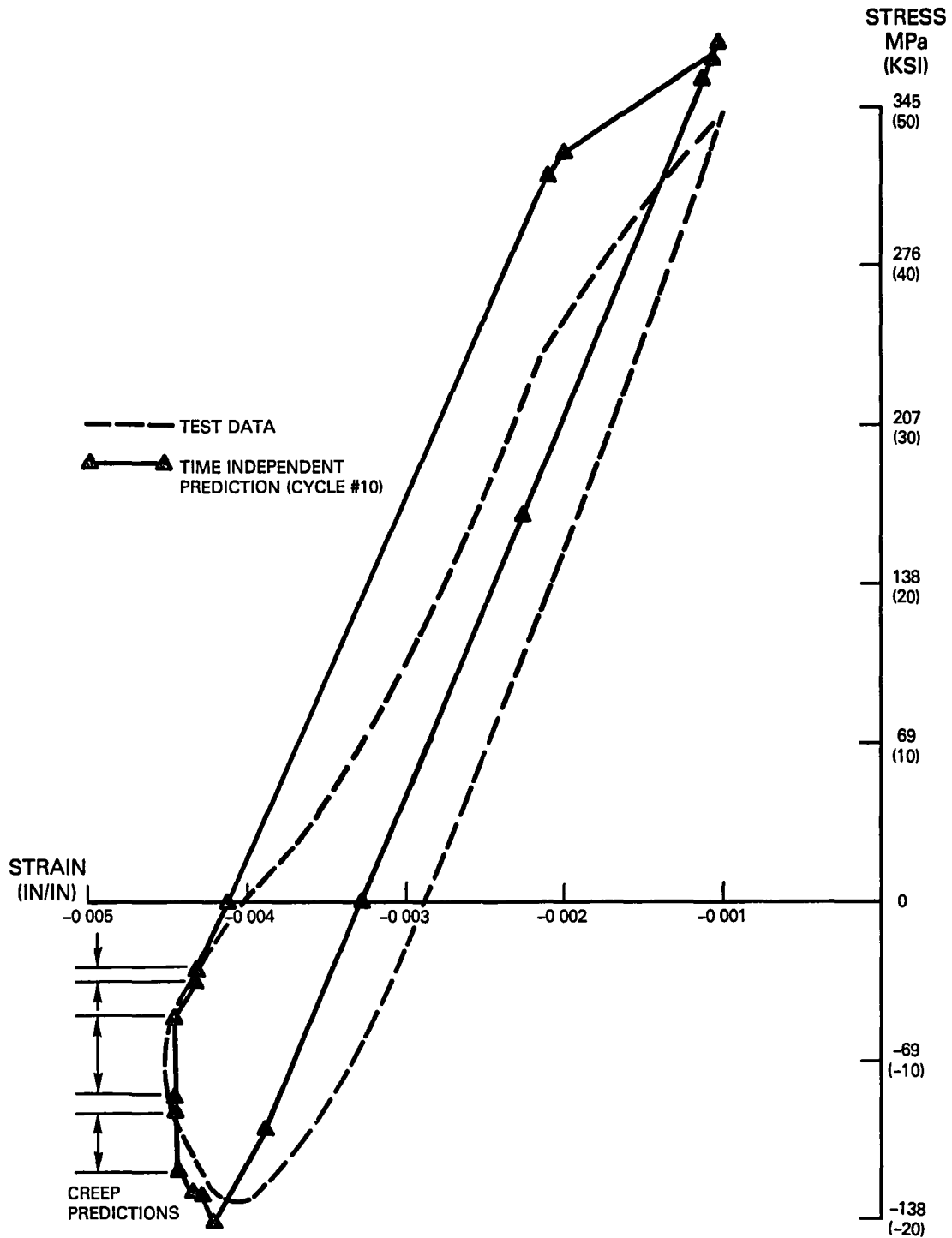
Figure 5.3-6  Prediction  of  Faithful  Cycle  Response  by  Time  Independent
Plasticity  and  Creep Model  (10th  Cycle)

Prediction of the faithful cycle thermomechanical response with the rate dependent model is shown in Figure 5.3-7. Overall, the model predicts a more accurate response than the prediction generated by the rate independent model. Both the loading and unloading slopes closely agree with the data and the loading yield point is overpredicted by approximately 10 percent in stress, -145 MPa versus -131 MPa, (-21 ksi versus -19 ksi). The model predicts the nonlinear response on unloading, but at a lower temperature than observed in the experiment. This results in the greatest discrepancy between the prediction and the data. The predicted stress levels are lower and the reverse yield point is not as well defined. In this area, the temperatures are decreasing and the material is becoming less rate sensitive. Further development of the model to improve the rate independent response prediction is in progress. This should improve the overall thermomechanical cyclic response prediction.

The prediction using the simplified procedure is presented in Figure 5.3-8. The results are of comparable accuracy to the results predicted by the other two models. Reverse yielding on the cool-down is predicted at 276 MPa (+40 ksi) at 721°C (1330°F) as shown in Figure 5.3-9 (Point B). The area of greatest discrepancy, on the cool-down, is also implied in Figure 5.3-8 where the stress history comes close to, but does not penetrate, the yield surface boundary. The stress at which yielding occurs on the heatup is also closely predicted by the method, -152 Mpa versus -131 MPa (-22 ksi versus -19 ksi) (Point D). Consistent with the other simulations using the simplified procedure, only the first complete loading cycle is considered in the prediction of the stable response.
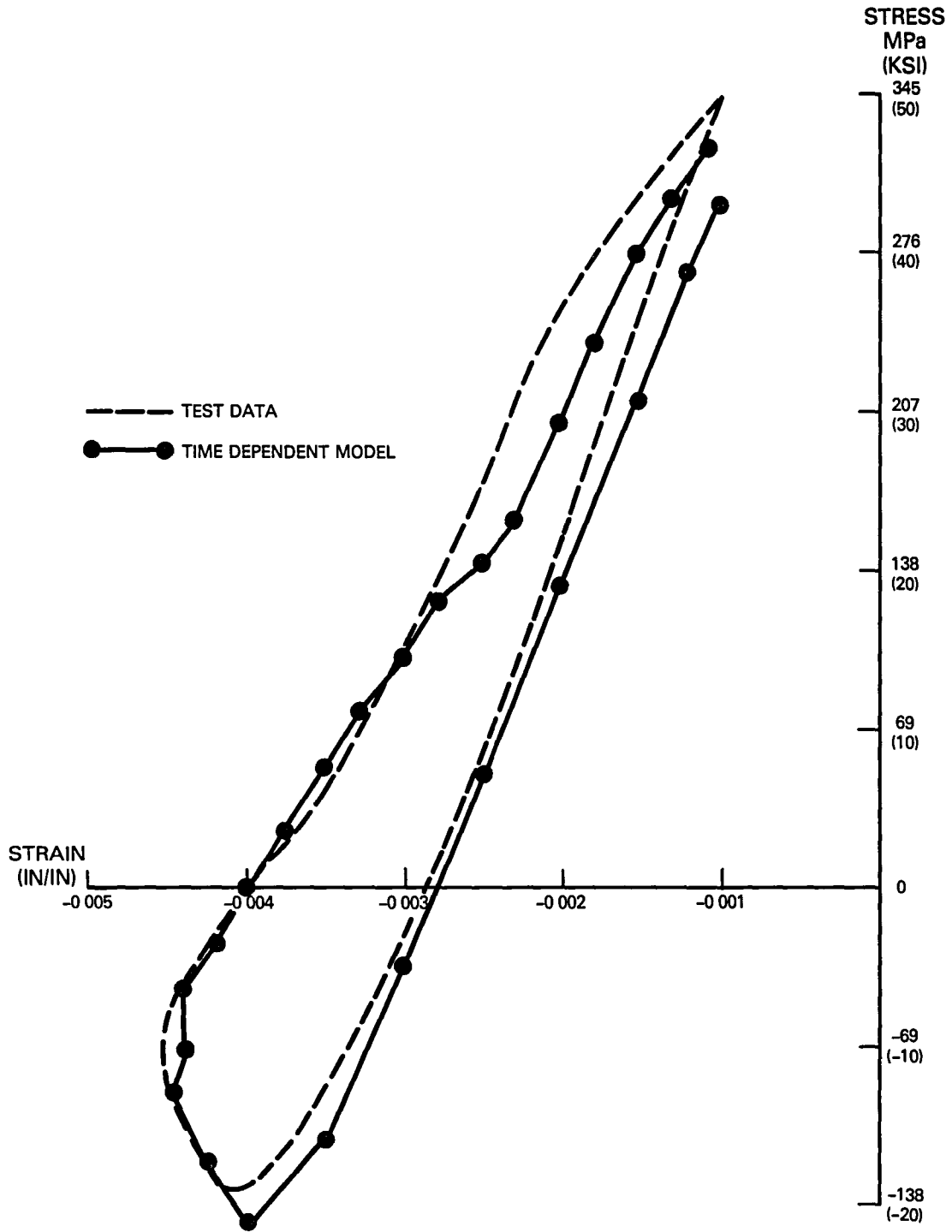
Figure 5.3-7  Prediction of Faithful Cycle Response by Time Dependent Model

60
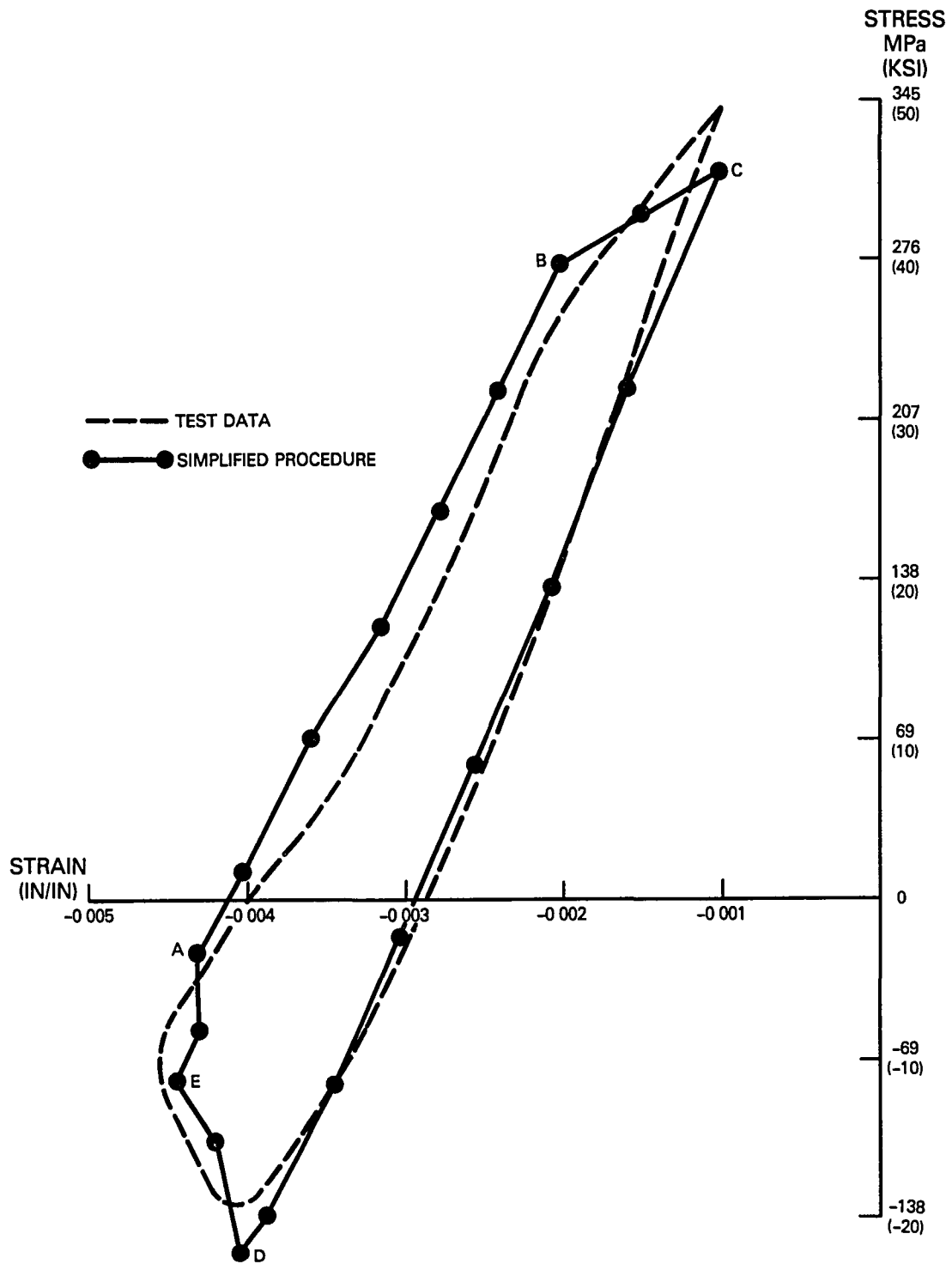
Figure 5.3-8  Prediction of Faithful Cycle Response by Simplified Procedure
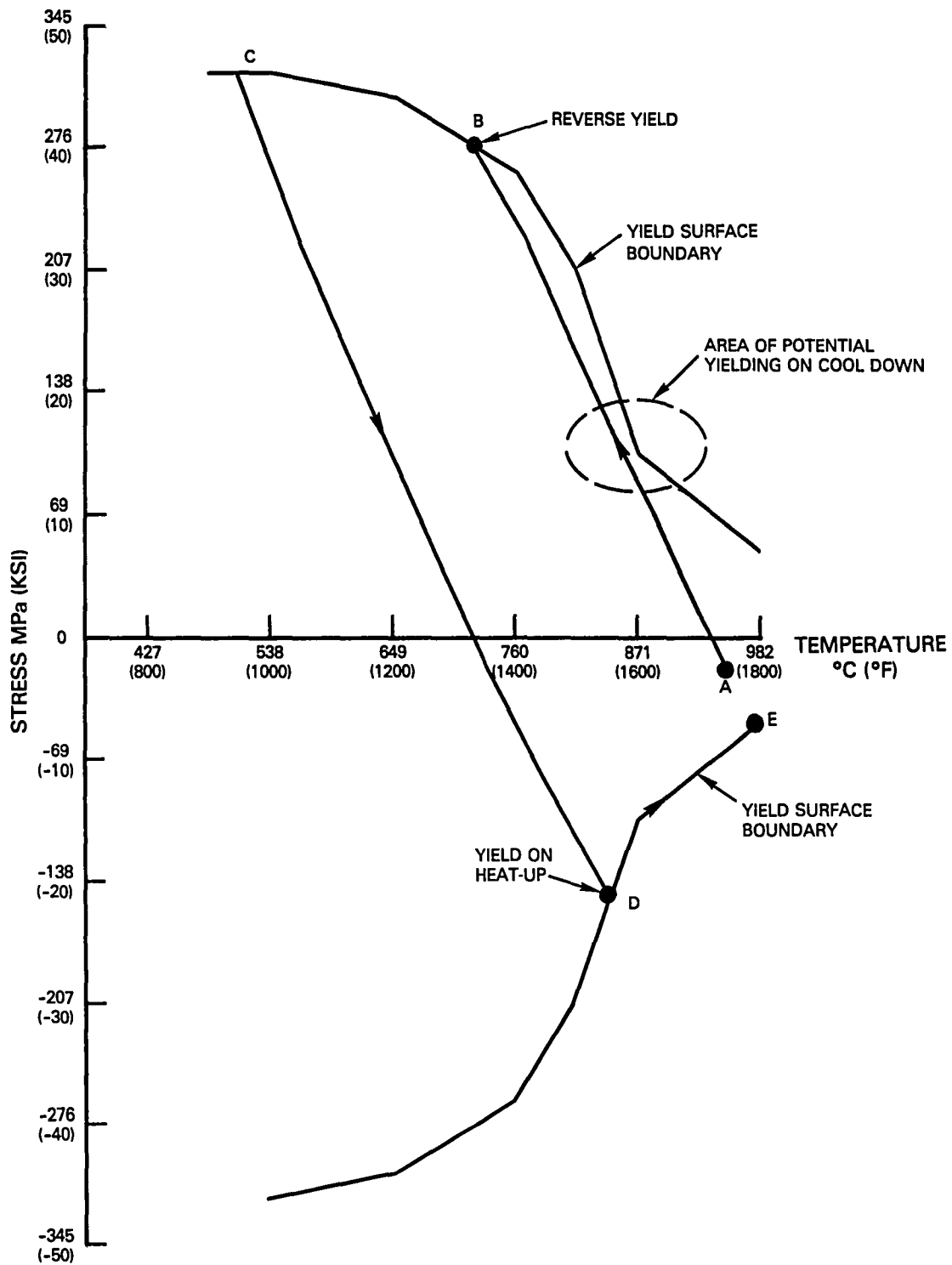
Figure 5.3-9   Prediction of Yield Points for Faithful Cycle

62

## 6.0 SUMMARY OF RESULTS

A simplified analytical procedure for estimating the local stress-strain response in a high temperature structural component has been developed.

The simplified procedure relies on the assumption that local inelastic response in a high temperature structure is constrained by the surrounding elastic material. The mechanical strain-temperature history can then be approximated with a linear elastic analysis. The procedure further assumes that the local response is composed of elastic, time independent plastic, and creep components. A conventional yield surface concept is used to determine the onset of plastic action. At all other times within a loading cycle, the response is assumed to be a combination of creep and elastic action. A nonlinear differential equation is used to predict an incremental history recognizing the elastic and creep response. Short time (primary) creep data is used in the creep model development.

Simulations of a series of Hastelloy X thermomechanical uniaxial specimen tests have shown that the simplified procedure accurately predicts the major characteristics of the cyclic stress-strain response. Simulations of the same thermomechanical cycles with nonlinear finite element analysis using time independent plasticity and creep, and unified time dependent material behavior models have also been conducted. The time dependent material model produced the better overall prediction of the cyclic response. Prediction results with the simplified procedure are of comparable accuracy to the two finite element solutions.

Further development of the simplified procedure should consider application to a higher strength, less time dependent, high temperature material. The current calculation procedure has been demonstrated for the prediction of cyclic response after the first complete loading cycle. Development of a relaxation model to predict the shift in the mean stress associated with continued cycling of the high strength materials is desirable.

A Hastelloy X unified data base has been developed and is presented in Appendix A. The data base includes stress-strain response for both isothermal and thermomechanical loading cycles of varying degrees of loading complexity. The data has been used in the evaluation of the three models discussed in this report. It may also be useful in the development and simulations of alternate models.

APPENDIX A

EXPERIMENTAL DATA GENERATED FOR DATA BASE
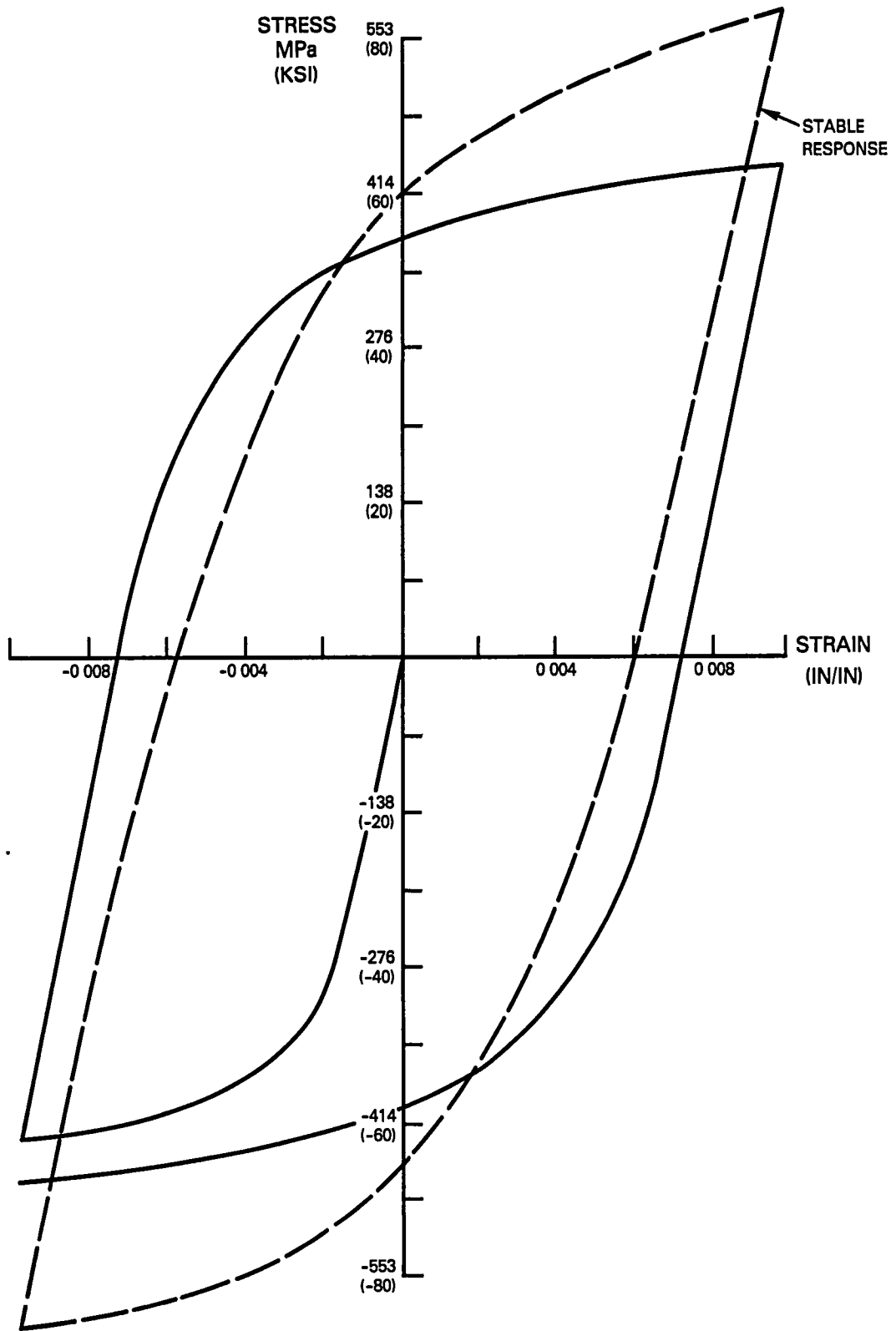
Figure A-1    Fully Reversed Strain (Condition a) at 538°C (1000°F)
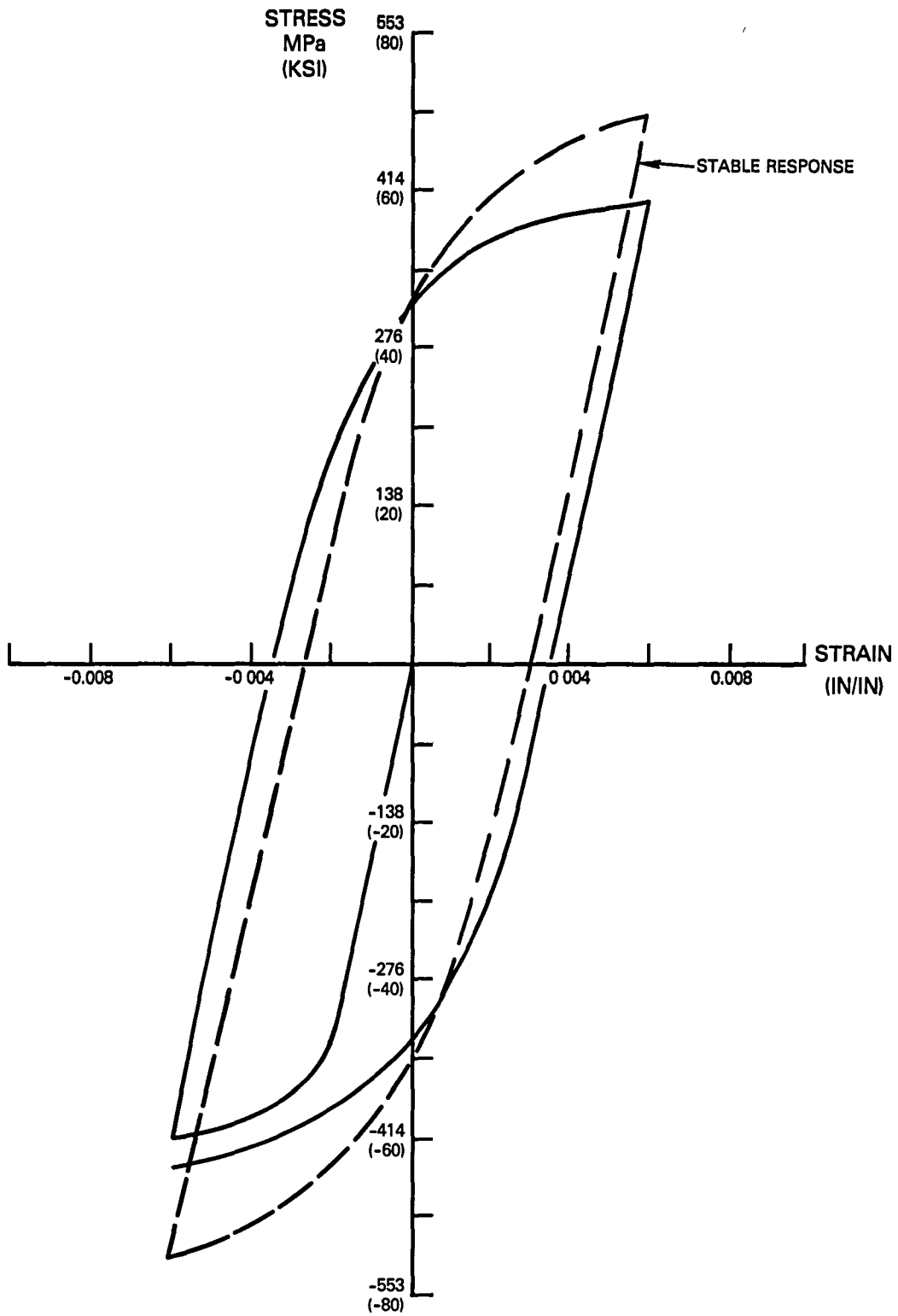
Figure A-2    Fully Reversed Strain (Condition a) at 649°C (1200°F)
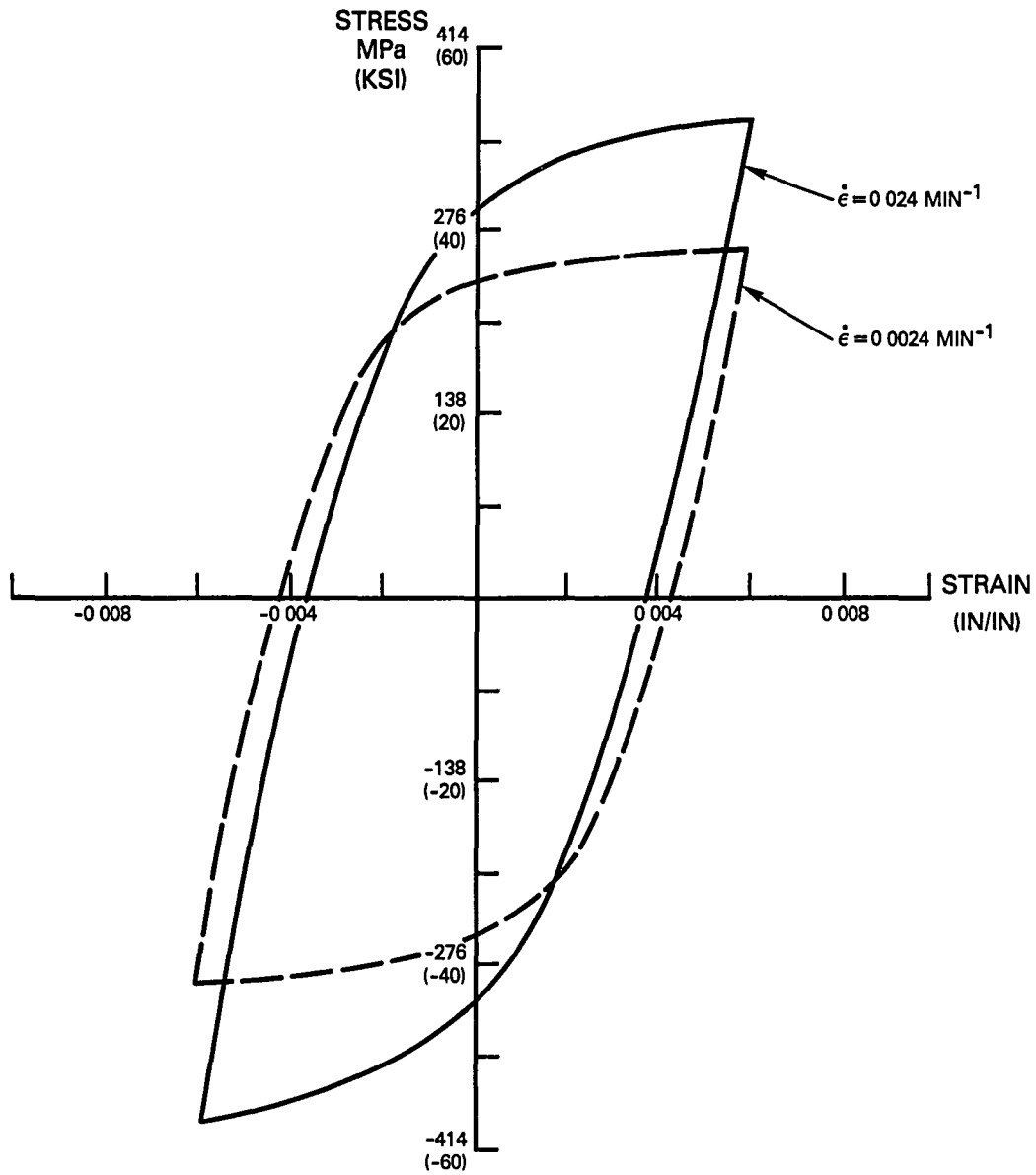
Figure A-3     Fully Reversed Strain (Condition a) at 760°C (1400°F)
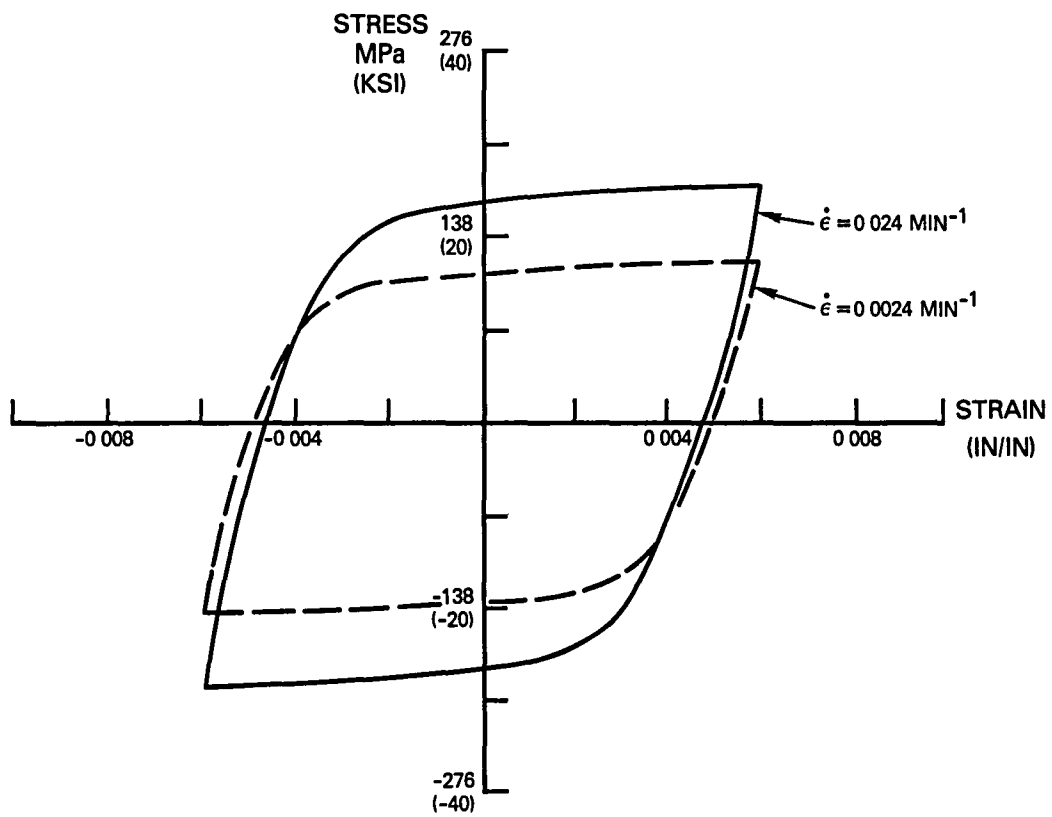
Figure A-4    Fully Reversed Strain (Condition a) at 871°C (1600°F)
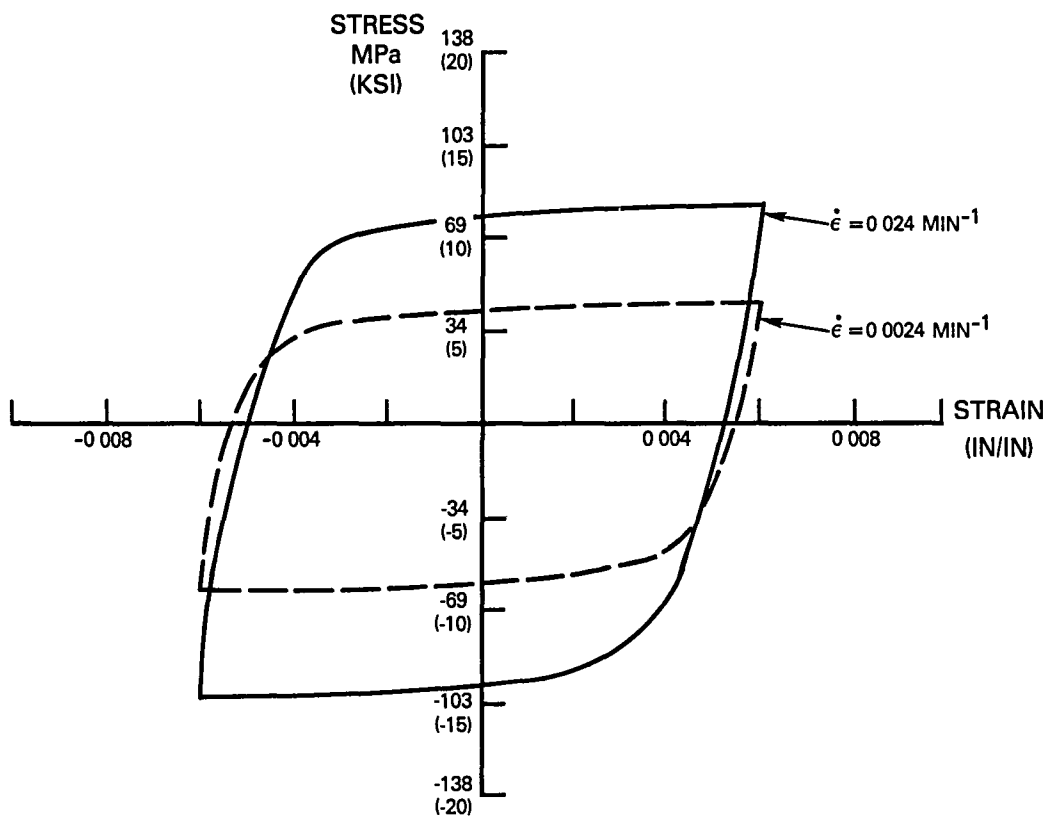
Figure A-5    Fully Reversed Strain (Condition a) at 982°C (1800°F)
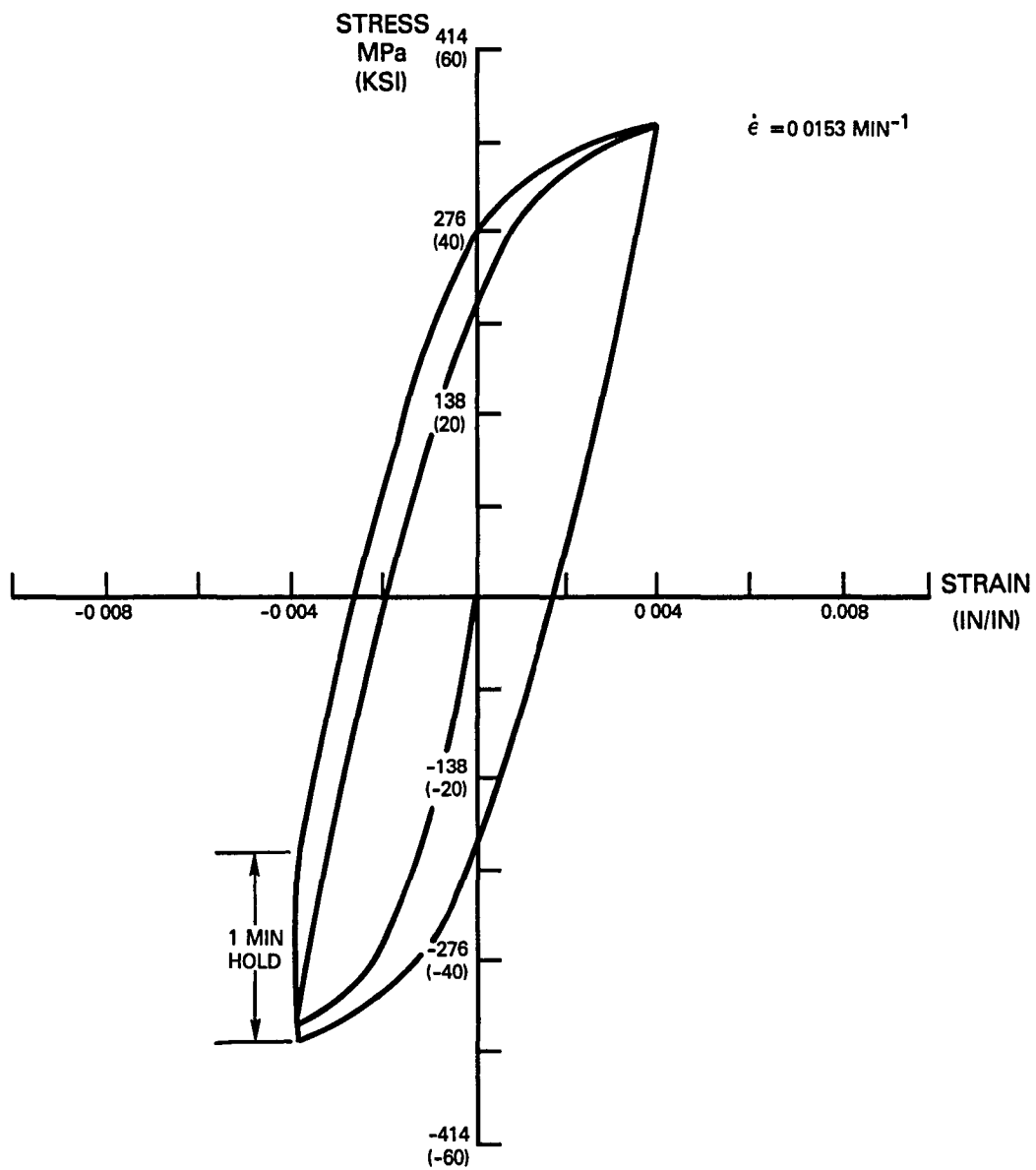
Figure A-6    Fully Reversed with 1 Minute Strain Hold (Condition b) at 760°C
(1400°F)

STRESS
MPa
(KSI)

CONTINUOUS
CYCLING
RESPONSE

$\dot{\epsilon} = 0\ 015\ MIN^{-1}$

1 MIN
HOLD

STRAIN
(IN/IN)

STRESS
MPa
(KSI)

CONTINUOUS
CYCLING
RESPONSE

$\dot{\epsilon} = 0\ 004\ MIN^{-1}$

1 MIN
HOLD
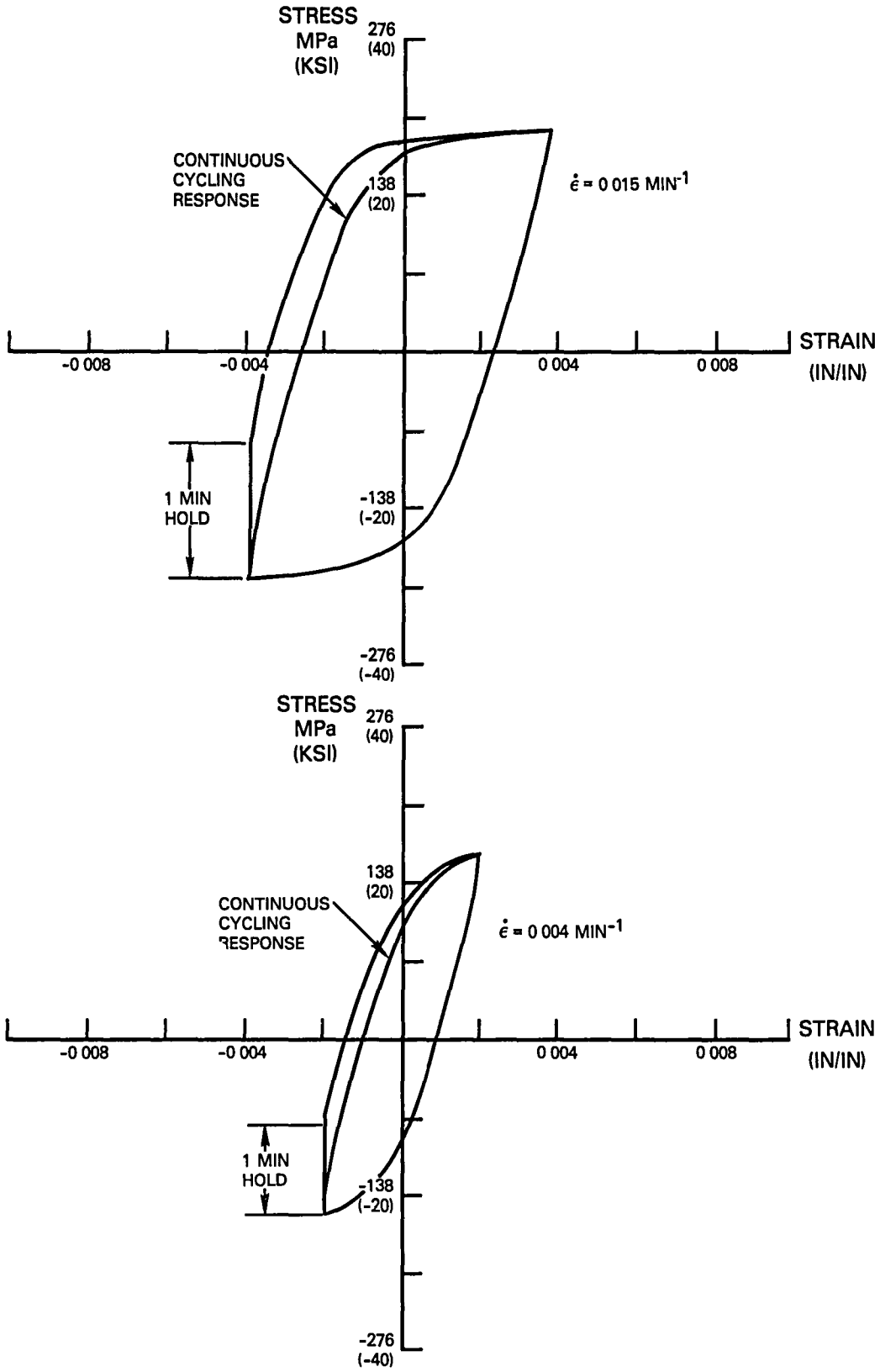
STRAIN
(IN/IN)

Figure A-7    Fully Reversed with 1 Minute Strain Hold (Condition b) at 871°C
(1600°F)

71
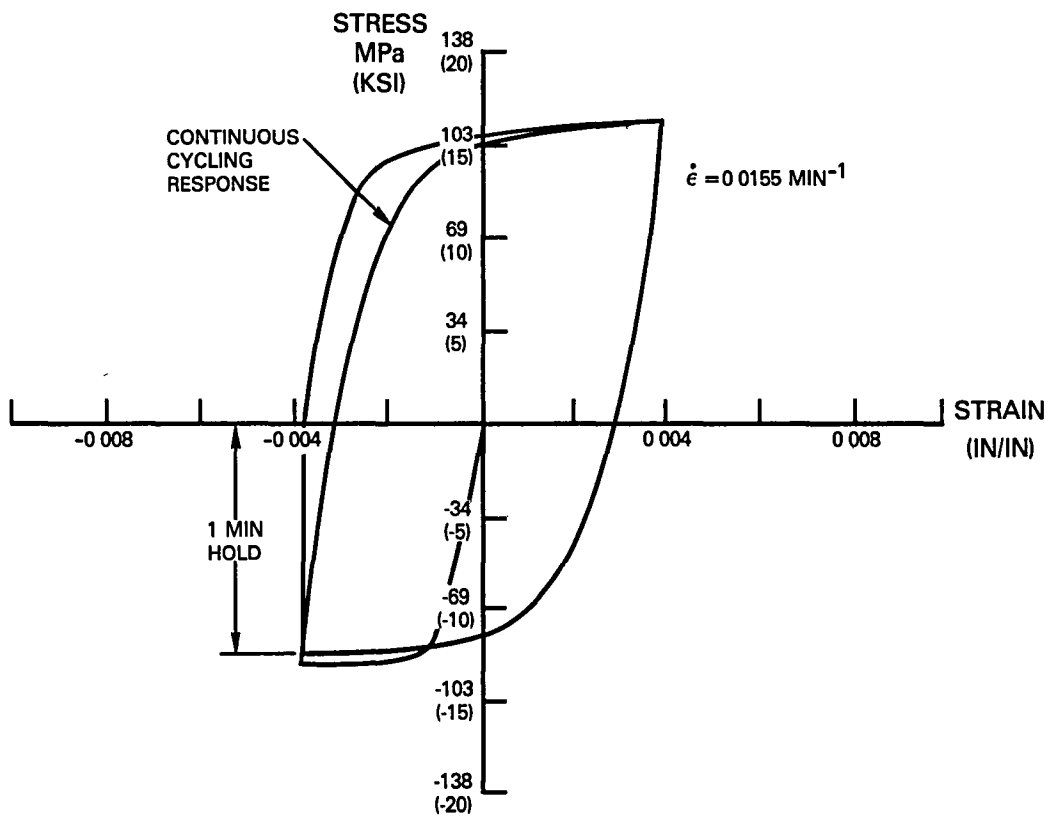
Figure A-8    Fully Reversed with 1 Minute Strain Hold (Condition b) at 982°C
             (1800°F)
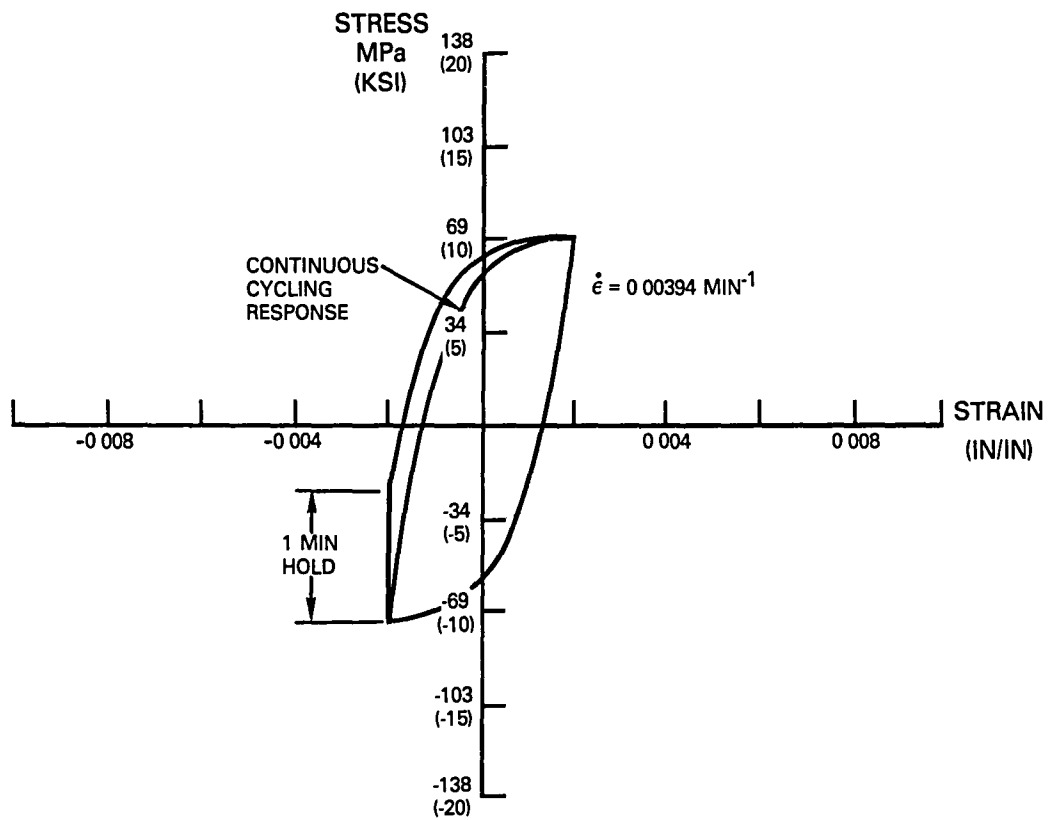
Figure A-9    Fully Reversed with 1 Minute Strain Hold (Condition b) at 982°C
              (1800°F)
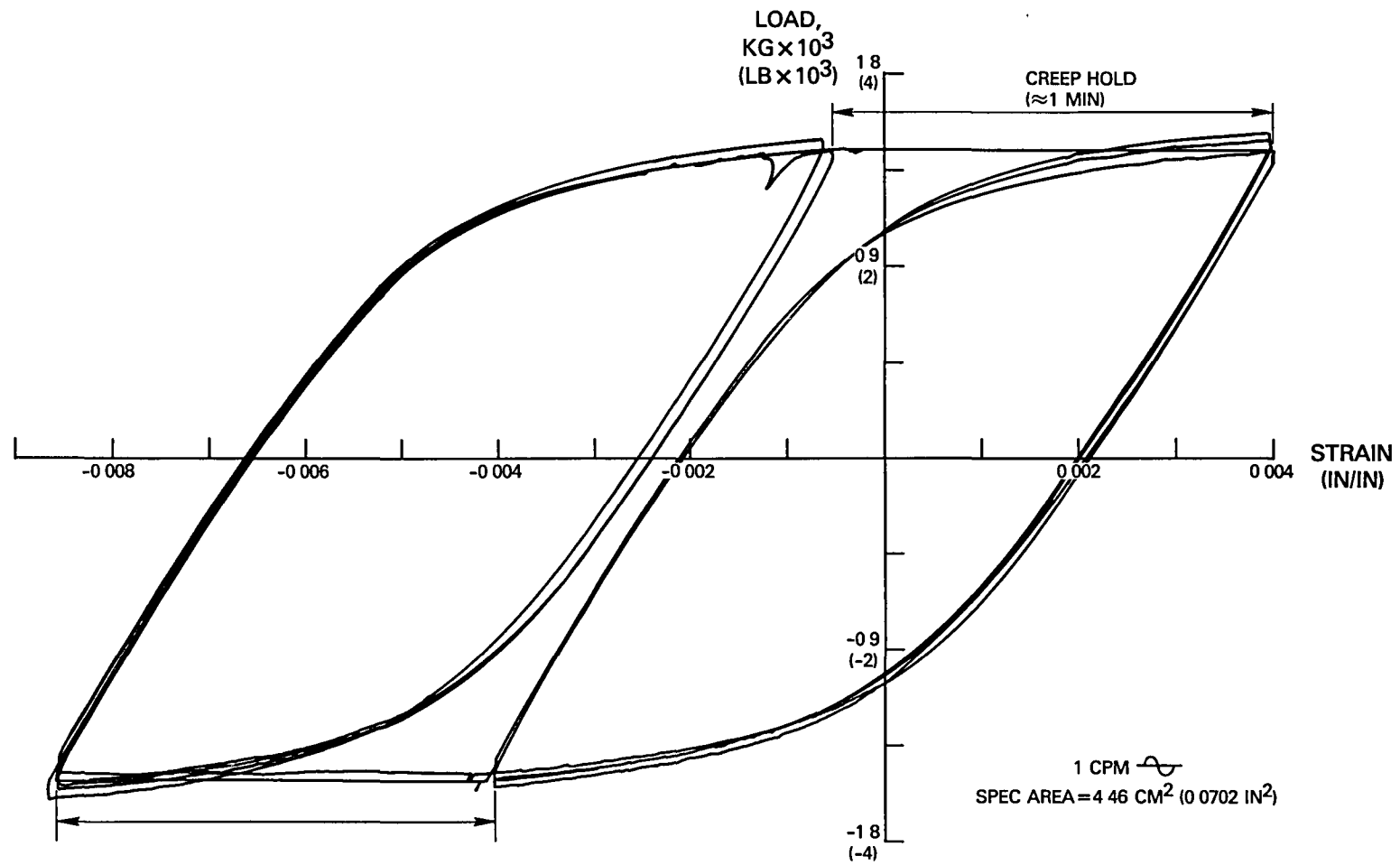
Figure A-10    Cyclic Response with Creep Hold (Condition c) at 760°C (1400°F)
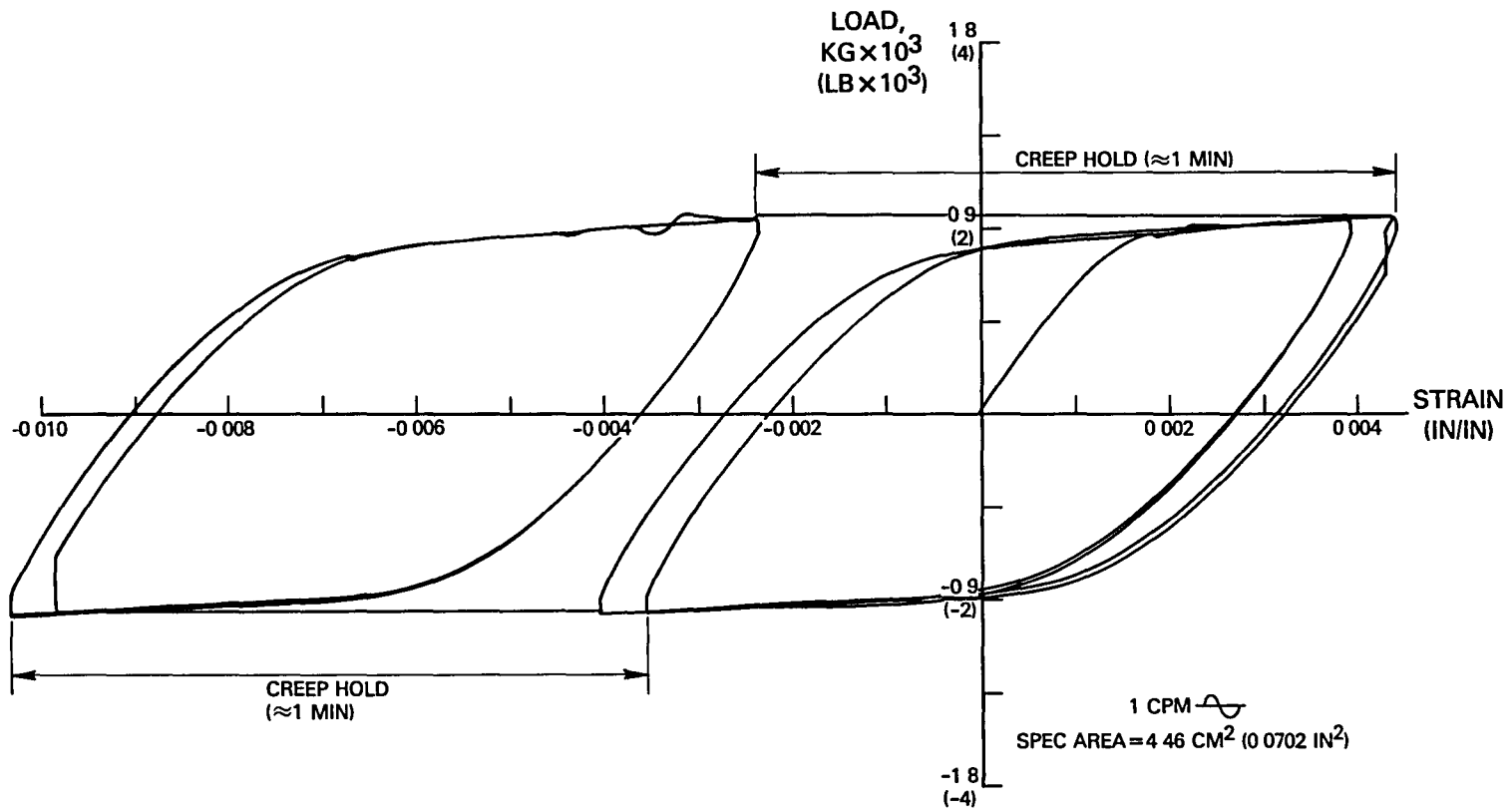
Figure A-11    Cyclic Response with Creep Hold (Condition c) at 871°C (1600°F)
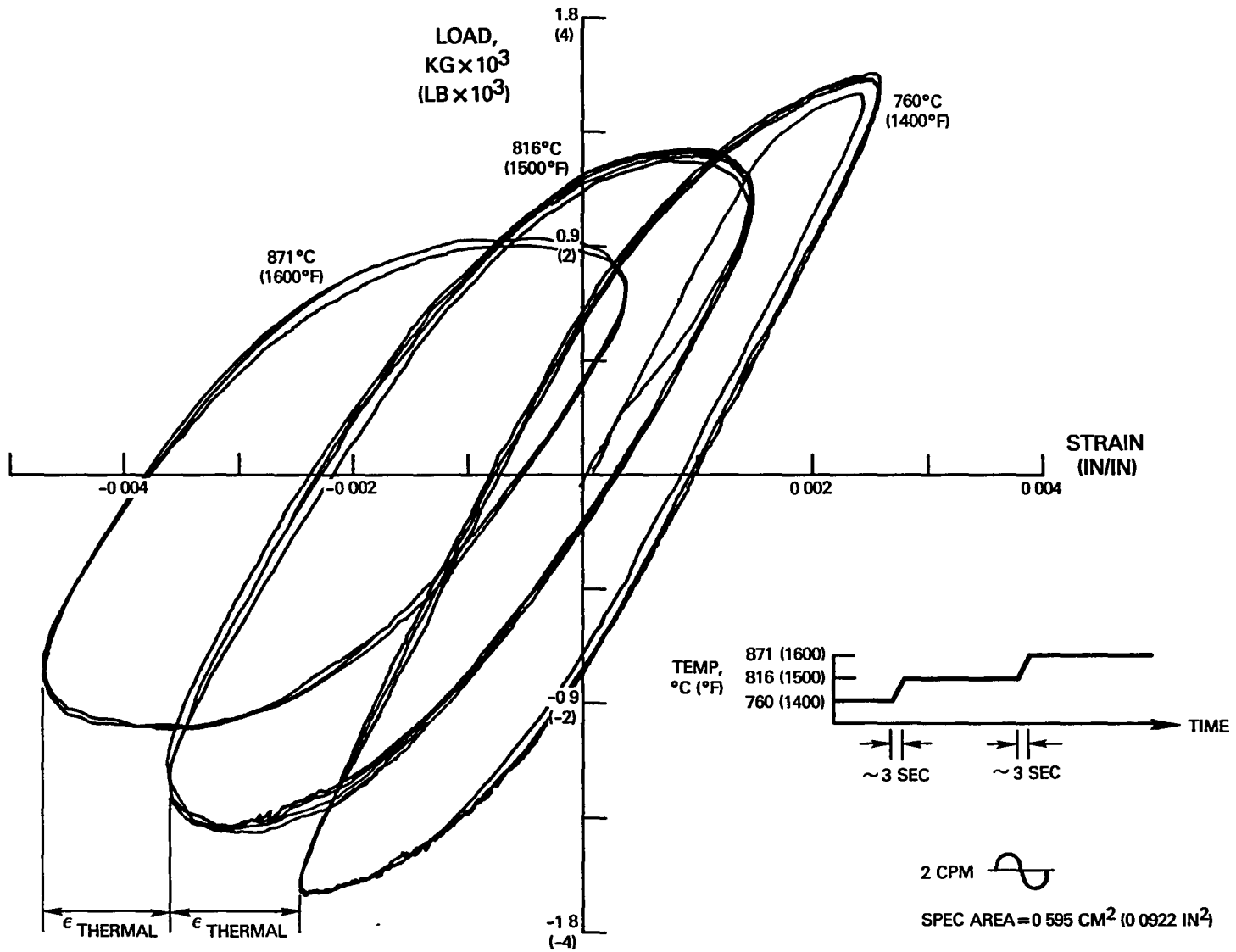
Figure A-12    Step Temperature Cycling (Condition d) at 2 cpm
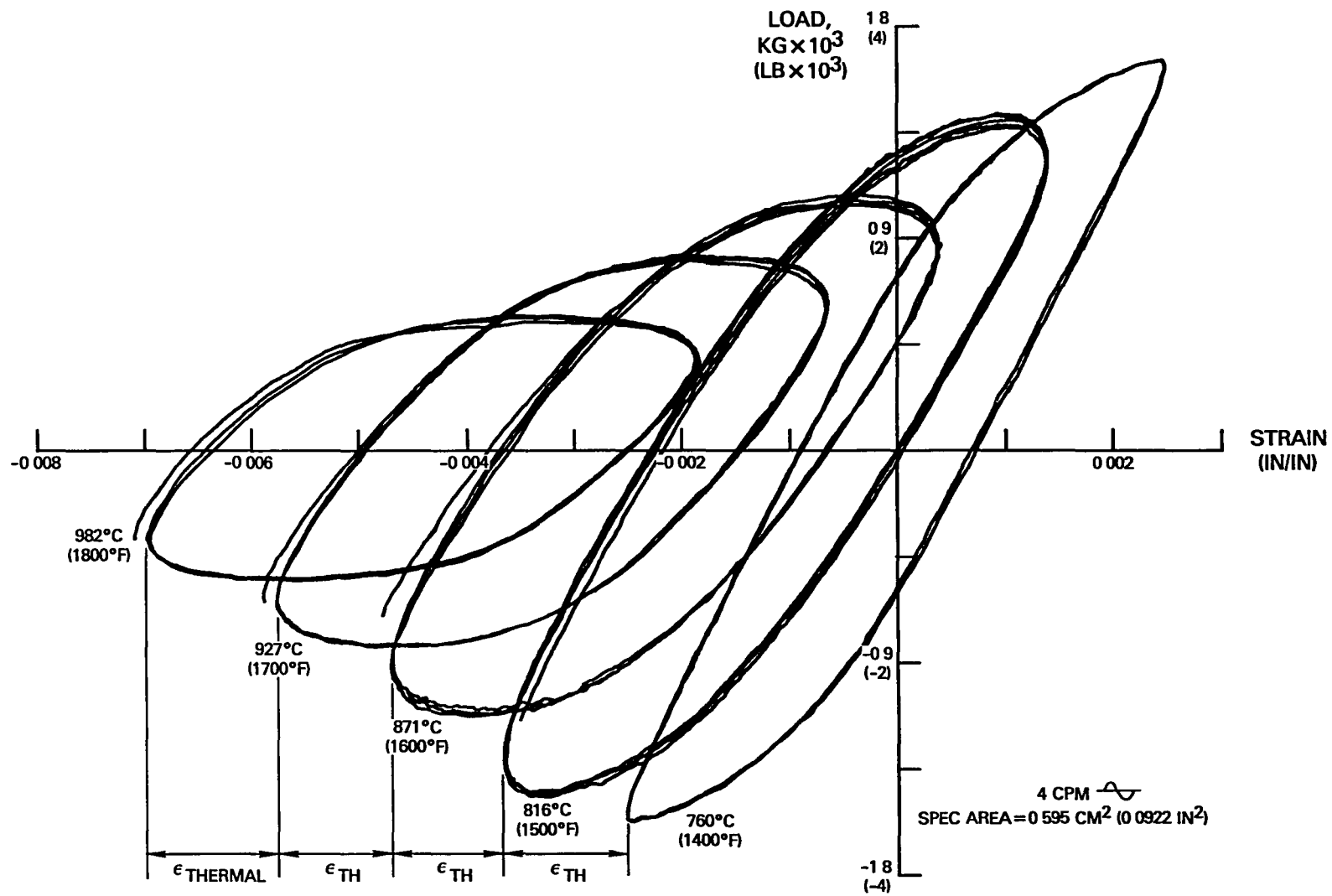
Figure A-13    Step Temperature Cycling (Condition d) at 4 cpm
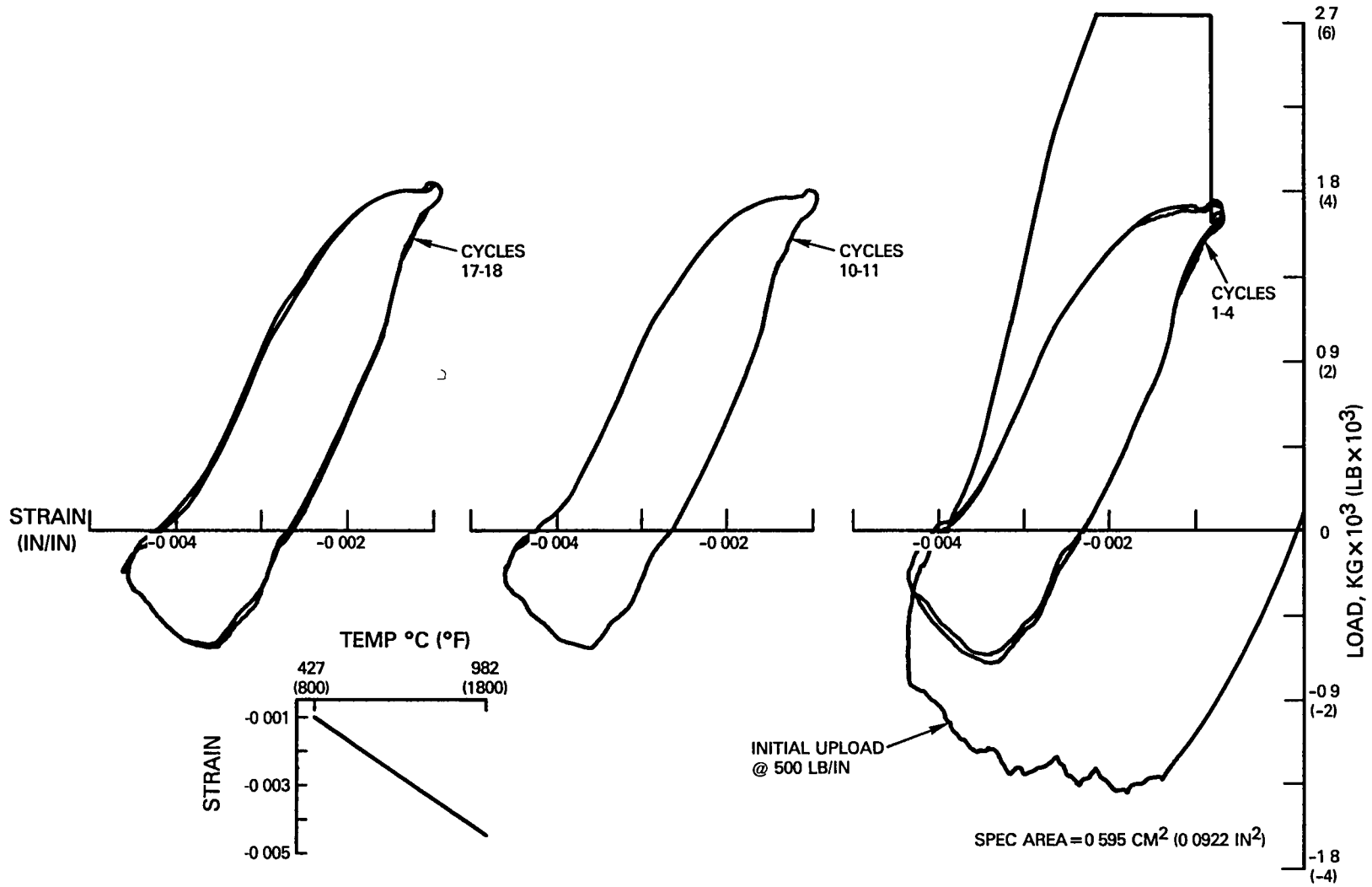
Figure A-14  Thermomechanical Cycling (Condition e) 427 to 982°C (800 to 1800°F)
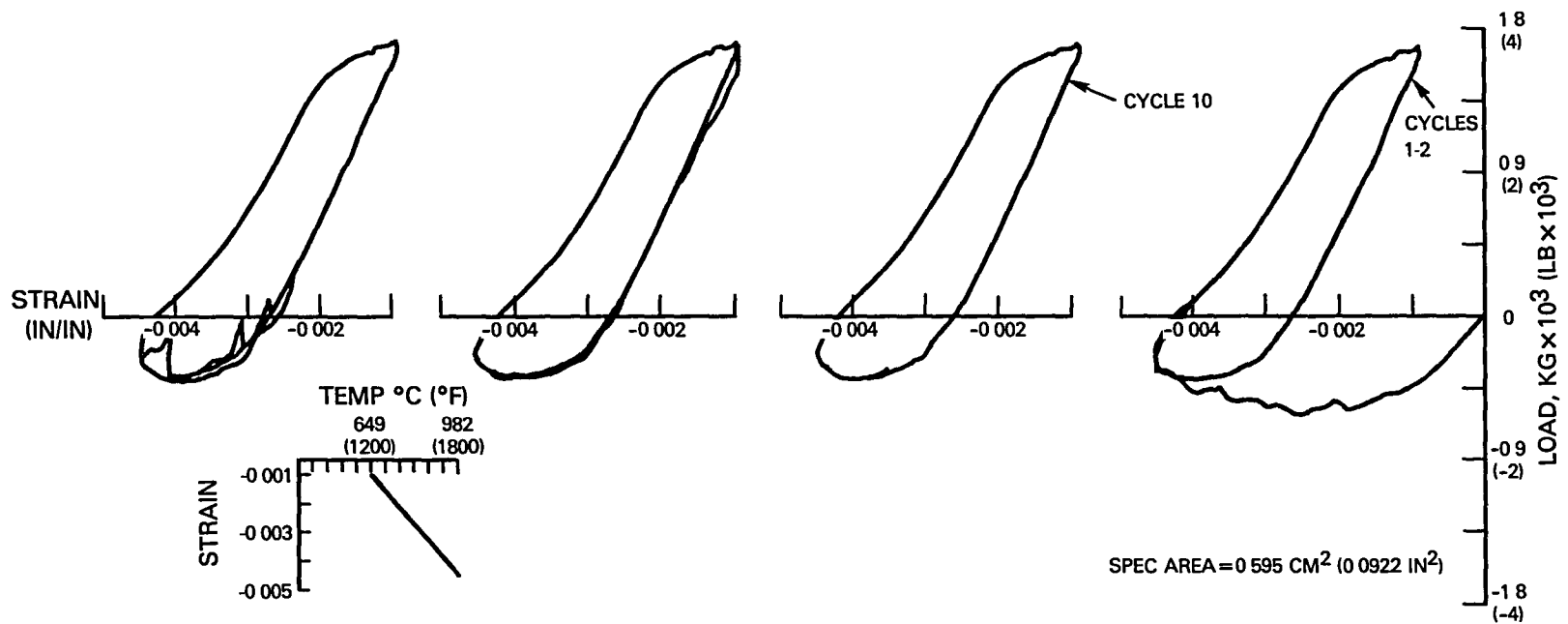
Figure A-15    Thermomechanical Cycling (Condition e) 649 to 982°C (1200 to 1800°F)
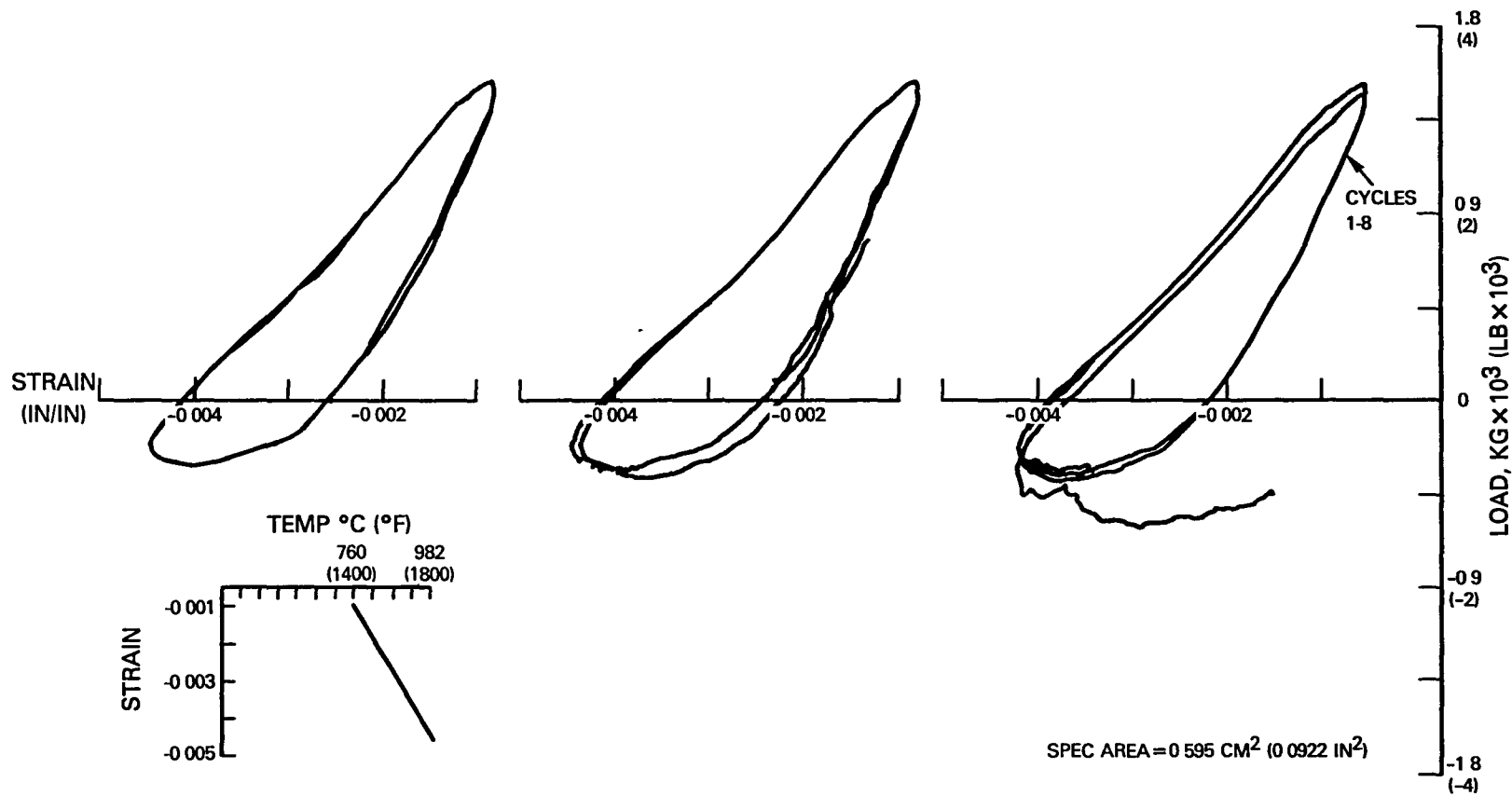
Figure A-15    Thermomechanical Cycling (Condition e) 750 to 982°C (1400 to 1800°F)

6th Cycle Mechanical Strain-Temperature History



SPECIMEN AREA = 0 057 CM$^2$ (0 0786 IN $^2$)
GAGE LENGTH = 2 5 CM (1 0 IN )
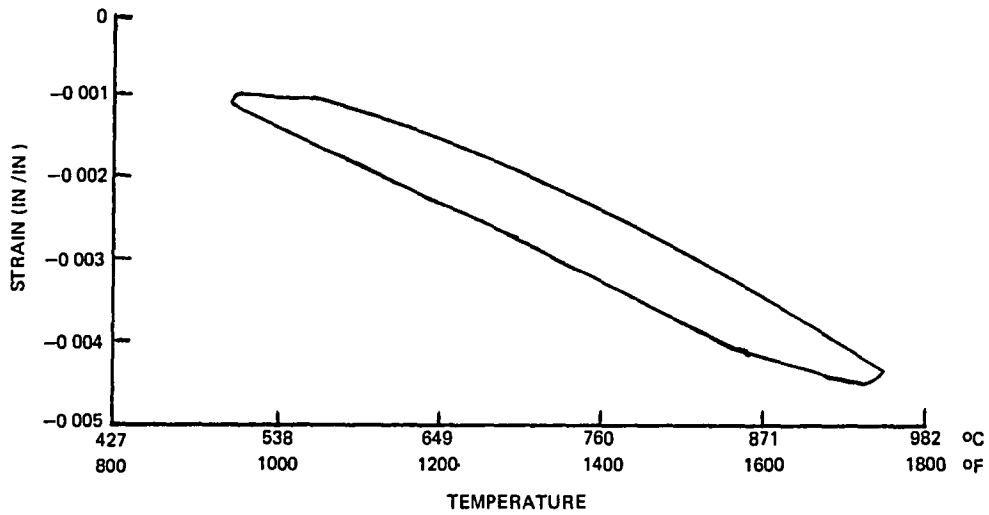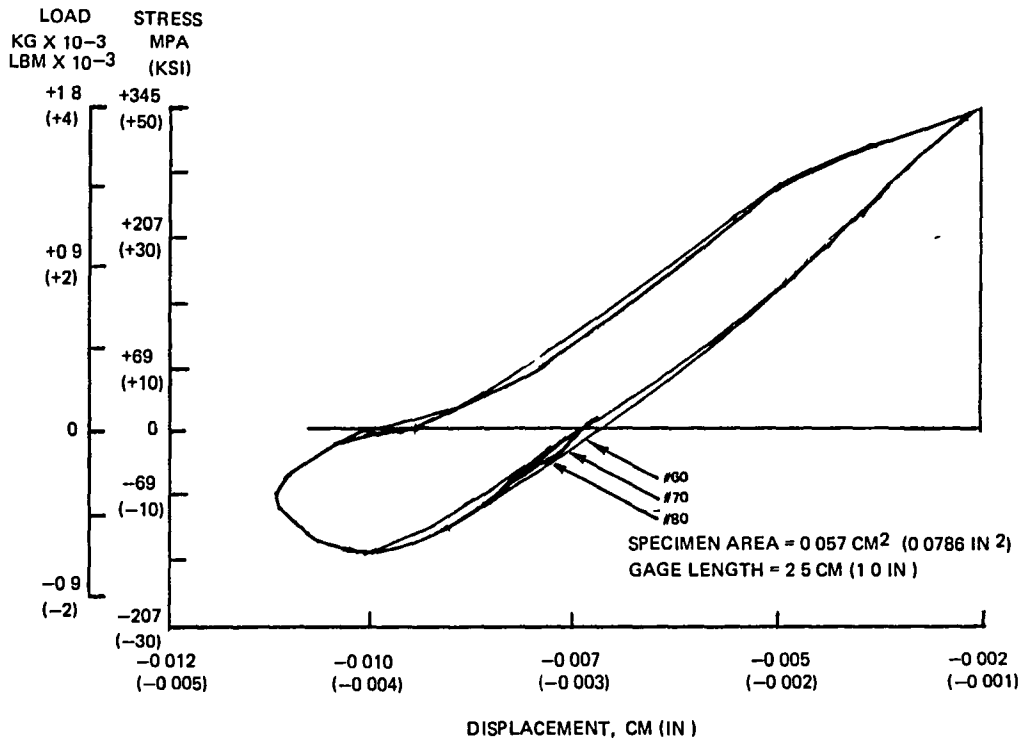
Test Specimen Response at Cycles 60, 70 & 80

Figure A-17    Faithful Cycle Strain-temperature and Stress-Strain Response (Condition f)

81

# APPENDIX B

## SUMMARY OF KEY EQUATIONS FOR SIMPLIFIED PROCEDURE

$$\Delta\varepsilon = \Delta\varepsilon_{plastic} + \Delta\varepsilon_{elastic} + creep \tag{1}$$

$$\Delta\sigma_{plastic} = \sigma y_{i+1} - \sigma y_i \quad \text{for } \sigma_i = \sigma y_i \text{ and } T_{i+1} \geq T_i \tag{16}$$

$$\Delta\sigma_{plastic} = \frac{E_{p\,i+1} + E_{p\,i}}{2}\,\Delta\varepsilon \quad \text{for } \sigma_i = \sigma y_i \text{ and } T_{i+1} < T_i \tag{17}$$

$$\Delta\sigma_{elastic + creep} = E\Delta\varepsilon_{total} - EA\sigma^{n}\Delta t \tag{23}$$

$$\sigma_{i+1} = \sigma_i + \dot{\sigma}_i\,\Delta t + \frac{\ddot{\sigma}_i\Delta t^2}{2!} + \frac{\dddot{\sigma}_i\Delta t^2}{3!} \tag{24}$$

$$\dot{\sigma} = E\dot{\varepsilon}_{total} - EA|\sigma|^{n-1}\sigma$$

$$\ddot{\sigma} = -nEA|\sigma|^{n-2}\sigma\dot{\sigma}$$

$$\dddot{\sigma} = -n(n-1)\,EA|\sigma|^{n-3}\sigma\dot{\sigma}^2 - nEA|\sigma|^{n-2}\sigma\ddot{\sigma}$$

For cyclic loading

$$\Delta\sigma^{*}_{elastic+creep} = E\Delta\dot{\varepsilon}_{total} - EA\sigma^{*n}\Delta t \tag{25}$$

$$\sigma^{*} = \sigma - \Omega \tag{26}$$

$$\Omega = \sigma_{max} - \sigma_{yield} \quad \text{for } \sigma_{max} \leq 2\sigma_{yield} \tag{27}$$

$$\Omega = \sigma_{yield} \quad \text{for } \sigma_{max} > 2\sigma_{yield} \tag{28}$$

[1]numbers refer to equations in text.

# APPENDIX C

## HEWLETT PACKARD HP67 PROGRAM FOR INCREMENTAL
## SOLUTION OF EQUATION 24

Input:  E (KSI) - STO1          $\sigma_i$(KSI) - STO4
$\dot{\epsilon}_{TOTAL}$ (hr$^{-1}$) - STO2   n - STO5
A - STO3          $\Delta$t (hr) - STO6

---

STEP

| | | | | | | | |
|---|---|---|---|---|---|---|---|
| 1 | fLBL A | 26 | RCL 4 | 51 | hy$^X$ | 76 | 3 |
| 2 | RCL 1 | 27 | X | 52 | RCL 4 | 77 | hy$^X$ |
| 3 | RCL 3 | 28 | RCL 3 | 53 | X | 78 | X |
| 4 | X | 29 | X | 54 | RCL 8 | 79 | 6 |
| 5 | RCL 5 | 30 | RCL 1 | 55 | X | 80 | ÷ |
| 6 | X | 31 | X | 56 | RCL 0 | 81 | RCL 8 |
| 7 | STO 0 (nEA) | 32 | CHS | 57 | X | 82 | RCL 6 |
| 8 | RCL 5 | 33 | RCL 2 | 58 | CHS | 83 | gx$^2$ |
| 9 | 1 | 34 | RCL 1 | 59 | RCL 7 | 84 | X |
| 10 | - | 35 | X | 60 | gx$^2$ | 85 | 2 |
| 11 | STO A (n-1) | 36 | + | 61 | RCL 4 | 86 | ÷ |
| 12 | RCL 5 | 37 | STO 7 ($\dot{\sigma}$) | 62 | X | 87 | + |
| 13 | 2 | 38 | RCL D | 63 | RCL D | 88 | RCL 7 |
| 14 | - | 39 | RCL B | 64 | RCL C | 89 | RCL 6 |
| 15 | STO B (n-2) | 40 | hy$^X$ | 65 | hy$^X$ | 90 | X |
| 16 | RCL 5 | 41 | RCL 4 | 66 | X | 91 | + |
| 17 | 3 | 42 | X | 67 | RCL 0 | 92 | RCL 4 |
| 18 | - | 43 | RCL 7 | 68 | X | 93 | + |
| 19 | STO C (n-3) | 44 | X | 69 | RCL A | 94 | STO 4 |
| 20 | RCL 4 | 45 | RCL 0 | 70 | X | 95 | hrtn |
| 21 | hABS | 46 | X | 71 | CHS | | |
| 22 | STO D (1σ1) | 47 | CHS | 72 | + | $\sigma_{i+1}$ output |  |
| 23 | RCL D | 48 | STO 8 ($\ddot{\sigma}$) | 73 | STO 9 ($\dddot{\sigma}$) | | |
| 24 | RCL A | 49 | RCL D | 74 | RCL 9 | | |
| 25 | hy$^X$ | 50 | RCL B | 75 | RCL 6 | | |

83

## REFERENCES

1. Moreno, V., "Combustor Liner Durability Analysis", National Aeronautics and Space Administration Report, Lewis Research Center, NASA CR 165250 (Contract NAS3-21836).

2. Walker, K. P.,"Research and Development Program for Nonlinear Structural Modeling with Advanced Time-Temperature Constitutive Relationships," NASA CR-165533 (Contract NAS3-22055), 1981.

3. "MARC General Purpose Finite Element Analysis Program", User's Manual, Volumes A-E, MARC Analysis Research Corporation, 1980.

Aerojet Liquid Rocket
Attn: Tech Info Ctr
Box 1322
Sacramento, CA 98513

AFOSR/NA
Attn: Capt David Glasgow
Mgr, Aerospace Sci
Bolling AFB
Washington, DC 20332

AFWAL/MLLN
Attn: Jack Henderson
Area B, Bldg 32
WPAFB, OH 45433

AFWAL/POTC
Attn: Richard Hill
Area B, Bldg 18
WPAFB, OH 45433

AFWAL/MLLN
Attn: Ted Nicholas
WPAFB, OH 45433

AFWAL/MLLN
Attn: Dr. Walt Reimann
WPAFB, OH 45433

AFWAL/MLLAM
Attn: Library
WPAFB, OH 45433

AiResearch Mfg Co
Attn: Richard Graves
2525 W 190th St
Torrance, CA 90509

University of Akron
Attn: Prof Paul Chang
Dept Civil Eng
Akron, OH 44325

Univ of Alabama
Attn: Dr. A. E. Carden
AME Dept
Box 2908
University, AL 35486

Univ of Arizona
Attn: Dr. Paul H. Wirsching
Dept. Aero & Mech Eng
Tucson, AZ 85721

Army Applied Tech Lab
Attn: Jan Lane
DAVDL-ATL-ATP
Fort Eustis, VA 23604

Army Applied Tech Lab
Attn: Library
Fort Eustis, VA 23604

AVCO - Space Systems Div
Attn: Library
Lowell Industrial Pk
Lowell, MA 01851

AVCO - Lycoming Div
Attn: Jerry Walters
550 S. Main St.
Stratford, CT 06497

Battelle Columbus Lab
Attn: Brian Leis
505 King ASve.
Columbus, OH 43201

Boeing
Attn: Library
3801 S. Oliver
Wichita, KS 67210

Case Western Reserve Univ
Attn: Prof. A. Chudnovski
205 Bingham Bldg
10900 Euclid Ave.
Cleveland, OH 44106

Case Western Reserve Univ
Attn: Prof. S. S. Manson
619 Glennan Bldg
10900 Euclid Ave.
Cleveland, OH 44106

Case Western Reserve Univ
Attn: Dr. Alex Mendelson
Glennan Bldg
10900 Euclid Ave.
Cleveland, OH 44106

Univ of Cincinnati
Attn: Dr. S. Antolovich
Dept. Matl's Sci & Met Eng
489 Rhodes Hall
Cincinnati, OH 45221

Univ of Cincinnati
Attn: Dr. Donald Stouffer
Dept Eng Sci
Cincinnati, OH 45221

Univ of Connecticut
Attn: Dr. Eric Jordan
Mech Eng Dept U-139
Storrs, CT 05268

Univ of Dayton
Attn: Dr. Joseph Gallagher
Research Institute
Rm 563 Kettering Bldg
Dayton, OH 45469

Defense Documentation Ctr
Cameron Station
5010 Duke St
Alexandria, VA 22314

Denver Research Institute
Attn: Library
University Park
Denver, CO 80210

Detroit Diesel Allison
Attn: Dr. Mehmet Doner
Matl's Research & Eng
Box 894 - W5
Indianapolis, IN 46206

FAA - New England Reg.
Attn: Vic Salvano
12 New England Exec Park
Burlington, MA 01803

Failure Analysis Assoc.
Attn: Dr. Clifford Wells
750 Welch Rd.
Suite 116
Palo Alto, CA 94304

Ford Motor
Attn: Dr. Ronand Landgraf
Scientific Research Staff
Box 2053
Dearborn, MI 48121

Garrett Turbine Eng Co
Attn: Lee Matsch
111 S 34th St
Box 5217
Phoenix,AZ 85010

Georgia Inst of Tech
Attn: Prof S. Atluri
225 North Ave
Atlanta, GA 30332

General Electric Company
Attn: Dr. Len Beitch K-221
Mgr, EM & LM
Evandale, Oh 45215

General Electric Company
Attn: J. H. Laflen
MS K-71
Evandale, OH 45215

General Electric Company
Attn: Library
1000 Western Ave.
Lynn, MA 01905

General Electric Company
Attn: Library
Box 8
Schenectady, NY 12301

General Electric Company
Attn: R. L. McKnight
Mail Drop K-69
Evandale, OH 45215

General Electric Company
Attn: Donald Mowbray
Bldg 55-219
1 River Rd.
Schenectady, NY 12345

General Electric Company
Attn: Warren Ostergren
Bldg 53-317
Gas Turbine Dept
Schenectady, NY 12345

General Electric Company
Attn: Dr. Mel Roberts
Mail Drop K-69
Evandale, OH 45215

General Electric Company
Attn: R. A. Sprague
Mail Drop M-82
Evandale, OH 45231

Hibbitt, Karlsson &
   Sorensen, Inc.
Attn: Dr. Kevin Walker
35 South Angell St
Providence, RI 02906

Univ of Illinois
Attn: Prof JoDean Morrow
321A Talbot Lab
Urbana, IL 61801

Univ of Illinois
Attn: Prof. D. Socie
Talbot Lab
Urbana, IL 61801

ITT Research Inst
Attn: Kenneth Hofer
10 W 35th St
CHicago, IL 60616

Int'l Harvester Co - Solar
Attn: Library
2200 Pacific Hwy
San Diego, CA 92101

Lockheed California
Attn: Library
Burban, CA 91503

Lockheed Huntsville
Attn:  W. H. Armstrong
Mgr, Struct & Mech
Huntsville, AL 35806

Mass Institute of Tech
Attn: Prof Ted Pian
Rm 33-311
77 Mass. Ave.
Cambridge, MA 02139

Mass Institute of Tech
Attn: Prof Regi Pelloux
Rm 8-237
77 Mass. Ave.
Cambridge, MA 02139

McDonnell Douglas
Attn: Library
Missiles & Space Div
5301 Bolsa Ave
Huntington Beach, CA 92647

McDonnell Douglas
Attn: Library
3852 Lakewood Blvd
Long Beach, CA 90801

Michigan State Univ
Attn: Dr. John Martin
MMM Dept
330 Engineering Bldg
E. Lansing, MI 48824

Univ of Minnesota
Attn: Dr. W. W. Gerberich
Dept Chem Eng & Matl Sci
Minneapolis, MN

NASA-AFWAL Tech Liaison
Attn: Everett Bailey
AFWAL/DO
WPAFB, OH 45433

NASA Headquarters
Attn: Dr. M. Greenfield
RTM-6, M&S Div
Washington, DC 20546

NASA Langley Research Ctr
Attn: Library
MS-185
Langley Field, VA 23365

NASA - Lewis Research Center
Attn: J. Acurio, Director
USAR&TL Propulsion Lab
Cleveland, OH 44135

NASA - Lewis Research Center
Attn: Dr. Robert Bill
Head, Fatigue Res Sect
MS 49-6
Cleveland, OH 44135

NASA - Lewis Research Center
Attn: Dr. Gary Halford
MS 49-6
Cleveland, OH 44135

NASA - Lewis Research Center
Attn: Marv Hirschberg
Chief, Fatigue & Fracture
MS 49-6
Cleveland, OH 44135

NASA - Lewis Research Center
Attn: Tech Utilization
MS 3-19
Cleveland, OH 44135

NASA - Lewis Research Center
Attn: Report Control
MS 5-5
Cleveland, OH 44135

NASA - Lewis Research Center (2)
Attn: Library
MS 60-3
Cleveland, OH 44135

NASA - Lewis Research Center
Attn: S&T Section
MS 501-11
Cleveland, OH 44135

NASA - Lewis Research Center
Attn: AR&TL Office
MS 77-5
Cleveland, OH 44135

NASA - Lewis Research Center
Attn: AFSC Liaison Office
MS 501-3
Cleveland, OH 44135

NASA - Lewis Research Center (2)
Attn: S&MT Div Files
MS 49-6
Cleveland, OH 44135

NASA - Lewis Research Center
Attn: Albert Kaufman
MS 49-6
Cleveland, OH 44135

NASA Marshall Space Center
Attn: Library
Huntsville, AL 35812

NASA Marshall Space Center
Attn: Norm Schlemmer
Huntsville, AL 35812

NASA Sci & Tech Info (25)
Attn: Accessioning Dept
Box 8757
Balt/Wash Intn'l Airport
Maryland 21240

Naval Air Systems Command
Attn: Irving Machlin
Code AIR-52031B
Washington, DC 20361

Naval Ship R&D Center
Attn: Library
Code 522.1
Bethesda, MD 20084

Northwestern Univ
Attn: Prof S. Nemat-Nasser
Dept of Civil Eng
Evanston, IL 60201

ORNL Box X
Attn: Dr. Charles Brinkman
Metals & Ceramics Div
Oak Ridge, TN 37830

ORNL Box X
Attn: Dr. Rod Ellis
Metals & Ceramics Div
Oak Ridge, TN 37830

Pennsylvania State Univ
Attn: Dr. Sam Zamrik
121 Hammond Bldg
University Park, PA 16802

Rensselaer Polytech Inst
Attn: Dr. D. Duquette
Matl's Eng Dept
Troy, NY 12181

Rensselaer Polytech Inst
Attn: Dr. Erhard Krempl
Mech & Aero Eng Dept
Troy, NY 12181

Rensselaer Polytech Inst
Attn: Prof Norman Stoloff
Dept of Matl's Eng
Troy, NY 12181

Rocketdyne
Attn: Al Hallden
Dept 545-126, Code AC20
6633 Canoga Ave.
Canoga Pk, CA 91304

Rockwell Int'l
Attn: Library
6633 Canoga Ave
Canoga Pk, CA 91304

Sandia Labs
Attn: Library
Albuquerque, NM 87115

Scientific Info Service
Attn: Ref. USZ
7 Woodland Ave.
Larchmont, NY 10538

Southern Rsearch Inst
Attn: Library
2000 9th Ave S
Birmingham, AL 35205

Southwest Research
Attn: Library
8500 Culebra Rd
San Antonio, TX 78284

Stanford Univ
Attn: Prof Alan K. Miller
Dept Matl's Sci & Eng
Stanford, CA 94305

Syracuse Univ
Attn: Dr. H. W. Liu
409 Link Hall
Syracuse, NY 13210

Teledyne CAE
Attn: Tom Moyer
Box 6971
Toledo, OH 43612

Texas A&M Univ
Attn: Dr. W. L. Bradley
College Station, TX 77843

Texas A&M Univ
Attn: Dr. Walter Haisler
Aerospace Eng Dept
College Station, TX 77843

Westinghouse - R&D Center
Attn: Robert Johnson
Bldg 401, Rm 2X9G
Pittsburgh, PA 15235

Westinghouse - ARD
Attn: Alfred Snow
Box 158
Madison, PA 15663

Univ of Wisconsin
Attn: A. Freed
Dept Eng Mech
Engineering Bldg
Madison, WI 53706

**End of Document**